

There and back again – Closed timelike curves as EFT selection principle

Bum-Hoon Lee ^{1,2,3,*} Nils A. Nilsson ^{4,5,†} and Somyadip Thakur ^{2,‡}

¹*Department of Physics, Shanghai University, Shanghai, 200444, China*

²*Center for Quantum Spacetime, Sogang University, Seoul 121-742, Korea*

³*Department of Physics, Sogang University, Seoul 121-742, Korea*

⁴*Cosmology, Gravity and Astroparticle Physics Group,*

Center for Theoretical Physics of the Universe, Institute for Basic Science, Daejeon 34126, Korea

⁵*LTE, Observatoire de Paris, Université PSL, CNRS, LNE,*

Sorbonne Université, 61 avenue de l'Observatoire, 75 014 Paris, France

(Dated: February 23, 2026)

Modified gravity is often approached in the context of effective-field theory (EFT), with the view that the EFT corrections permit a more desirable theory. In this paper, we posit that this should extend to the causal structure of curved spacetime in addition to the standard demands such that of flat spacetime positivity and unitarity. We propose a new guiding principle for modified-gravity theories, namely that closed timelike curves should always be *harder* to obtain than in General Relativity. By demanding this, one can place powerful constraints on modified gravity. To elucidate this claim, we investigate modified-gravity EFTs on rotating black-hole backgrounds, focusing on the appearance/disappearance of closed timelike curves, and provide parameter bounds which only partly overlap with other approaches based on time delay. We construct perturbative rotating black-hole solutions in modified-gravity EFTs based on the Horndeski class and provide parameter bounds necessary to preserve causality and stability. Finally, we present a novel probe for the existence of closed timelike curves through quasinormal modes and black-hole echoes. This can be used to diagnose spacetime causality once next-generation gravitational-wave data becomes available.

CONTENTS

I. Introduction	2
II. Warmup and choosing the model	5
III. K-essence model	14
IV. Einstein-dilaton Gauss-Bonnet model	25
V. Gravitational-wave echoes as probes of causality	35
VI. Discussion & Outlook	45
Acknowledgments	48
A. Rotating-cylinder backreaction	50
B. Gauge invariance of the CTC criterion under radial shifts	52
C. Vacuum $\ell = 2$ Kerr-(A)dS Hartle-Thorne treatment	53

* bhl@sogang.ac.kr

† nilsson@ibs.re.kr

‡ somyadip@sogang.ac.kr

I. INTRODUCTION

General Relativity (GR) has met with remarkable success since its conception over a century ago. Starting with the accurate prediction of the perihelion advance of Mercury, the theory has successfully passed every observational test to date. In the Solar system, tests such as lunar laser ranging [1, 2] and planetary ephemerides [3, 4] have now shown GR to hold to more than one part in one hundred million. On larger scales, gravitational lensing have provided strong proof that GR is the correct theory of gravity [5], and with the advent of gravitational-wave astronomy and the LIGO/Virgo/Kagra interferometers, general relativity is being probed in truly strong-gravity regimes [6–8], and the number of observed events are rapidly increasing, constraining the parameter space for modified-gravity models. Furthermore, next-generation gravitational-wave observatories such as LISA, Cosmic Explorer, and the Einstein Telescope will be significantly more sensitive to beyond-GR effects [9, 10]. Finally, on cosmological scales, the detection of the accelerated expansion of the Universe firmly indicates that the Lambda-Cold-Dark-Matter (LCDM) should be considered the currently leading cosmological model [11, 12].

Although a great success in terms of a classical theory of gravitation, GR has a number of undesirable features: firstly, it is famously non-renormalisable, making quantisation difficult; further, the measured value of the cosmological constant differs by 55 orders of magnitude as compared to QFT calculations [13]. It also features curvature singularities at the center of black holes as well as at the time of the Big Bang. At the cosmological level, the Hubble tension, the discrepancy in the value of the Hubble constant when measured by early and late-time probes is one of the most pervasive problems of the LCDM model [14]. Finally, the existence of Closed Timelike Curves (CTCs, which in GR are usually hidden behind a horizon), the topic of the present paper, can in certain circumstances allow observers to travel to their own causal past, creating a slew of problems such as the Grandfather Paradox [15]. In geometries without such curves, cause precedes effect in a determined temporal order, which defines the notion of causality, and great care has to be taken to avoid causality violation when constructing realistic theories. In flat spacetime, this entails ensuring that superluminal speeds cannot be maintained in such a way that the retarded propagator has support outside the local Minkowski lightcone, and causality is therefore a rather straightforward concept in flat spacetime, where the local lightcone coincides with the global one. In this context, commutation of scalars (spin-0 fields) for spacelike separations (outside the lightcone), i.e. $[\phi(x), \phi(y)] = 0, (x - y)^2 < 0$ is enough to guarantee causality of the full theory,¹ but when working in an EFT framework, the situation becomes more subtle, even on a flat background. Working in a low-energy EFT limit and including only the relevant operators requires additional constraints on the EFT coefficients in order to guarantee unitarity and causality. A standard tactic (see for example [16, 17] and references therein) is to study dispersion relations in $2 - 2$ scattering processes; from these, one can obtain positivity bounds on the Wilson coefficients.

If the notion of causality in Minkowski space is conceptually straightforward, the situation is decidedly less so on a curved background. A significant amount of work has been carried out in context of GREFT [18], an effective-field theory approach to higher-order curvature corrections to GR. Characterising the properties of such EFTs has been the subject of much recent work, including the swampland conjecture [19, 20] and quasinormal mode causality [21]. In gravity, one is dealing with scales significantly larger than that of scattering amplitudes², and as such, the notion of *IR* causality is introduced, and its consequences on non-trivial (i.e. curved) backgrounds were considered in for example [17, 21–24] and references therein. For higher-derivative scalar-tensor theory on a black hole background, it was shown

¹ This in fact guarantees that all spin-0 fields are bosons. For fermions and higher-spin objects, the situation is more subtle, but we will not consider it here.

² In the context of cosmological perturbations, the so-called high-momentum limit is often used, but this is relative to the Hubble radius and we are firmly in the infrared as compared to scattering amplitudes.

in [22, 25] that the Shapiro time delay obtains a correction from the higher-curvature terms as $t_{\text{Shapiro}} = t_{\text{GR}} + t_{\text{EFT}}$, and as long as the time delay does not become a resolvable time *advance*, the bounds are in agreement with those from 2–2 scattering. In other words, since even an ideal detector is bounded by the uncertainty principle and we have that, for IR causality, $-\omega t_{\text{EFT}} \lesssim 1$ [21], which can be related to the Eisenbud-Wigner time delay for gravitational waves.³ These IR causality bounds can be complemented with UV causality, which is a property of scattering amplitudes on a Minkowski background – this becomes subtle on non-trivial spacetimes, especially cosmological ones, where the expanding background breaks time diffeomorphisms. As such, a hierarchy of scales emerges, and one can only consider EFT operators on comoving scales below some cutoff, as was outlined in detail in Section 4 of [22], where it was found that the distance a gravitational wave may travel outside the local Minkowski lightcone without offering support to the Green’s function (and thus breaking causality) must be smaller than the physical wavelength $2\pi a/k$ of the GW. In addition, it was recently shown that causal propagation of scalar modes on dS space requires bounds on the Wilson coefficients, but that the corresponding positivity bounds in Minkowski space are stronger [27].

Motivated in part by the challenges and tensions faced by general relativity outlined above, the field of modified gravity has gained great traction in recent decades, and has become increasingly important with the advent of gravitational-wave astronomy, which probes such strong-gravity environments where we may expect corrections to general relativity to appear. Nevertheless, constructing a consistent extension to GR is not an easy task, as shown in the form of Lovelock’s theorem, which proves that the Einstein-Hilbert action is the only possible action constructed solely from the metric tensor which also gives second-order equations of motion (and which has two propagating degrees of freedom) in four spacetime dimensions [28–30]. Therefore, the only way to move beyond general relativity is to add a new degree of freedom in some way, for example by higher-curvature operators (the minimal choice can be said to be the Starobinsky model or quadratic gravity which has a third (scalar) propagating degree of freedom, but no cutoff scale [31]) or by breaking one of the symmetries of the underlying theory. Modifying GR in this way in an excellent way to learn more about the gravitational interaction, and many models exist, based for example on higher-curvature terms, e.g quadratic gravity, massive gravity (e.g [32]), theories with broken assumptions (e.g non-commutative spacetime [33], which is equivalent to the violation of local Lorentz symmetry, or Hořava-Lifshitz gravity [34], which is known to be Lorentz breaking), and theories with extra fields (e.g Horndeski gravity [35, 36], which introduces a new scalar degree of freedom). These are just a few of the existing models in what has grown into a veritable “zoo” of modified-gravity models.⁴ In this paper, we choose Horndeski gravity as our tool to modify gravity, as it is the most general scalar-tensor theory which gives second-order field equations.

This paper focuses on Closed-Timelike Curves (CTCs) as a probe of modified gravity: in principle, CTCs allow observers to travel back in time and meet themselves in the past; therefore, there can be no doubt that such an action breaks causality without appealing to time delay or scattering amplitudes. CTCs were first described by Van Stockum in 1937 [39] and Gödel in 1949 [40] using a rotating cosmological solution to general relativity which contains CTCs. Since then, several other solutions containing CTCs have been discovered, for example the well-known solution of a Kerr black hole (although in this case, the CTC appears inside the inner horizon) and the solution of a rotating cosmic string known as the Tipler cylinder [39, 41, 42]. Such solutions are in conflict with the Chronology Protection Conjecture, stating that the laws of physics does not allow closed timelike curves [43]. Taking this at face value, any UV completion of general relativity, which we can consider to be the IR limit of some theory of quantum gravity, must somehow prevent the appearance of CTCs and rescue causality⁵. We therefore posit in this paper that when considering any type of modified gravity, it should be demanded that any modification to general relativity should make it harder, and never easier, to generate closed timelike curves. Given this, the existence of CTCs can be used as a guiding principle for modified gravity, and in this paper, we develop this notion in the context of scalar-tensor theories. We provide bounds on EFT coefficients akin to those obtained from time delay and scattering amplitudes

³ Similar techniques were applied to gauge fields in e.g. [26].

⁴ For a more complete picture of the modified-gravity landscape, see the reviews [37] and [38].

⁵ The Universe does indeed seem to be causal: apart from agreeing with human intuition (which admittedly means little in relativity), Stephen Hawking can be quoted as “*There is also strong experimental evidence in favour of the [Chronology Protection] conjecture from the fact that we have not been invaded by hordes of tourists from the future*” [43].

described above, and we present an observational smoking gun to identify the existence of a CTC around compact-binary coalescence remnants. We choose as our starting point the most general Horndeski action and then study two physically motivated subsets in detail.

Causality is one of the most fundamental principles underlying any relativistic field theory: geometrically, causality is encoded in the structure of the light cones defined by the spacetime metric $g_{\mu\nu}$, which determine the set of events that can influence or be influenced by a given observer [44]. When this causal structure breaks down, the spacetime may admit CTCs, timelike trajectories $\gamma(\lambda)$ satisfying $g_{\mu\nu} \dot{\gamma}^\mu \dot{\gamma}^\nu < 0$, $\gamma(\lambda_1) = \gamma(\lambda_2)$, allowing an observer to return to their own past. The existence of CTCs signals the failure of global hyperbolicity, implying that the Cauchy problem is no longer well-posed and chronological order ceases to be globally defined. In this sense, CTCs represent the geometric manifestation of causality violation. From the effective field theory point of view, the same pathology appears dynamically through superluminal propagation, time advance, or negative Shapiro delays at the level of perturbation. These arise when higher-derivative operators or non-canonical kinetic terms deform the propagation cone of fluctuations, as defined by an effective metric $G_{\text{eff}}^{\mu\nu} = g^{\mu\nu} + \Delta^{\mu\nu}(\phi, \nabla\phi, R, \dots)$, so that null or timelike trajectories of $G_{\text{eff}}^{\mu\nu}$ may close within the physical spacetime. In scalar-tensor EFTs such as k-essence or Einstein-dilaton-Gauss-Bonnet (EdGB) gravity, these deformations are controlled by higher-derivative coefficients (α, β, \dots) that modify both the background geometry and the causal cone for perturbations. Regions of parameter space that permit closed trajectories in $G_{\text{eff}}^{\mu\nu}$ therefore correspond to low-energy violations of causality, or the onset of CTC-like behaviour. The formation of CTCs is also deeply connected to the violation of the classical energy conditions; for example, the Null Energy Condition (NEC), which can be written as $T_{\mu\nu} k^\mu k^\nu \geq 0$ for all null k^μ , ensures the focusing of null geodesics via the Raychaudhuri equation and is essential for preserving global hyperbolicity. When the NEC is violated, as is the case in certain higher-derivative or non-canonical scalar theories, the focusing theorem no longer holds (see for example [45]), allowing the light cones to tip and reconnect. By way of illustration, the Raychaudhuri equation for a null congruence with tangent k^μ reads

$$\frac{d\theta}{d\lambda} = -\frac{1}{2}\theta^2 - \sigma_{\mu\nu}\sigma^{\mu\nu} + \omega_{\mu\nu}\omega^{\mu\nu} - R_{\mu\nu}k^\mu k^\nu,$$

where $\theta = \nabla_\mu k^\mu$ is the expansion scalar and $\sigma_{\mu\nu}, \omega_{\mu\nu}$ are the shear and vorticity tensors. For hypersurface-orthogonal congruences ($\omega_{\mu\nu} = 0$) obeying the NEC, the Einstein equations imply $R_{\mu\nu}k^\mu k^\nu \geq 0$, yielding $d\theta/d\lambda \leq -\theta^2/2$, which guarantees that initially converging null rays ($\theta < 0$) focus within a finite affine parameter, maintaining causal order. However, if the NEC is violated we have $R_{\mu\nu}k^\mu k^\nu < 0$ and the inequality reverses, leading to $d\theta/d\lambda > 0$, leading to defocusing of null congruences, and local light cones then expand and may eventually overlap, creating regions where null or timelike curves close upon themselves. The surface where $g_{\varphi\varphi} = 0$ (or equivalently where $G_{\text{eff}}^{tt} = 0$) defines a *chronology horizon* [46], beyond which CTCs can form. From the ultraviolet (UV) perspective of string theory, such causality violations signal the breakdown of the low-energy EFT expansion. The full string amplitude satisfies analyticity and Regge boundedness, ensuring that all time delays remain positive [47, 48]. Apparent CTCs or superluminal propagation in truncated EFTs are thus artifacts of neglecting higher-order α' corrections. When the infinite tower of stringy states is included, these corrections restore the positivity of $R_{\mu\nu}k^\mu k^\nu$ and preserve global hyperbolicity; hence, in a UV-complete theory, causality and chronology protection should be maintained, while CTC-like behaviour in the EFT marks the boundary of EFT expansion validity.

This paper is organised as follows: in Section II, we introduce the notation and notions used in the rest of the paper by studying a rotating cylinder in vacuum; in Section II A, we show the existence of a gauge-invariant criterion for CTCs; in Section II B, we review the Horndeski action and choose two subsets to examine further; in Section III, we pick up quadratic k-essence and generate a rotating solution and provide a bound on the coupling constants from CTC avoidance; in Section IV, we do the same for the EdGB model using a different technique; in Section V we show that breaking causality can generate GW echoes in the ringdown signal, which can be used as a new observational probe; in Section VI we discuss our findings and conclude with some comments about potential future work. We use units where $c = \hbar = 1$ and the metric signature $(-+++)$ throughout the paper.

II. WARMUP AND CHOOSING THE MODEL

We begin the discussion with a simple generalisation of an infinitely long rotating cylinder in flat space. Minkowski space in cylindrical coordinates can be written as

$$ds^2 = -dt^2 + dr^2 + r^2 d\varphi^2 + dz^2, \quad (2.1)$$

which enjoys cylindrical symmetry, and where r is now the radius of the cylinder perpendicular to the axis of symmetry z . We can generalize the above to that of a spinning cylinder by introducing a $dt d\varphi$ coupling as

$$ds^2 = -dt^2 + 2\omega dt d\varphi + (r^2 - \omega^2) d\varphi^2 + dr^2 + dz^2, \quad (2.2)$$

where ω is the angular velocity. One can easily check that this is a vacuum solution of the Einstein-Hilbert action. This solution is different from that of Van Stockum or Tipler [39, 42] as these are not vacuum solutions but instead are found in the presence of dust. Here, we are interested in vacuum solutions in order to isolate the effects of the CTC, and therefore proceed with Eq. (2.2). To make the causal structure more transparent one might try to diagonalise the metric to remove the off-diagonal $dt d\varphi$ term by a corotating shift,

$$\varphi = \varphi' - \Omega(r) t, \quad \Omega(r) \equiv \frac{\omega}{r^2 - \omega^2}. \quad (2.3)$$

However, since Ω depends on r , the differential is

$$d\varphi = d\varphi' - \Omega(r) dt - t \Omega'(r) dr, \quad \Omega'(r) = -\frac{2\omega r}{(r^2 - \omega^2)^2}. \quad (2.4)$$

Substituting this into (2.2), the $dt d\varphi'$ term cancels, but one generically generates new t -dependent cross-terms. The metric becomes

$$ds^2 = -\frac{r^2}{r^2 - \omega^2} dt^2 + (r^2 - \omega^2) d\varphi'^2 - 2t(r^2 - \omega^2)\Omega'(r) d\varphi' dr + [1 + (r^2 - \omega^2)t^2\Omega'(r)^2] dr^2 + dz^2, \quad (2.5)$$

We can now use the standard criteria (see e.g [49]) for the existence of a CTC: when the angular component changes sign

$$g_{\varphi\varphi} < 0, \quad (2.6)$$

and we can see from the metric that the roles of t and φ is exchanged at this point, akin to that of a black-hole horizon. Therefore, there exists a critical angular momentum directly related to the cylinder where the angular-momentum Killing vector becomes timelike; equivalently, we may say that $r_{ctc} < |\omega|$. Around the CTC, lightcones tilt in a manner such that at every point, the curve is timelike and in the causal future of an observer sitting at that point; we depict this behaviour schematically in Figure 1.

In order to illustrate the techniques used in the rest of the paper, we add a matter sector to the above action in the form of a massless scalar field ψ and investigate its effect on the formation of the CTC by solving the backreacted solutions in a perturbative series. As such, we consider the Einstein-Hilbert action with a minimally coupled scalar as

$$S = \int d^4x \sqrt{-g} \left[\frac{R}{2\kappa} - \frac{1}{2} (\partial_\mu \psi)^2 \right], \quad (2.7)$$

where R is the curvature scalar and $\kappa \equiv 8\pi G$. We adopt cylindrical coordinates (t, r, φ, z) and choose the background

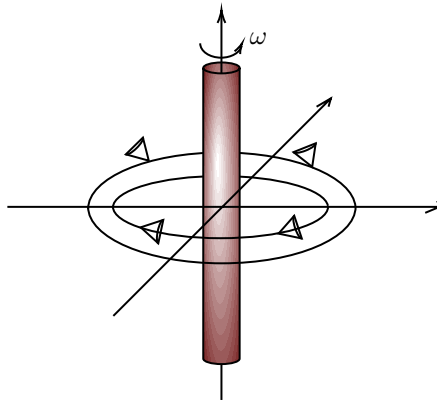


FIG. 1: Rotating cylinder and the appearance of the closed timelike curve (inner circle), represented by the tilted lightcones with the curve in its causal future.

metric⁶ in Eq. (2.2). The vacuum background satisfies $G_{\mu\nu}[g^{(0)}] = 0$, and CTCs occur where $g_{\varphi\varphi}^{(0)} = r^2 - \omega^2 < 0$, so the vacuum chronology horizon can be defined as the critical radius $r_{\text{ctc}}^{(0)} = |\omega|$.

Perturbative solution

We now compute the backreaction corrections to the background metric by the scalar field by solving the equations of motion order by order by defining

$$\psi(r) = q\tilde{\psi}(r) + \mathcal{O}(q^3), \quad g_{\mu\nu} = g_{\mu\nu}^{(0)} + \varepsilon h_{\mu\nu} + \mathcal{O}(\varepsilon^2), \quad (2.8)$$

where we have introduced a small scalar amplitude q and expanded in powers of q using the bookkeeping parameter $\varepsilon \equiv \kappa q^2$, keeping the leading backreaction terms in the metric, which enter at order q^2 . Throughout this section, we work consistently to linear order in ε and drop $\mathcal{O}(\varepsilon^2)$ terms. We choose a radial gauge $h_{rr} = 0$, after which the remaining perturbations are described by four functions of r ,

$$h_{tt} = -a(r), \quad h_{t\varphi} = \omega a(r) + b(r), \quad h_{\varphi\varphi} = c(r) - 2\omega b(r) - \omega^2 a(r), \quad h_{zz} = s(r), \quad h_{rr} = 0. \quad (2.9)$$

This ansatz may a-priori seem ad-hoc; however, it leads to a very simple set of linear differential equations controlling the backreaction and suffices to illustrate the techniques used in this paper. We refer to Appendix A for further details of calculation.

To $\mathcal{O}(\varepsilon)$, the metric reads

$$ds^2 = -[1 + \varepsilon a(r)]dt^2 + 2[\omega + \varepsilon b(r)]dt d\varphi + [r^2 - \omega^2 + \varepsilon c(r)]d\varphi^2 + dr^2 + dz^2. \quad (2.10)$$

In order to avoid divergencies on the surface of the cylinder and simultaneously model a finite-width geometry, we choose a smooth log-profile for the scalar of the form

$$\tilde{\psi}(r) = \frac{1}{2} \ln\left(\frac{r^2 + r_0^2}{r_0^2}\right), \quad r_0 > 0, \quad (2.11)$$

where r_0 is a regulator radius introduced to avoid the central singularity when integrating and is effectively the radius

⁶ We denote “background” as well as quantities evaluated on the background with a sub- or superscript “(0)”; we adopt the same convention throughout this paper, where relevant.

of the cylinder. Then, $\partial_r \psi = q r / (r^2 + r_0^2)$ and

$$(\partial\psi)^2 = q^2 \frac{r^2}{(r^2 + r_0^2)^2}. \quad (2.12)$$

For $r \gg r_0$ one has $\psi \simeq q \ln r$ as expected for a free scalar in a cylindrically symmetric exterior region. To linear order in ε the field equations read

$$\delta G_{\mu\nu}[h] = \kappa T_{\mu\nu}^{(0)}, \quad (2.13)$$

and evaluating the resulting stress tensor on the background (2.2) gives the leading $\mathcal{O}(q^2)$ components

$$\begin{aligned} T_{tt}^{(0)} &= \frac{1}{2} q^2 \frac{r^2}{(r^2 + r_0^2)^2}, & T_{t\varphi}^{(0)} &= -\frac{1}{2} \omega q^2 \frac{r^2}{(r^2 + r_0^2)^2}, & T_{\varphi\varphi}^{(0)} &= -\frac{1}{2} (r^2 - \omega^2) q^2 \frac{r^2}{(r^2 + r_0^2)^2}, \\ T_{rr}^{(0)} &= \frac{1}{2} q^2 \frac{r^2}{(r^2 + r_0^2)^2}, & T_{zz}^{(0)} &= -\frac{1}{2} q^2 \frac{r^2}{(r^2 + r_0^2)^2}. \end{aligned} \quad (2.14)$$

In the gauge (2.9) the independent radial equations reduce to

$$(tt) : \quad -\mathcal{B} = \Sigma(r), \quad (2.15)$$

$$(t\varphi) : \quad \omega \mathcal{B} - \frac{1}{2} b'' + \frac{1}{2r} b' = -\omega \Sigma(r), \quad (2.16)$$

$$(rr) : \quad \frac{1}{2r} (a' + s') = \Sigma(r), \quad (2.17)$$

$$(zz) : \quad \frac{1}{2} a'' + \frac{1}{2r} a' + \left(\frac{c''}{2r^2} - \frac{c'}{r^3} + \frac{c}{r^4} \right) = -\Sigma(r), \quad (2.18)$$

$$(\varphi\varphi) : \quad \frac{1}{2} r^2 (a'' + s'') + \omega b'' - \frac{\omega}{r} b' - \omega^2 \mathcal{B} = -(r^2 - \omega^2) \Sigma(r). \quad (2.19)$$

where we have defined

$$\mathcal{B}(r) \equiv \frac{1}{2} s'' + \frac{1}{2r} s' + \frac{c''}{2r^2} - \frac{c'}{r^3} + \frac{c}{r^4}, \quad \Sigma(r) \equiv \frac{1}{2} \frac{r^2}{(r^2 + r_0^2)^2}. \quad (2.20)$$

Using the (tt) and $(t\phi)$ equations, we get a decoupled set of equation for the $b(r)$ as

$$b'' - \frac{1}{r} b' = 0, \quad \Rightarrow \quad b(r) = B_0 + B_2 r^2, \quad (2.21)$$

and we determine the constant B_0 and B_2 by physical requirement that there is no growth in the perturbations for large r , which sets $B_2 = 0$; we keep a constant B_0 mode for the $b(r)$. we now define the new variables

$$u \equiv a + s, \quad w \equiv s - a, \quad (2.22)$$

and we have from Eq. (2.17) that

$$u'(r) = 2r \Sigma(r) \quad \Rightarrow \quad u'(r) = \frac{r^3}{(r^2 + r_0^2)^2}. \quad (2.23)$$

By subtracting Eq. (2.15) from Eq. (2.18) we obtain

$$w'' + \frac{1}{r} w' = 0, \quad (2.24)$$

and from (2.15) we find the following equation

$$\frac{c''}{2r^2} - \frac{c'}{r^3} + \frac{c}{r^4} = -\Sigma(r) - \frac{1}{2} \left(s'' + \frac{s'}{r} \right). \quad (2.25)$$

Substituting now $s = (u + w)/2$ and using $w'' + \frac{w'}{r} = 0$ gives

$$\frac{c''}{2r^2} - \frac{c'}{r^3} + \frac{c}{r^4} = -\Sigma(r) - \frac{1}{4} \left(u'' + \frac{u'}{r} \right), \quad (2.26)$$

and we use that $u' = 2r\Sigma$ and $\Sigma = \frac{1}{2} \frac{r^2}{(r^2 + r_0^2)^2}$ to finally find

$$u'' + \frac{u'}{r} = \frac{4r^2 r_0^2}{(r^2 + r_0^2)^3}. \quad (2.27)$$

Therefore the decoupled equation becomes

$$c'' - \frac{2}{r}c' + \frac{2}{r^2}c = -\frac{r^4(r^2 + 3r_0^2)}{(r^2 + r_0^2)^3}. \quad (2.28)$$

The homogeneous solutions of (A11) are $c_h = C_1 r + C_2 r^2$. Regularity at the axis sets $C_1 = 0$, and imposing the point condition $c(r_0) = 0$ to ensure that the solution does not diverge on the “surface” of the cylinder fixes C_2 and yields the final regular solution

$$c(r) = \frac{1}{2} r^2 \ln \left(\frac{2r_0^2}{r^2 + r_0^2} \right) + \frac{2 + 3\pi}{16} r^2 - \frac{3}{4} r r_0 \arctan \left(\frac{r}{r_0} \right) - \frac{r^2 r_0^2}{4(r^2 + r_0^2)}. \quad (2.29)$$

Now we turn our attention in solving the equations for $a(r)$ and $s(r)$ in terms of the difference mode $w(r) \equiv s(r) - a(r)$. One may rewrite the same relation as

$$w'' + \frac{1}{r}w' = 0, \quad w(r) \equiv s(r) - a(r), \quad (2.30)$$

which we detail in Appendix A. The general solution of Eq. (2.30) is $w(r) = W_0 \ln r + W_1$, and regularity at the axis requires no logarithmic divergence as $r \rightarrow 0$, which implies that $W_0 = 0 \Rightarrow w(r) = W_1 = \text{const}$. For the same reason, we impose

$$a(r_0) = 0, \quad s(r_0) = 0, \quad (2.31)$$

leading to $w(r_0) = s(r_0) - a(r_0) = 0$, so $W_1 = 0$ and therefore

$$s(r) = a(r). \quad (2.32)$$

We now solve the sum mode $u(r) \equiv a(r) + s(r)$. From Eq. (2.17) we find that

$$u'(r) = 2r \Sigma(r) = \frac{r^3}{(r^2 + r_0^2)^2}. \quad (2.33)$$

Integrating this equation and fixing the integration constants by using (2.31) (from which we find $u(r_0) = a(r_0) + s(r_0) = 0$), we find the solution

$$u(r) = \frac{1}{2} \left[\ln \left(\frac{r^2 + r_0^2}{2r_0^2} \right) + \frac{r_0^2}{r^2 + r_0^2} - \frac{1}{2} \right]. \quad (2.34)$$

Using (2.32) we have $u(r) = a(r) + s(r) = 2a(r) = 2s(r)$, and hence

$$a(r) = s(r) = \frac{1}{4} \left[\ln \left(\frac{r^2 + r_0^2}{2r_0^2} \right) + \frac{r_0^2}{r^2 + r_0^2} - \frac{1}{2} \right], \quad a(r_0) = s(r_0) = 0. \quad (2.35)$$

Now that we have the solution to $\mathcal{O}(\varepsilon)$, we examine the azimuthal component in order to identify the causal structure: the full azimuthal metric component is

$$g_{\varphi\varphi}(r) = r^2 - \omega^2 + \varepsilon \left(c(r) - 2\omega b(r) - \omega^2 a(r) \right), \quad (2.36)$$

and the azimuthal CTC condition therefore reads

$$r^2 - \omega^2 + \varepsilon \left(c(r) - 2\omega b(r) - \omega^2 a(r) \right) < 0. \quad (2.37)$$

We define r_{ctc} as the smallest radius where $g_{\varphi\varphi}$ vanishes as $g_{\varphi\varphi}(r_{\text{ctc}}) = 0$. Expanding about the background root $r = \omega$ using

$$r_{\text{ctc}} = \omega + \varepsilon \delta r + \mathcal{O}(\varepsilon^2), \quad (2.38)$$

and using $g_{\varphi\varphi}(\omega) = \varepsilon (c(\omega) - 2\omega b(\omega) - \omega^2 a(\omega))$ and $\partial_r(r^2 - \omega^2)|_{r=\omega} = 2\omega$ we find that

$$\delta r = - \frac{c(\omega) - 2\omega b(\omega) - \omega^2 a(\omega)}{2\omega}, \quad (2.39)$$

and to first order in ε we have

$$r_{\text{ctc}} = \omega - \varepsilon \frac{c(\omega) - 2\omega b(\omega) - \omega^2 a(\omega)}{2\omega} + \mathcal{O}(\varepsilon^2). \quad (2.40)$$

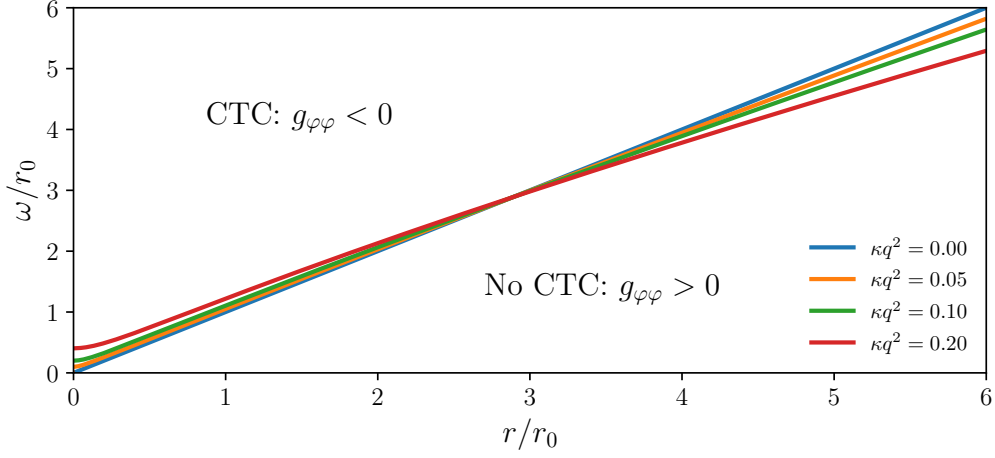
If one chooses the static branch $b(r) = B_0$ (constant), then Eq. (2.40) becomes

$$r_{\text{ctc}} = \omega - \varepsilon \frac{c(\omega) - 2\omega B_0 - \omega^2 a(\omega)}{2\omega} + \mathcal{O}(\varepsilon^2). \quad (2.41)$$

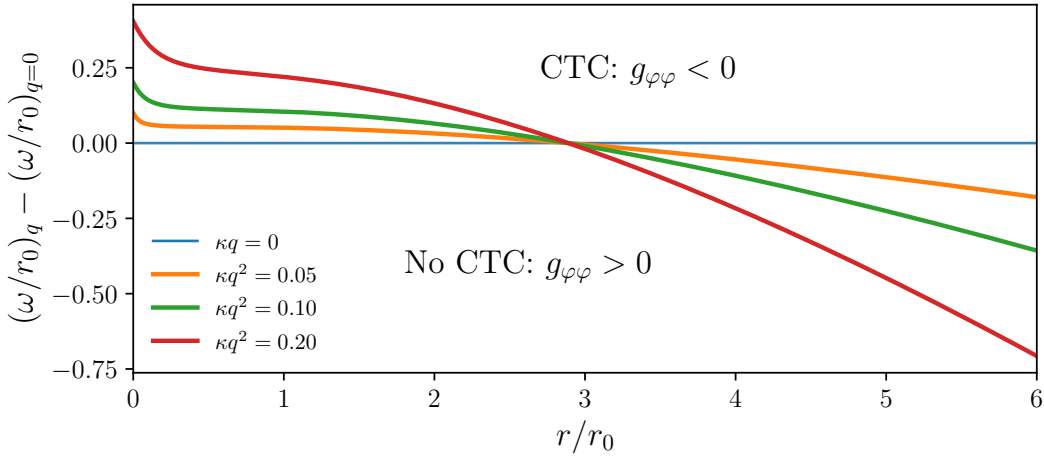
Figure 2 shows the CTC “phase diagram” in the $(r/r_0, \omega/r_0)$ plane obtained from the sign of the azimuthal metric component $g_{\varphi\varphi}$. Since azimuthal closed timelike curves correspond to closed φ -loops becoming timelike, the chronology-violating region is defined by $g_{\varphi\varphi} < 0$, while the causal region has $g_{\varphi\varphi} > 0$. The boundary $g_{\varphi\varphi} = 0$ (black curve) is the chronology horizon for azimuthal loops. In the unperturbed rotating-cylinder background one has $g_{\varphi\varphi}^{(0)} = r^2 - \omega^2$, so the chronology horizon lies on the straight line $r = \omega$. Including the scalar backreaction at $\mathcal{O}(\varepsilon)$ deforms this line through

$$g_{\varphi\varphi}(r) = r^2 - \omega^2 + \varepsilon \left(c(r) - 2\omega B_0 - \omega^2 a(r) \right), \quad (2.42)$$

where the functions $a(r)$ and $c(r)$ encode the backreacted response to the scalar stress tensor and therefore shift the radius at which the azimuthal Killing direction becomes timelike. As ε is increased the deformation becomes more pronounced, reflecting the growing influence of the scalar energy density (peaked around $r \sim r_0$) on the location of the chronology horizon. While this is a purely classical backreaction analysis, it provides a natural way to discuss Hawking’s chronology protection viewpoint: the appearance of a chronology horizon is precisely where one expects semiclassical effects, such as vacuum polarization where a large renormalized stress tensor $\langle T_{\mu\nu} \rangle_{\text{ren}}$ can become important and potentially destabilize or prevent the formation of CTCs. In this sense, our plots identify the parameter region where a semiclassical chronology-protection mechanism would be most relevant, namely near the $g_{\varphi\varphi} = 0$



(a) Sign of $g_{\varphi\varphi}$ as a function of r and ω . The coloured line denotes $g_{\varphi\varphi} = 0$. The bottom right region is causal and chronologically safe, and CTCs appear in the lower right region



(b) Deviation of $g_{\varphi\varphi}$ from the $q = 0$ case.

FIG. 2: CTC regions for an infinite rotating cylinder for different values of q . The boundary line between the regions is impacted when matter is added.

boundary where the would-be chronology horizon first develops.

In the rest of the paper, we build on this idea to investigate how chronology protection can be used as a quantitative constraint on modified gravity EFTs. In particular, we use the requirement that no physically admissible solution should develop a chronology horizon (or enter a CTC region) within the regime of validity of the effective theory to carve out the allowed parameter space. Concretely, by tracking how the would-be chronology horizon shifts under scalar–tensor backreaction and demanding the absence of azimuthal (and, where relevant, helical) CTCs outside the cutoff scale, we translate chronology-protection criteria into bounds on the associated EFT parameters and gravity couplings.

A. Gauge-Invariant Criterion for the existence of Closed Timelike Curves

To parameterize small-spin departures from the Schwarzschild geometry, we employ the Hartle–Thorne slow-rotation expansion [50], i.e. an expansion in the dimensionful spin parameter a , or equivalently in the dimensionless ratio

$\varepsilon_a \equiv a/(GM) \ll 1$.⁷ Starting from the Schwarzschild metric

$$ds^2 = -f(r) dt^2 + f(r)^{-1} dr^2 + r^2 d\Omega^2, \quad f(r) \equiv 1 - \frac{2GM}{r}, \quad (2.43)$$

one constructs a stationary, axisymmetric spacetime that reproduces the Kerr metric order-by-order in χ . Retaining terms through $\mathcal{O}(a^4)$, it is convenient to organize the result as

$$ds^2 = ds_{\text{Sch}}^2 + ds_{\text{rot}}^2 + ds_{\text{quad}}^2 + ds_{\text{hex}}^2, \quad (2.44)$$

where $ds_{\text{rot}}^2 \sim \mathcal{O}(a)$ encodes frame dragging, $ds_{\text{quad}}^2 \sim \mathcal{O}(a^2)$ captures the leading even-parity ($\ell = 2$) deformation, and $ds_{\text{hex}}^2 \sim \mathcal{O}(a^4)$ contains the next even-parity corrections (including $\ell = 0, 2, 4$ pieces). The angular dependence in the even-parity sector is naturally expanded in Legendre polynomials $P_2(\cos\theta)$ and $P_4(\cos\theta)$, with corresponding radial coefficient functions (see [50]).

A necessary condition for *azimuthal* closed timelike curves (CTCs)—closed loops along the integral curves of the azimuthal Killing vector $\xi_{(\varphi)} \equiv \partial_\varphi$ at fixed t, r, θ —is that the azimuthal direction become timelike,

$$g_{\varphi\varphi}(r, \theta) < 0. \quad (2.45)$$

In the slow-rotation expansion, the azimuthal metric component can be written through $\mathcal{O}(a^4)$ as

$$g_{\varphi\varphi}(r, \theta) = r^2 \sin^2 \theta \left[1 + \frac{2a^2}{r^2} f_2(r) P_2(\cos\theta) + \frac{a^4}{r^4} f_4(r, \theta) \right] + \mathcal{O}(a^6), \quad (2.46)$$

where $f_2(r)$ is the standard $\mathcal{O}(a^2)$ Hartle–Thorne even-parity radial coefficient multiplying the $\ell = 2$ mode, and $f_4(r, \theta)$ collects the $\ell = 0, 2, 4$ contributions at $\mathcal{O}(a^4)$. For the Kerr-matched Hartle–Thorne exterior one may take

$$f_2(r) = 1 + \frac{2GM}{r} + \frac{18G^2M^2}{5r^2}, \quad f_4(r, \theta) = C_1(r) + C_2(r)P_2(\cos\theta) + C_3(r)P_4(\cos\theta), \quad (2.47)$$

with $C_i(r)$ given in standard references [50]. The key point is that Hartle–Thorne is an *exterior* slow-rotation expansion, controlled only when $|a|/r \ll 1$ (and hence $\varepsilon_a \ll 1$) so that each successive order in a is parametrically smaller. In this regime, the bracket multiplying $r^2 \sin^2 \theta$ remains a perturbative deformation of unity, and $g_{\varphi\varphi}$ stays positive throughout the exterior, so azimuthal CTCs are absent. If, however, one extrapolates the $\mathcal{O}(a^4)$ -truncated expression into a region where $|a|/r \not\ll 1$ (for instance deep in the interior where the exterior expansion is not applicable), the formally higher-order $\mathcal{O}(a^4)$ term can dominate the truncated series and may spuriously drive $g_{\varphi\varphi}$ negative. Such sign changes should therefore be interpreted as an indicator that the slow-rotation truncation is being used outside its domain of validity, rather than as a physical prediction. It is nevertheless useful as a diagnostic to see how a sign change could arise within the truncated series. From the above expression, the condition $g_{\varphi\varphi} < 0$ implies

$$f_4(r, \theta) < -\frac{r^4}{a^4} \left[r^2 + 2a^2 f_2(r) P_2(\cos\theta) \right], \quad (2.48)$$

i.e. the $\mathcal{O}(a^4)$ sector must be sufficiently negative to overwhelm the leading positive term in the square bracket. Restricting to the equatorial plane $\theta = \pi/2$, where $\sin^2 \theta$ is maximal and frame dragging effects are strongest, one has $P_2(0) = -1/2$ and $P_4(0) = 3/8$, so that

$$f_4(r, \pi/2) = C_1(r) - \frac{1}{2}C_2(r) + \frac{3}{8}C_3(r), \quad (2.49)$$

⁷ In the literature, χ is often used to denote ε_a .

and Eq. (2.48) becomes an inequality for this particular linear combination of the $C_i(r)$. Solving it within the $\mathcal{O}(a^4)$ truncation defines a *formal* “CTC radius” r_{ctc} , and dimensional analysis then implies the scaling

$$\frac{r_{\text{ctc}}}{GM} \approx \alpha \varepsilon_a^2 + \mathcal{O}(\varepsilon_a^3), \quad (2.50)$$

where α is a numerical coefficient determined by the explicit Hartle–Thorne functions $C_i(r)$. We emphasize that any positive- r solution for r_{ctc} obtained in this manner arises precisely where the exterior slow-rotation truncation ceases to be controlled, and should therefore be viewed as a truncation artifact rather than a physical CTC prediction for the Kerr exterior.⁸ For comparison, in the exact Kerr spacetime the inner horizon lies at

$$r_- = GM - \sqrt{(GM)^2 - a^2}, \quad (2.51)$$

and azimuthal CTCs occur only in the maximal analytic extension, confined to the negative- r region behind the inner horizon. Thus, any positive- r CTCs encountered in the truncated Hartle–Thorne series do not reflect the causal structure of the exact Kerr exterior.

In the remainder of this paper we derive CTC existence criteria using expressions that are exact in a , and only at the final stage, when analytic intuition is useful, do we expand in ε_a . In doing so, it is essential to account for the residual gauge freedom of the slow-rotation ansatz: matching a perturbative Kerr form to the exact geometry requires the fixing of this freedom, conveniently implemented as a radial redefinition (a “radial shift”). After this gauge choice, the CTC existence criterion can be expressed in a manifestly gauge-invariant form; details are provided in Appendix B. As a starting point, we have that stationary and axisymmetric spacetimes admit two commuting Killing vector fields

$$\xi_{(t)}^\mu = (\partial_t)^\mu, \quad \xi_{(\varphi)}^\mu = (\partial_\varphi)^\mu, \quad (2.52)$$

associated with time translation and axial rotation, respectively. The integral curves of $\xi_{(\varphi)}^\mu$ are closed curves, and thus a necessary (but as we shall see, *not* sufficient) condition for the absence of CTCs is that these orbits remain spacelike. A naive test based solely on $g_{\varphi\varphi} > 0$ is commonly used when the coordinates are already in Boyer–Lindquist (BL) form, since in that gauge $\xi_{(\varphi)}^\mu$ is orthogonal to the (r, θ) surfaces; however, in more general gauges, including the Hartle–Thorne slow-rotation coordinates, the metric components do not guarantee that the coordinate basis vector ∂_φ is aligned with the axial Killing direction in a way that preserves length comparison under coordinate transformations. Therefore, the sign of $g_{\varphi\varphi}$ alone is *not* a gauge-invariant diagnostic of CTC formation; instead, a fully invariant criterion can be obtained by restricting the metric to the two-dimensional space of Killing orbits spanned by $\{\xi_{(t)}, \xi_{(\varphi)}\}$ [51, 52]. The induced metric on this subspace is

$$g_{AB} \equiv \begin{pmatrix} g_{tt} & g_{t\varphi} \\ g_{t\varphi} & g_{\varphi\varphi} \end{pmatrix}, \quad A, B \in \{t, \varphi\}. \quad (2.53)$$

Physically, the orbits of the Killing group must possess one timelike and one spacelike direction for the spacetime to have Lorentzian signature and free of causal pathologies in the t - φ sector: this requirement is equivalent to the following pair of inequalities:

$$g_{\varphi\varphi} > 0, \quad \det(g_{AB}) = g_{tt}g_{\varphi\varphi} - g_{t\varphi}^2 < 0, \quad (2.54)$$

which when taken together ensure that the axial Killing vector has positive norm (i.e. that it is spacelike) and that

⁸ Defining the CTC limit in the equatorial plane is a conservative diagnostic: since $\sin^2 \theta$ is maximal there, the truncated criterion is most easily violated.

the t - φ subspace has Lorentzian signature [53, 54]. Importantly, both expressions in Eq. (2.54) are invariant under all coordinate transformations that do *not* mix the axial Killing direction with time, i.e. under $(t, r, \theta) \rightarrow (t', r', \theta')$ with φ fixed. This covers Hartle–Thorne gauges, quasi-isotropic gauges, and horizon-regular ingoing gauges [51]. Thus, the gauge-invariant statement of “no CTCs” is:

$$\text{No CTCs} \iff g_{\varphi\varphi} > 0 \text{ and } g_{tt}g_{\varphi\varphi} - g_{t\varphi}^2 < 0 \quad \text{everywhere for } r \geq r_+,$$

where r_+ is the outer horizon. By contrast, a test using only $g_{\varphi\varphi} > 0$ without imposing Boyer-Lindquist (or areal) gauge can produce spurious “CTC regions” that arise solely from coordinate distortions, particularly in slow-rotation Hartle-Thorne metrics where the $l = 2$ radial perturbation has not been gauge-fixed.

B. Choosing the model

Horndeski theory [35] is the most general scalar-tensor theory which produces second-order equations of motion without imposing degeneracy conditions, and has been the subject of a great deal of study; for example, see [55] for a review. The full Horndeski Lagrangian reads

$$\begin{aligned} \mathcal{L} = \sqrt{-g} & \left[G_2(\phi, X) - G_3(\phi, X)\square\phi + G_4(\phi, X)R + G_{4X}[(\square\phi)^2 - \phi^{\mu\nu}\phi_{\mu\nu}] \right. \\ & \left. + G_5(\phi, X)G^{\mu\nu}\phi_{\mu\nu} - \frac{1}{6}G_{5,X}[(\square\phi)^3 - 3\square\phi\phi^{\mu\nu}\phi_{\mu\nu} + 2\phi_{\mu\nu}\phi^{\nu\lambda}\phi_\lambda^\mu] \right], \end{aligned} \quad (2.55)$$

where $\{G_2, G_3, G_4, G_5\}$ are arbitrary functions of ϕ and X , $\phi_{\mu_1\dots\mu_n} \equiv \nabla_{\mu_1}\dots\nabla_{\mu_n}\phi$, $X \equiv -g^{\mu\nu}\phi_\mu\phi_\nu/2$. In this paper, we focus on two interesting subsets of the above Horndeski action, namely Einstein-Scalar-Gauss-Bonnet gravity [30, 56] (EdGB) and k-essence theory [55, 57]. The Gauss-Bonnet term reads

$$\mathcal{G} = R^2 - 4R_{\mu\nu}R^{\mu\nu} + R_{\mu\nu\alpha\beta}R^{\mu\nu\alpha\beta}, \quad (2.56)$$

and since it is topological in $D = 4$ spacetime dimensions, we introduce the non-minimal coupling $f(\phi)\mathcal{G}$. Using this, one can obtain the EdGB Lagrangian from Eq. (2.55) by choosing (see [55, 58])

$$\begin{aligned} G_2 &= 8f^{(4)}X^2(3 - \ln X), \quad G_3 = 4f^{(3)}X(7 - 3\ln X), \\ G_4 &= 4f^{(2)}X(2 - \ln X), \quad G_5 = -4f^{(1)}\ln X, \end{aligned} \quad (2.57)$$

where the linear X term in G_2 accounts for the scalar-field kinetic term. It is known [55, 58] that the above subset reproduces the Gauss-Bonnet term. In order to capture the Einstein-Hilbert and scalar-field kinetic term pieces, we perform the following redefinition

$$G_2 \rightarrow G_2 + \beta X, \quad G_4 \rightarrow G_4 + \frac{1}{2\kappa}, \quad (2.58)$$

where $\kappa \equiv 8\pi G$. We specify the non-minimal coupling function as $f(\phi) = \alpha e^\vartheta$, with $\alpha = \text{const}$ and write the Lagrangian in the following simple form

$$\mathcal{L}_{\text{EdGB}} = \sqrt{-g} \left[\frac{R}{2\kappa} + \alpha e^\vartheta \mathcal{G} - \frac{\beta}{2} \partial_\mu \vartheta \partial^\mu \vartheta \right], \quad (2.59)$$

where we make the non-canonical choice to keep ϑ dimensionless in order to avoid introducing an extra parameter in the exponential coupling function. As such, we have that α is also dimensionless and that $[\beta] = M^2$, so we can write

it in terms of a dimensionless variable $\tilde{\beta}$ as

$$\text{For EdGB: } \beta \equiv \tilde{\beta} M_*^2, \quad (2.60)$$

where M_* is a mass scale which is not necessarily equal to the mass of the black hole.

We find the equations of motion for the inverse metric $g^{\mu\nu}$ and scalar field ϑ as

$$\frac{1}{\kappa} G_{\mu\nu} + \alpha e^{\vartheta} D(\vartheta)_{\mu\nu} - \frac{1}{2} T_{\mu\nu}^{(\vartheta)} = 0, \quad \square\vartheta + \frac{\alpha}{\beta} e^{\vartheta} \mathcal{G} = 0, \quad (2.61)$$

where the Gauss-Bonnet contribution $D(\vartheta)_{\mu\nu}$ and stress-energy tensor $T_{\mu\nu}^{\vartheta}$ are defined as

$$\begin{aligned} D(\vartheta)_{\mu\nu} = & 2R\nabla_{\mu}\nabla_{\nu}\vartheta - 2(g_{\mu\nu}R - 2R_{\mu\nu})\nabla_{\lambda}\nabla^{\lambda}\vartheta + 8R_{\lambda(\mu}\nabla^{\lambda}\nabla_{\nu)}\vartheta \\ & - 4g_{\mu\nu}R^{\lambda\rho}\nabla_{\lambda}\nabla_{\rho}\vartheta + 2R_{\mu\lambda\nu\rho}\nabla^{\lambda}\nabla^{\rho}\vartheta, \\ T_{\mu\nu}^{\vartheta} = & \beta \left(\nabla_{\mu}\vartheta\nabla_{\nu}\vartheta - \frac{1}{2}g_{\mu\nu}\nabla_{\lambda}\nabla^{\lambda}\vartheta \right), \end{aligned} \quad (2.62)$$

which we study further in Section IV.

III. K-ESSENCE MODEL

Another interesting subset is that of k-essence [57], the Lagrange density of which reads

$$\mathcal{L}_{\text{k-ess}} = \sqrt{-g} \left[\frac{R}{2\kappa} + P(X) \right], \quad (3.1)$$

from which we obtain the equations of motion for the inverse metric and scalar field as

$$G_{\mu\nu} - \frac{1}{2\kappa} g_{\mu\nu} P(X) - \frac{1}{2\kappa} \partial_{\mu}\phi\partial_{\nu}\phi P'(X) = 0, \quad \square\phi - \frac{P''(X)}{P'(X)} \partial^{\mu}\phi\partial^{\nu}\phi\partial_{\mu}\partial_{\nu}\phi = 0. \quad (3.2)$$

For the k-essence model defined by the action (3.1) and the field equations (3.2), we pick up the quadratic case which constitutes choosing the function $P(X)$ as

$$P(X) \equiv \alpha X + \beta X^2, \quad (3.3)$$

where α and β are constants. In these units, α is dimensionless and $[\beta] = M^{-4}$, which we note is different from our choice in the EdGB model in Section IV. In order to express β in terms of a dimensionless variable $\tilde{\beta}$ we define

$$\text{For k-essence: } \beta \equiv \frac{\tilde{\beta}}{M_*^4}, \quad (3.4)$$

where the mass scale M_* is not necessarily that of the black hole. In the rest of our treatment of k-essence, we express β in terms of $\tilde{\beta}$ when convenient.

For the choice of scalar sector (3.3), we can write the equations of motion in the following convenient form

$$G_{\mu\nu} = \kappa T_{\mu\nu}, \quad T_{\mu\nu} \equiv P_X \partial_{\mu}\phi\partial_{\nu}\phi + g_{\mu\nu} P(X), \quad \nabla_{\mu} (P_X \nabla^{\mu}\phi) = 0, \quad (3.5)$$

where we have defined $P_X \equiv \partial P / \partial X = \alpha + 2\beta X$. The limit $P_X \rightarrow 0$ implies that $X = -\alpha/2\beta$ and reduces the first equation in (3.5) to that of GR in vacuum. Black holes typically obey “no-hair” theorems [59, 60] unless one allows

time-dependence of the scalar field, and the simplest stationary configuration consistent with the symmetries of the Kerr geometry is a shift-symmetric profile of the form

$$\phi(t, r) = \phi_*(t, r) + \delta\phi(t, r, \theta), \quad \phi_*(t, r) = \phi_0(r) + qt, \quad (3.6)$$

where $\delta\phi(t, r, \theta)$ contains $\mathcal{O}(q^2)$ corrections; q is a dimension-2 constant which we call the charge parameter. Since the energy-momentum tensor only depends on derivatives of ϕ , the metric remains stationary and axisymmetric even though ϕ itself has a time-dependent profile. With the spatial background Our choice of $P(X)$ in Eq. (3.3) admits two branches of stationary solutions:

- a zero-charge branch, where $X = X_* = -\alpha/(2\beta)$ and the stress tensor is proportional to $g_{\mu\nu}$, producing Kerr-(A)dS geometry without additional momentum flow;
- a nonzero-charge branch, where $\partial_t\phi = q \neq 0$ produces a finite energy and momentum density.

In the zero-charge case, we have that X is negative outside the horizon, which can be avoided by requiring $\alpha/\beta > 0$ to be satisfied. The other case can also be considered by introducing a field configuration where $\partial_t\phi$ is included in P_X already at the background level.

Although the k-essence α term is marginal, the β term is suppressed by some new mass scale and we can view it as an EFT correction; as such, we need to take care to work in the regime of EFT validity. A sufficient condition is that the horizon length scale of the black hole (which constitutes the background geometry) is parametrically larger than the cutoff length $\ell_* \sim M_*^{-1}$

$$GM \gg \frac{1}{M_*}, \quad (3.7)$$

restricting our choice of EFT cutoff scale. Assuming now a small charge parameter, we expand ϕ as

$$\phi(t, r, \theta) = \phi_0(r) + qt + \varepsilon_q^2 \left[\Phi_0(r) + \Phi_2(r)P_2(\cos\theta) \right] + \mathcal{O}(q^3), \quad (3.8)$$

where the small-charge expansion is controlled by the geometrically defined

$$\varepsilon_q \equiv q(GM)^2 \quad (3.9)$$

which controls the small backreaction by the matter sector. Independently of the definition (3.9) which encodes the geometry, we also ensure control of the EFT by imposing that

$$q \ll M_*^2, \quad (3.10)$$

which naturally mixes all mass scales in the system when expressed as

$$\varepsilon_q \ll \frac{1}{8\pi} \left(\frac{MM_*}{M_{\text{Pl}}^2} \right)^2, \quad (3.11)$$

where we have used that $G = (8\pi M_{\text{Pl}}^2)^{-1}$. Since $M_*/M_{\text{Pl}} < 1$, this EFT constraint is easily satisfied.

With the ansatz in Eq. (3.8), the derivatives of ϕ in four dimensions are

$$\partial_t\phi = q + \mathcal{O}(q^2), \quad (3.12)$$

$$\partial_r\phi = \phi'_0(r) + \varepsilon_q^2 \left[\Phi'_0(r) + \Phi'_2(r)P_2(\cos\theta) \right] + \mathcal{O}(q^3), \quad (3.13)$$

$$\begin{aligned} \partial_\theta\phi &= q^2 \Phi_2(r) \partial_\theta P_2(\cos\theta) + \mathcal{O}(q^3) \\ &= -3q^2 \Phi_2(r) \cos\theta \sin\theta + \mathcal{O}(q^3), \end{aligned} \quad (3.14)$$

where we used $P_2(\cos\theta) = (3\cos^2\theta - 1)/2$ and $\partial_\theta P_2(\cos\theta) = -3\cos\theta\sin\theta$. Thus the only *leading* charge dependence in the derivatives appears through the constant time derivative $\partial_t\phi = q + \dots$, and the radial and angular charge contributions start at $\mathcal{O}(q^2)$. Since the stress-energy tensor (3.5) only depends on derivatives of ϕ , the charge-induced contribution scales parametrically as $T_{\mu\nu}^{(\text{charge})} \sim q^2$. For $\varepsilon_q^2 \ll 1$ this is small compared with the curvature scale of the Kerr-(A)dS background, where the Kretschmann scalar scales as $R_{\mu\nu\rho\sigma}R^{\mu\nu\rho\sigma} \sim 1/M^4$. The momentum density carried by the scalar is thus perturbative, and the geometry deviates from Kerr-(A)dS only by small $\mathcal{O}(q^2)$ corrections. Furthermore, the configuration remains stationary and axisymmetric; indeed, the charge contribution is linear in t but constant in time derivatives,

$$\partial_t\phi = q = \text{constant}, \quad \partial_\varphi\phi = 0, \quad (3.15)$$

so that the stress-energy tensor is invariant under the background Killing vectors

$$\mathcal{L}_{\xi_t}T_{\mu\nu} = 0, \quad \mathcal{L}_{\xi_\varphi}T_{\mu\nu} = 0, \quad \xi_t = \partial_t, \quad \xi_\varphi = \partial_\varphi, \quad (3.16)$$

and the full solution therefore remains stationary and axisymmetric. We are therefore free to proceed with the Hartle-Thorne slow-rotation formalism. In four dimensions, the rotation parameter a has dimensions of inverse mass, so the dimensionless spin appropriate for a slow-rotation approximation is

$$\varepsilon_a \equiv \frac{a}{GM}, \quad (3.17)$$

and in the Hartle-Thorne regime one expands in powers of ε_a^2 . Since both the charge and slow-rotation corrections enter at quadratic order in their respective small parameters, the metric can be written as a double expansion

$$g_{\mu\nu} = g_{\mu\nu}^{(0)} + \varepsilon_a^2 g_{\mu\nu}^{(a^2)} + \varepsilon_q^2 g_{\mu\nu}^{(q^2)} + \mathcal{O}(\varepsilon_a^4, \varepsilon_q^4, \varepsilon_a^2\varepsilon_q^2), \quad (3.18)$$

where $g_{\mu\nu}^{(0)}$ is the Kerr-(A)dS background in Boyer-Lindquist-type coordinates. The tensor $g_{\mu\nu}^{(a^2)}$ denotes the standard vacuum Hartle-Thorne correction at order a^2 , while $g_{\mu\nu}^{(q^2)}$ is the charge-induced correction at order q^2 . At order ε_a^2 order, the perturbations obey

$$\delta G_{\mu\nu}[g^{(a^2)}] + \Lambda_{\text{eff}} g_{\mu\nu}^{(a^2)} = 0, \quad (3.19)$$

where $\delta G_{\mu\nu}$ is the linearised Einstein tensor evaluated on the Kerr-(A)dS background, and Λ_{eff} is the effective cosmological constant arising from the zero-charge k-essence sector. At $\mathcal{O}(\varepsilon_q^2)$ the charge-corrected perturbations satisfy the equations of motion (3.2) at the same order

$$\delta G_{\mu\nu}[g^{(q^2)}] + \Lambda_{\text{eff}} g_{\mu\nu}^{(q^2)} = T_{\mu\nu}^{(q^2)}[\phi_0, q], \quad (3.20)$$

with the same linear differential operator on the left-hand side. This is because the k-essence stress-energy tensor is already quadratic in q , so the metric correction enters only linearly at this order, and no new derivatives appear in the Einstein tensor at $\mathcal{O}(q^2)$ beyond those already present in the vacuum Hartle-Thorne sector. Therefore the $\mathcal{O}(q^2)$ problem is a sourced version of the vacuum Hartle-Thorne equations, with the source determined by the non-zero charge. After spherical-harmonic decomposition into monopole ($\ell = 0$) and quadrupole ($\ell = 2$) multipoles, the Einstein and scalar equations at $\mathcal{O}(\varepsilon_a^2)$ and $\mathcal{O}(\varepsilon_q^2)$ reduce to linear elliptic equations in the radial coordinate. For the monopole ($\ell = 0$) one obtains linear first-order ODEs for $m_0(r)$ and $h_0(r)$, and a linear second-order elliptic ODE for the scalar monopole $\Phi_0(r)$. Conversely, for the quadrupole ($\ell = 2$) part, the metric perturbations can be combined into a function $H_2(r)$ obeying a second-order linear elliptic ODE, while the quadrupole scalar $\Phi_2(r)$ satisfies an ODE

of the same type. Schematically, all these equations take the form

$$\mathcal{F}[f(r)] = S(r), \quad (3.21)$$

where \mathcal{F} is the Hartle–Thorne radial operator (a Fuchsian ODE with three regular singular points for Kerr-(A)dS), and $S(r)$ is a source determined by the zero-charge background and the charge parameter q . Since \mathcal{F} does not mix ε_a and ε_q at this order, there are no cross-couplings at $\mathcal{O}(\varepsilon_a^2 \varepsilon_q^2)$.

A. Zero-charge branch

It is particularly illuminating to study the zero-charge branch of quadratic k-essence, i.e. the case where q in Eq. (3.6) vanishes. In this case, the scalar equation of motion is

$$\nabla_\mu (P_X \nabla^\mu \phi) = 0, \quad (3.22)$$

so the zero-charge condition implies that $P_X(X_\star) = 0$ where X_\star denotes the kinetic term evaluated on this branch. For the quadratic model $P(X) = \alpha X + \beta X^2$, this yields

$$P_X = \alpha + 2\beta X = 0 \quad \Rightarrow \quad X_\star = -\frac{\alpha}{2\beta}. \quad (3.23)$$

Even though perturbations are strongly coupled in this limit, it is instructive to examine its consequence thanks to its relative simplicity. The k-essence function and the stress-energy tensor are now constants and read $P(X_\star) = -\alpha^2/4\beta$, $T_{\mu\nu}^{(0)} = P(X_\star) g_{\mu\nu}^{(0)}$, and the Einstein equations reduce to the Kerr-(A)dS equation with an effective cosmological constant determined by the k-essence couplings

$$G_{\mu\nu}[g^{(0)}] + \Lambda_{\text{eff}} g_{\mu\nu}^{(0)} = 0, \quad \Lambda_{\text{eff}} = \frac{\kappa\alpha^2}{4\beta}, \quad (3.24)$$

where the effective cosmological constant can equivalently be expressed in terms of dimensionless variables as $\Lambda_{\text{eff}} = 2\pi G M_\star^4 \alpha^2 / \tilde{\beta}$. Any Kerr-(A)dS solution with cosmological constant Λ_{eff} is an exact solution of the zero-charge branch. Starting from the Kerr-AdS metric in Boyer-Lindquist coordinates

$$ds^2 = -\frac{\Delta_r}{\rho^2} \left(dt - \frac{a \sin^2 \theta}{\Xi} d\varphi \right)^2 + \frac{\rho^2}{\Delta_r} dr^2 + \frac{\rho^2}{\Delta_\theta} d\theta^2 + \frac{\Delta_\theta \sin^2 \theta}{\rho^2} \left(a dt - \frac{r^2 + a^2}{\Xi} d\varphi \right)^2 \quad (3.25)$$

where

$$\begin{aligned} \rho^2 &\equiv r^2 + a^2 \cos^2 \theta, & \Xi &\equiv 1 + \frac{\Lambda_{\text{eff}}}{3} a^2, \\ \Delta_r &\equiv (r^2 + a^2) \left(1 - \frac{\Lambda_{\text{eff}}}{3} r^2 \right) - 2GM r, & \Delta_\theta &\equiv 1 + \frac{\Lambda_{\text{eff}}}{3} a^2 \cos^2 \theta, \end{aligned} \quad (3.26)$$

we have that to first order in the slow-rotation parameter a , the metric takes Hartle-Thorne form

$$ds^2 = -N^2(r) dt^2 + \frac{dr^2}{N^2(r)} + r^2 d\Omega^2 - 2\omega(r) r^2 \sin^2 \theta dt d\varphi + \mathcal{O}(a^2), \quad (3.27)$$

with the metric functions determined as

$$N^2(r) = 1 - \frac{2GM}{r} - \frac{\Lambda_{\text{eff}}}{3} r^2, \quad \omega(r) = \frac{2aGM}{r^3} + \mathcal{O}(a^3). \quad (3.28)$$

From the solution, we demand stationarity and axisymmetry, and so we adopt the ansatz $\phi_0(r, \theta) = S_r(r) + S_\theta(\theta)$, after which the kinetic term can be written as

$$X(r, \theta) = -\frac{1}{2}[g^{rr}(S'_r)^2 + g^{\theta\theta}(S'_\theta)^2] = X_\star. \quad (3.29)$$

Using now that $g^{rr} = N^2(r)$ and $g^{\theta\theta} = 1/r^2$, the zero-charge condition becomes

$$N^2(r) [S'_r(r)]^2 + \frac{1}{r^2} [S'_\theta(\theta)]^2 = -2X_\star = \frac{\alpha}{\beta}. \quad (3.30)$$

Furthermore, it is convenient to define $C \equiv \alpha/\beta$, $X_\star = -C/2$, and we can separate these variables by introducing a constant $K \geq 0$, after which the radial and angular dependence decouples

$$[S'_\theta(\theta)]^2 = K, \quad N^2(r) [S'_r(r)]^2 = C - \frac{K}{r^2}. \quad (3.31)$$

By considering $K = 0$, we achieve the minimal-separation case with trivial angular sector $S_\theta(\theta) = \text{const.}$, and the radial equation integrates to give the radial profile of the form

$$S_r(r) = \pm\sqrt{C} \int^r \frac{dr'}{N(r')}. \quad (3.32)$$

With a non-zero effective cosmological constant,

$$\Delta_0(r) \equiv r^2 N^2(r) = r^2 - 2GMr - \frac{\Lambda_{\text{eff}}}{3} r^4, \quad (3.33)$$

the zero-charge solution takes the exact form

$$S_r(r) = \pm\sqrt{C} \int^r \frac{r'}{\sqrt{\Delta_0(r')}} dr'. \quad (3.34)$$

Since $\Delta_0(r)$ is a quartic polynomial with (in general) three real roots (inner, outer, cosmological), the integral can be expressed in terms of standard incomplete elliptic integrals. Thus $S_r(r)$ is known exactly, in elementary form for $\Lambda_{\text{eff}} = 0$ and in terms of elliptic functions for $\Lambda_{\text{eff}} \neq 0$. We note that the GR limit can still be accessed inside the zero-charge branch by taking $\Lambda_{\text{eff}} \rightarrow 0$, which is equivalent to taking $\alpha^2/\beta \rightarrow 0$. Then, by taking β to be finite, we obtain $\phi = \text{const.}$ and $T_{\mu\nu} = 0$, which is nothing but the Kerr solution under GR.

B. Nonzero-flux branch

We now deform the $P_X(X_\star) = 0$ (vacuum-energy) branch by turning on a small time-gradient and by allowing the kinetic term to depart from X_\star at order ε_q^2 . We use the shift-symmetric ansatz defined in Eq. (3.6) and we organise the expansion in the dimensionless parameter ε_q . We note now that a purely spatial background gradient (e.g. $\phi_0 = \phi_0(r, \theta)$ and $q = 0$) gives $X \leq 0$ outside the horizon. Therefore, a real $q = 0$ realization of $P_X(X_\star) = 0$ requires

$$X_\star = -\frac{\alpha}{2\beta} < 0 \quad \iff \quad \alpha/\beta > 0. \quad (3.35)$$

If instead we wish to consider $\alpha\beta < 0$ (so that $X_\star > 0$), then the *zeroth-order* $P_X = 0$ configuration must include a timelike component in $\partial_\mu\phi$ at the background level, so that X_\star can be positive. The perturbation theory below is written in a way that is consistent in both cases: the expansion parameter is the deviation of X away from X_\star at

order ε_q^2 .

We use the Hartle–Thorne expansion up to $\mathcal{O}(\varepsilon_a^2)$,

$$ds^2 = -N^2(r) e^{2\delta(r)} \left[1 + \varepsilon_a^2 h_2(r) P_2(\cos \theta) \right] dt^2 + \frac{dr^2}{N^2(r)} \left[1 + \varepsilon_a^2 m_2(r) P_2(\cos \theta) \right] \\ + r^2 \left[1 + \varepsilon_a^2 k_2(r) P_2(\cos \theta) \right] \left(d\theta^2 + \sin^2 \theta d\varphi^2 \right) - 2\omega(r) r^2 \sin^2 \theta dt d\varphi + \mathcal{O}(\varepsilon_a^3), \quad (3.36)$$

with lapse (fixed by the $P(X_*)$ vacuum energy) defined as in Eq. (3.28). At $\varepsilon_q = 0$ we recover the vacuum Kerr–(A)dS slow-rotation functions as $\delta = 0$, $\omega = \omega_{\text{vac}}$, and $(h_2, k_2, m_2) = (h_2^{\text{vac}}, k_2^{\text{vac}}, m_2^{\text{vac}})$. The off-diagonal component is $g_{t\phi} = -\omega(r) r^2 \sin^2 \theta$. We decompose $\omega(r) = \omega_{\text{vac}}(r) + \varepsilon_q^2 \omega_2(r) + \dots$, where ω_2 is fixed by the (t, φ) Einstein equation at $\mathcal{O}(\varepsilon_a \varepsilon_q^2)$.

Even- ε_q expansion

We expand all backreaction quantities in even powers of ε_q

$$\phi(t, r, \theta) = \phi_0(r, \theta) + qt + \varepsilon_q^2 \left[\Phi_0(r) + \Phi_2(r) P_2(\cos \theta) \right] + \mathcal{O}(\varepsilon_q^4), \quad (3.37)$$

$$\delta(r) = \varepsilon_q^2 \delta_2(r) + \mathcal{O}(\varepsilon_q^4), \quad \omega(r) = \omega_{\text{vac}}(r) + \varepsilon_q^2 \omega_2(r) + \mathcal{O}(\varepsilon_q^4), \quad (3.38)$$

$$h_2(r) = h_2^{\text{vac}}(r) + \varepsilon_q^2 H_2(r) + \mathcal{O}(\varepsilon_q^4), \quad k_2(r) = k_2^{\text{vac}}(r) + \varepsilon_q^2 K_2(r) + \mathcal{O}(\varepsilon_q^4), \quad (3.39)$$

and we use the Hartle–Thorne-compatible gauge choice

$$m_2(r) = m_2^{\text{vac}}(r) - \varepsilon_q^2 H_2(r) + \mathcal{O}(\varepsilon_q^4). \quad (3.40)$$

Further, we expand the kinetic term around the zero-charge limit X_* as

$$X(r, \theta) = X_* + \varepsilon_q^2 \left[X_{2,0}(r) + X_{2,2}(r) P_2(\cos \theta) \right] + \mathcal{O}(\varepsilon_q^4), \quad (3.41)$$

and since we have $P_X = \alpha + 2\beta X$ and $P_{XX} = 2\beta$, and since $P_X(X_*) = 0$ we have

$$P(X) = P(X_*) + \mathcal{O}(\varepsilon_q^4), \quad (3.42)$$

$$P_X(X) = 2\beta \varepsilon_q^2 \left[X_{2,0}(r) + X_{2,2}(r) P_2(\cos \theta) \right] + \mathcal{O}(\varepsilon_q^4). \quad (3.43)$$

Substituting this into the expression for the stress-energy tensor $T_{\mu\nu} = P_X \partial_\mu \phi \partial_\nu \phi + P g_{\mu\nu}$ we get

$$T_{\mu\nu} = \underbrace{P(X_*) g_{\mu\nu}}_{\text{vacuum energy } (\Lambda_{\text{eff}})} + \underbrace{2\beta \varepsilon_q^2 \left[X_{2,0} + X_{2,2} P_2 \right] \partial_\mu \phi_* \partial_\nu \phi_*}_{\text{leading nonzero-flux source}} + \mathcal{O}(\varepsilon_q^4). \quad (3.44)$$

At this order it is sufficient to evaluate $\partial_\mu \phi$ using the zeroth-order expression $\phi_* = \phi_0 + qt$ since any addition of Φ_0, Φ_2 into $\partial_\mu \phi \partial_\nu \phi$ produces terms of $\mathcal{O}(\varepsilon_q^4)$. At $\mathcal{O}(\varepsilon_q^2)$, the scalar equation fixes one functional degree of freedom, but in practice it is convenient to treat the radial functions $X_{2,0}(r)$ and $X_{2,2}(r)$ as initial data and then reconstruct Φ_0, Φ_2 by integration once $X_{2,0}, X_{2,2}$ are fixed. This is the approach we choose for our numerical implementation.

Monopole sector ($\ell = 0$)

We first set $\varepsilon_a = 0$ and solve the $\ell = 0$ nonzero-flux backreaction at $\mathcal{O}(\varepsilon_q^2)$. We adopt a general separable form of the

scalar of the form

$$\phi_0(r, \theta) = S_r(r) + S_\theta(\theta). \quad (3.45)$$

At $\varepsilon_q = 0$, the condition $X = X_\star$ is

$$X_\star = -\frac{1}{2} \left[N^2 (S'_r)^2 + \frac{1}{r^2} (S'_\theta)^2 \right], \quad (\varepsilon_a = 0), \quad (3.46)$$

which can be realized, for example, by either a radial-only background ($S'_\theta = 0$), where we have $N^2 (S'_r)^2 = -2X_\star$ so this requires $X_\star < 0$ (equivalently $\alpha/\beta > 0$). Another option is a stealth time-gradient background (in order to obtain $X_\star > 0$), where one takes a nonzero time-dependent contribution at zeroth order and adjusts S_r, S_θ such that Eq. (3.46) is replaced by $X_\star = q_0^2/2N^2 - [N^2 (S'_r)^2 + (S'_\theta)^2/r^2]/2$. In what follows we keep the monopole equations in a general form so that we are not required to choose one of these two realizations until the end.

The scalar equation is $\nabla_\mu (P_X \nabla^\mu \phi) = 0$, which implies conservation of some current J^μ as

$$J^\mu \equiv P_X \nabla^\mu \phi, \quad \nabla_\mu J^\mu = 0. \quad (3.47)$$

In the monopole sector ($\varepsilon_a = 0$, $\partial_\theta = \partial_\varphi = 0$ for perturbations), which can be integrated once to give

$$r^2 e^\delta N P_X \partial_r \phi = \mathcal{Q}, \quad (3.48)$$

where \mathcal{Q} is a radial current which we set to zero from now on. At leading nontrivial order, using $P_X = 2\beta \varepsilon_q^2 X_{2,0} + \mathcal{O}(\varepsilon_q^4)$, this implies

$$X_{2,0}(r) S'_r(r) = 0 \quad (3.49)$$

for a radial-only monopole perturbation; therefore, in the simplest radial-only configuration (where $S'_r \neq 0$), the no-current branch we have chosen implies

$$X_{2,0}(r) = 0, \quad (3.50)$$

which is exactly the constant- X case, as $X = X_\star + \mathcal{O}(\varepsilon_q^4)$.⁹

It will be useful to note that at $\varepsilon_a = 0$, using $\phi = \phi_0 + qt + \varepsilon_q^2 \Phi_0 + \dots$ and the monopole metric $ds^2 = -N^2 e^{2\varepsilon_q^2 \delta_2} dt^2 + dr^2/N^2 + r^2 d\Omega^2$, one finds

$$X = -\frac{1}{2} \left(g^{tt} q^2 + g^{rr} (\partial_r \phi)^2 \right) = X_\star + \varepsilon_q^2 X_{2,0}(r) + \mathcal{O}(\varepsilon_q^4), \quad (3.51)$$

with

$$X_{2,0}(r) = \frac{1}{2N^2(r)} - N^2(r) S'_r(r) \Phi'_0(r) + \delta_2(r) \left(\frac{1}{N^2(r)} \right) \frac{q^2}{2M^4} + \dots \quad (3.52)$$

Working again with the constant- X case where $X_{2,0} = 0$, and (since δ_2 is then unsourced at the same order) one may set $\delta_2 = 0$ without loss of generality, yielding

$$X_{2,0} = 0 \quad \implies \quad \Phi'_0(r) = \frac{1}{2 S'_r(r) N^2(r)} \quad (\varepsilon_a = 0). \quad (3.53)$$

⁹ We could also have chosen to keep $X_{2,0}(r) \neq 0$ at $\mathcal{O}(\varepsilon_q^2)$. In this case, one must either allow a nontrivial angular background $S'_\theta(\theta) \neq 0$ configuration so that the monopole current constraint is modified by angle-dependent terms, or work on a different current branch with $\mathcal{Q} \neq 0$.

For the radial-only background with $N^2(S'_r)^2 = -2X_\star$, this becomes

$$\Phi'_0(r) = \frac{1}{2\sqrt{-2X_\star}} \frac{1}{N^3(r)} = \frac{1}{2\sqrt{C}} \frac{1}{N^3(r)}, \quad C \equiv -2X_\star = \frac{\alpha}{\beta}. \quad (3.54)$$

Monopole Einstein equations

We write the monopole metric as

$$ds^2 = -N^2(r) e^{2\varepsilon_q^2 \delta_2(r)} dt^2 + \frac{dr^2}{N^2(r)} + r^2 d\Omega^2, \quad N^2(r) = 1 - \frac{2GM}{r} - \frac{\Lambda_{\text{eff}}}{3} r^2, \quad (3.55)$$

and taking the Kerr limit, the Einstein equations (3.5) at $\mathcal{O}(\varepsilon_q^2)$ are sourced by

$$T_{\mu\nu}^{(q)} \Big|_{\ell=0} = 2\beta \varepsilon_q^2 X_{2,0}(r) \partial_\mu \phi_\star \partial_\nu \phi_\star + \mathcal{O}(\varepsilon_q^4), \quad (3.56)$$

which we can separate and express the metric functions as

$$\delta'_2(r) = \frac{\kappa r}{2N^2(r)} \left(T^{(q)r}_r - T^{(q)t}_t \right)_{\ell=0}, \quad (3.57)$$

$$(rN^2(r))' - 1 + \Lambda_{\text{eff}} r^2 = -\kappa r^2 \left(T^{(q)t}_t \right)_{\ell=0}. \quad (3.58)$$

In the constant- X case (3.50), $T_{\mu\nu}^{(q)}$ vanishes at $\mathcal{O}(\varepsilon_q^2)$, so $\delta_2 = 0$ and the monopole geometry remains exactly Schwarzschild-(A)dS at this order.

Finally, we turn to the monopole sector for the scalar field and define

$$x \equiv \frac{r}{GM}, \quad \lambda \equiv \Lambda_{\text{eff}} (GM)^2, \quad (3.59)$$

and

$$N^2(x) = 1 - \frac{2}{x} - \frac{\lambda}{3} x^2, \quad u(x) \equiv \sqrt{1 - \frac{2}{x}}. \quad (3.60)$$

In the constant- X monopole branch, we have from Eq. (3.51) that

$$\frac{d\Phi_0}{dx} = \frac{1}{2\sqrt{C}} \frac{1}{N^3(x)}, \quad C = \frac{\alpha}{\beta}, \quad (3.61)$$

and for $|\lambda| \ll 1$ one expands

$$\frac{1}{N^3(x)} = \frac{1}{u^3(x)} \left[1 + \frac{1}{2} \frac{\lambda x^2/3}{u^2(x)} + \mathcal{O}(\lambda^2) \right], \quad (3.62)$$

and therefore we have

$$\Phi_0(x) = \Phi_0(x_\infty) + \frac{1}{2\sqrt{C}} \left[\int_{x_\infty}^x \frac{dx'}{u^3(x')} + \frac{\lambda}{6} \int_{x_\infty}^x \frac{x'^2 dx'}{u^5(x')} + \mathcal{O}(\lambda^2) \right], \quad (3.63)$$

with explicit integrals given in Appendix C.

Quadrupole sector ($\ell = 2$)

At $\mathcal{O}(\varepsilon_a^2 \varepsilon_q^2)$ the nonzero-flux deformation is sourced by (H_2, K_2) , and the $\ell = 2$ projection of the Einstein equations (3.5) reduces to a linear first-order system

$$\frac{d}{dx} \begin{pmatrix} H_2 \\ K_2 \end{pmatrix} = A(x; \lambda) \begin{pmatrix} H_2 \\ K_2 \end{pmatrix} + S(x; \lambda), \quad (3.64)$$

where

$$A(x; \lambda) = \begin{pmatrix} c_{HH}(x; \lambda) - a_{KH}(x; \lambda) & -a_{KK}(x; \lambda) \\ a_{KH}(x; \lambda) & a_{KK}(x; \lambda) \end{pmatrix}, \quad S(x; \lambda) = \begin{pmatrix} -S_K(x; \lambda) \\ S_K(x; \lambda) \end{pmatrix}, \quad (3.65)$$

$$a_{KK}(x; \lambda) = \frac{6}{3 - \lambda x^3}, \quad a_{KH}(x; \lambda) = \frac{2(6 + 6x + \lambda x^3)}{x(3 - \lambda x^3)}, \quad c_{HH}(x; \lambda) = \frac{2(3 - \lambda x^3)}{x(6 - 3x + \lambda x^3)}, \quad (3.66)$$

and where the source is written as

$$S_K(x; \lambda) = \frac{3x^2}{4(3 - \lambda x^3)} \Pi_2(x; \lambda), \quad (3.67)$$

with the parametrization

$$\Pi_2(x; \lambda) = -4 X_{2,2}(x) m_{2,0}(x; \lambda), \quad (3.68)$$

where $m_{2,0}(x; \lambda)$ is the vacuum Kerr-(A)dS Hartle-Thorne $\ell = 2$ function (see Appendix C), and $X_{2,2}(x)$ is the kinetic deformation term in Eq. (3.41). The system (3.64) has regular singular points at any horizon where $N^2(x) = 0$. Let x_h denote the outer black-hole horizon, and for dS let x_c denote the cosmological horizon. Then, we fix one boundary condition by performing a near-horizon expansion about $x = x_h$ and demand that H_2, K_2 remain finite. This yields a linear relation between $H_2(x_h)$ and $K_2(x_h)$ which we show in Appendix C. We must also impose decay of the solutions on the outer boundary: for AdS/flat asymptotics, we impose decay at some large cutoff x_{out} such that

$$H_2(x_{\text{out}}) = 0, \quad K_2(x_{\text{out}}) = 0, \quad (3.69)$$

while for dS one imposes regularity at $x = x_h + \epsilon$, where ϵ is small, in order to avoid numerical divergencies.

Finally, we schematically compute the quadrupolar contribution to the scalar field by projecting $\nabla_\mu (P_X \nabla^\mu \phi) = 0$ onto $\ell = 2$; this gives a linear second-order ODE for $\Phi_2(x)$ which is lengthy, so we write it schematically as

$$\mathcal{D}_2[\Phi_2](x) = \mathcal{S}_\phi(x; \lambda; H_2, K_2; \Phi_0, \delta_2; X_{2,2}), \quad (3.70)$$

where \mathcal{D}_2 is the $\ell = 2$ radial operator determined by the Kerr-(A)dS Hartle-Thorne background.

C. CTC avoidance

In order to protect causality in our stationary and axisymmetric solutions, we demand the absence of azimuthal and helical CTCs. Azimuthal CTCs (constant t, r, θ loops) occur whenever the azimuthal Killing direction becomes timelike as $g_{\varphi\varphi}(r, \theta) < 0$; conversely, helical CTCs (closed orbits of $\partial_t + \Omega \partial_\varphi$) are defined through the 2-parameter family of vectors as

$$K(\Omega) = \partial_t + \Omega \partial_\varphi, \quad g(K, K) = g_{tt} + 2\Omega g_{t\varphi} + \Omega^2 g_{\varphi\varphi}. \quad (3.71)$$

For fixed (r, θ) this quadratic form is minimised at

$$\Omega_*(r, \theta) = -\frac{g_{t\varphi}}{g_{\varphi\varphi}}, \quad (3.72)$$

and the minimum value is

$$g(K, K)|_{\min} = g_{tt} - \frac{g_{t\varphi}^2}{g_{\varphi\varphi}} = -\frac{\mathcal{H}(r, \theta)}{g_{\phi\phi}}, \quad \mathcal{H}(r, \theta) \equiv g_{t\varphi}^2 - g_{tt}g_{\varphi\varphi}. \quad (3.73)$$

A sufficient helical-CTC condition in the stationary region is [51, 61]

$$\mathcal{H}(r, \theta) > 0 \quad \text{and} \quad g_{tt}(r, \theta) < 0, \quad (3.74)$$

since $\mathcal{H} > 0$ is the statement that the (t, φ) plane admits a timelike direction (while $g_{tt} < 0$ ensures we remain in the stationary region where ∂_t is timelike). Equivalently, one may work directly with

$$k_{\min}^2 \equiv g_{\varphi\varphi} - \frac{g_{t\varphi}^2}{g_{tt}}, \quad \text{CTCs when } k_{\min}^2 < 0 \text{ in a region with } g_{tt} < 0, \quad (3.75)$$

which is the form implemented in our numerical solutions. For either branch (zero charge with $P_X = 0$, or nonzero charge with the ε_q -deformed backreaction), the exterior is deemed chronology-safe iff for all $r \geq r_+$ one has no azimuthal CTCs and no helical CTCs, i.e. $g_{\varphi\varphi}(r, \theta) \geq 0$ and $k_{\min}^2(r, \theta) \geq 0$ (equivalently $\mathcal{H}(r, \theta) \leq 0$), implemented within the stationary region $g_{tt} < 0$. In the zero-charge branch, the separated scalar solution satisfies (see Section III A) $S'_r \sim \sqrt{2X_0}$ and $S'_\theta \sim \sqrt{2X_0}$, and we therefore must impose that $X_0 > 0$, leading to $-\alpha/2\beta > 0$, and we find that $\alpha/\beta < 0$ is necessary for the scalar field to be real. We therefore restrict our attention to the two physical regions of parameter space where α and β have the same sign. Furthermore, the energy density and pressure of the effective cosmological fluid are

$$\rho = -P(X_0) = \frac{\alpha^2}{4\beta}, \quad p = +P(X_0) = -\frac{\alpha^2}{4\beta}, \quad w = \frac{p}{\rho} = -1, \quad (3.76)$$

and in order for the weak and dominant energy conditions (WEC and DEC, respectively) to be satisfied, we must require $\rho > 0$, and β is therefore further restricted to the $\beta > 0$ half-plane, since ρ is quadratic in α but linear in β . The strong energy condition (SEC) is fulfilled by demanding that $\rho + 3p = -2P(X_0) \geq 0$, which implies $\beta < 0$, so the WEC and SEC can never be simultaneously satisfied. Together with the reality condition, the only two physical branches are:

- dS branch: $\alpha > 0$, $\beta > 0$, ($\tilde{\beta} > 0$) (WEC and DEC satisfied),
- AdS branch: $\alpha < 0$, $\beta < 0$, ($\tilde{\beta} < 0$) (SEC satisfied).

In each of these two branches, we impose further conditions to prevent the appearance of both helical and azimuthal CTCs. The azimuthal metric component to the required accuracy is

$$g_{\varphi\varphi} = \frac{\sin^2 \theta}{\rho^2 \Xi^2} \left[\Delta_\theta (r^2 + a^2)^2 - a^2 \sin^2 \theta \Delta_r \right] \equiv \frac{\sin^2 \theta}{\rho^2 \Xi^2} \mathcal{N}(r, \theta; \Lambda_{\text{eff}}), \quad (3.77)$$

and azimuthal CTCs occur when $\mathcal{N}(r, \theta; \Lambda_{\text{eff}}) < 0$. Conversely, helical CTCs occur when the discriminant of $g(K, K) = g_{\varphi\varphi} + 2\Omega g_{t\varphi} + \Omega^2 g_{tt}$ is positive (see Eq. (2.54)), leading to $\mathcal{H}(r, \theta; \Lambda_{\text{eff}}) \equiv g_{t\varphi}^2 - g_{tt}g_{\varphi\varphi} > 0$. Finally, we note that the existence of CTCs is determined by Λ_{eff} , which is a function of α and β , and we can therefore define a critical Λ which we call $\Lambda_{\text{crit}}(a, \theta)$ as the smallest (most negative) value of Λ_{eff} for which *either* of the CTC conditions is

violated somewhere outside the outer horizon r_+ . For fixed spin and polar angle, we define $\Lambda_{\text{crit}}(a, \theta)$

$$\Lambda_{\text{crit}}(a, \theta) = \min_{r \geq r_+} \left\{ \Lambda_{\text{eff}} : \mathcal{N}(r, \theta; \Lambda_{\text{eff}}) = 0 \text{ or } \mathcal{H}(r, \theta; \Lambda_{\text{eff}}) = 0 \right\}, \quad (3.78)$$

and the Kerr–AdS exterior is free of all (azimuthal and helical) CTCs iff $\Lambda_{\text{eff}} \geq \Lambda_{\text{crit}}(a, \theta)$. Combining all of the above constraints, we identify three distinct regions of parameter space and collect them in Table I. We evaluate Eq. (3.78)

Criteria	Geometry
$\alpha > 0, \tilde{\beta} > 0$	dS branch (physical and always causal)
$\alpha < 0, \tilde{\beta} < 0, \frac{\alpha^2}{ \tilde{\beta} } \leq \frac{4}{\kappa M_*^4} \Lambda_{\text{crit}}(a, \theta)$	AdS branch (physical and CTC-sensitive)
$\alpha < 0, \tilde{\beta} < 0, \frac{\alpha^2}{ \tilde{\beta} } > \frac{4}{\kappa M_*^4} \Lambda_{\text{crit}}(a, \theta)$	AdS acausal.

TABLE I: Geometries in k-essence with non-zero charge expressed in terms of $\tilde{\beta}$ as defined in Eq. (3.4).

numerically for different values of spin and equatorial angle and show the results in Figure 3 and 4. In Figure 3 we show the allowed and forbidden regions for both positive and negative α and β for a microscopic black hole and with $M_*/M = 10^{-5}$ and $\varepsilon_a = 0.4$. We notice that a small region of parameter space where CTCs are allowed appears for $\alpha < 0$ and $-0.25 \times 10^{-5} \lesssim \tilde{\beta} < 0$. The size and shape of this region and correspondingly the bound on $\tilde{\beta}$ strongly depends on the EFT cutoff scale M_* and the black-hole mass M , but we find that it depends only weakly on the spin parameter ε_a and equatorial angle θ . We show this dependence in Figure 4 where we show the third quadrant of Figure 3 in more detail for $M_*/M_{\text{Pl}} = \{0.01, 0.02, 0.03\}$ and $M/M_{\text{Pl}} = \{10^3, 2 \times 10^3, 3 \times 10^3\}$. In general, a lower EFT cutoff together with a smaller black hole corresponds to the CTC-allowed region being smaller, but the bounds on β do not scale linearly with increasing mass or cutoff scale; indeed, we observe crossing of CTC region boundary lines for $\{M_*/M_{\text{Pl}} = 0.02, M/M_{\text{Pl}} = 2 \times 10^3\}$ and $\{M_*/M_{\text{Pl}} = 0.03, M/M_{\text{Pl}} = 10^3\}$.

Non-zero charge case

Here, all conditions are evaluated on the corrected Hartle-Thorne metric in Eq. (3.36) with nonzero-flux backreaction included through $\mathcal{O}(\varepsilon_a^2 \varepsilon_q^2)$. Turning on a linear-time piece $\phi \propto qt$ moves us away from the pure vacuum-energy ($P_X = 0$) branch in a controlled way. A strictly constant- X configuration with $P_X(X_*) = 0$ continues to solve the scalar equation even after adding qt provided one simultaneously adjusts the spatial gradients so that $X = X_*$ remains exact. The nonzero-charge sector of interest here is instead the controlled deformation in which $q \neq 0$ is treated as a small parameter and the kinetic term is allowed to depart from X_* starting at order ε_q^2 as

$$\phi = \phi_0(r, \theta) + qt + \varepsilon_q^2 [\Phi_0(r) + \Phi_2(r)P_2(\cos \theta)] + \dots, \quad X = X_* + \varepsilon_q^2 [X_{2,0}(r) + X_{2,2}(r)P_2(\cos \theta)] + \dots \quad (3.79)$$

In this expansion, P_X becomes parametrically small but nonzero,

$$P_X(X) = 2\beta \varepsilon_q^2 [X_{2,0} + X_{2,2}P_2] + \mathcal{O}(\varepsilon_q^4), \quad (3.80)$$

and it is precisely this that produces a nontrivial charge stress tensor contribution at $\mathcal{O}(\varepsilon_q^2)$ as

$$T_{\mu\nu} = \underbrace{P(X_*) g_{\mu\nu}}_{\text{vacuum energy } (\Lambda_{\text{eff}})} + \underbrace{2\beta \varepsilon_q^2 [X_{2,0} + X_{2,2}P_2] \partial_\mu \phi_* \partial_\nu \phi_*}_{\text{leading charge source}} + \mathcal{O}(\varepsilon_q^4), \quad \phi_* \equiv \phi_0 + qt. \quad (3.81)$$

The energy conditions for the non-zero charge can be used to impose further constraints. For a purely spatial gradient,

we have $X \leq 0$ outside the horizon, whereas a time-gradient contributes as

$$X = \frac{q^2}{2(-g_{tt})} - \frac{1}{2} \left(g^{rr} (\partial_r \phi)^2 + g^{\theta\theta} (\partial_\theta \phi)^2 \right), \quad (\text{stationary region } g_{tt} < 0). \quad (3.82)$$

Consequently, if the zeroth-order profile has $q = 0$ and the scalar is realized purely by spatial gradients, then reality of the $P_X(X_\star) = 0$ background enforces $X_\star < 0$, i.e. $\alpha/\beta > 0$. If one instead aims to access $X_\star > 0$ (i.e. $\alpha/\beta < 0$), then one must include a timelike component already at the background level (a stealth $q_0 t$) so that Eq. (3.82) can be positive. The vacuum-energy contribution remains

$$\rho_\Lambda = -P(X_\star) = \frac{\alpha^2}{4\beta}, \quad p_\Lambda = +P(X_\star) = -\frac{\alpha^2}{4\beta}, \quad w_\Lambda = -1, \quad (3.83)$$

so $\rho_\Lambda > 0$ selects $\beta > 0$ (dS-like $\Lambda_{\text{eff}} > 0$) while the strong energy condition prefers $\beta < 0$ (AdS-like $\Lambda_{\text{eff}} < 0$). The flux sector in Eq. (3.81) adds $\mathcal{O}(\varepsilon_q^2)$ corrections whose sign and angular dependence are controlled by $\beta [X_{2,0} + X_{2,2} P_2]$ and can locally strengthen or weaken the energy inequalities depending on the chosen branch.

In the nonzero-charge branch, the metric functions $(g_{tt}, g_{t\varphi}, g_{\varphi\varphi})$ receive $\mathcal{O}(\varepsilon_q^2)$ corrections through

$$h_2 = h_2^{\text{vac}} + \varepsilon_q^2 H_2, \quad k_2 = k_2^{\text{vac}} + \varepsilon_q^2 K_2, \quad (3.84)$$

and these are sourced by the charge via Eq. (3.81). Therefore, both $\mathcal{H}(r, \theta)$ and $g_{\varphi\varphi}(r, \theta)$ acquire $\mathcal{O}(\varepsilon_q^2)$ deformations which shift the onset of chronology violation. For fixed $(\varepsilon_a, \theta, \varepsilon_q)$, the onset of CTCs is controlled by Λ_{eff} . We define the critical value as the smallest deformation (in the relevant sign direction) for which *either* the azimuthal or helical condition is saturated somewhere outside the outer horizon r_+ as

$$\Lambda_{\text{crit}}(\varepsilon_a, \theta, \varepsilon_q) = \min_{r \geq r_+} \left\{ \Lambda_{\text{eff}} : g_{\phi\phi}(r, \theta; \Lambda_{\text{eff}}) = 0 \text{ or } \mathcal{H}(r, \theta; \Lambda_{\text{eff}}) = 0 \right\}. \quad (3.85)$$

The exterior is free of both azimuthal and helical CTCs iff

$$\Lambda_{\text{eff}} \geq \Lambda_{\text{crit}}(\varepsilon_a, \theta, \varepsilon_q), \quad (3.86)$$

Equivalently, in dimensionless form we may work with $\lambda_{\text{crit}}(\varepsilon_a, \theta, \varepsilon_q) \equiv \Lambda_{\text{crit}}(\varepsilon_a, \theta, \varepsilon_q) (GM)^2$, and then map the critical curve to the microscopic couplings using the dimensionless variable λ defined in Eq. (3.59). Each critical curve $\lambda = \lambda_{\text{crit}}(\varepsilon_a, \theta, \varepsilon_q)$ therefore becomes a parabola in the (α, β) plane, which we combine with the corresponding reality and energy-condition branch to divide the parameter space into physical and unphysical regions. We evaluate Eq. (3.85) numerically and display the result in Figure 5. In contrast to the zero-charge case in Figure 4, the size of the acausal region in the third quadrant is highly sensitive to the spin parameter, equatorial angle, as well as the charge parameter ε_q . In Figure 5, we evaluate the acausal regions for a range of parameter values but for fixed EFT cutoff $M_\star/M_{\text{Pl}} = 0.01$ and black-hole mass $M/M_{\text{Pl}} = 10^3$, as this case shows more sensitivity to spin due to the matter backreaction. It is clear that in general, higher spin and more backreaction (larger ε_q) leads to a larger acausal region, and moving towards the equatorial plane (larger θ) enlarges the region further, due to the frame dragging term. Nevertheless, the bounds on $\tilde{\beta}$ are several orders of magnitude smaller than for the zero-charge case.

IV. EINSTEIN-DILATON GAUSS-BONNET MODEL

In order to solve the field equations in (2.61) with backreaction onto the Kerr geometry, we first note that these are significantly less trivial than the k-essence case, and it may therefore be necessary to change the computation scheme. On the one hand, we can tackle the problem by directly construct the spin-0 and spin-2 perturbations on

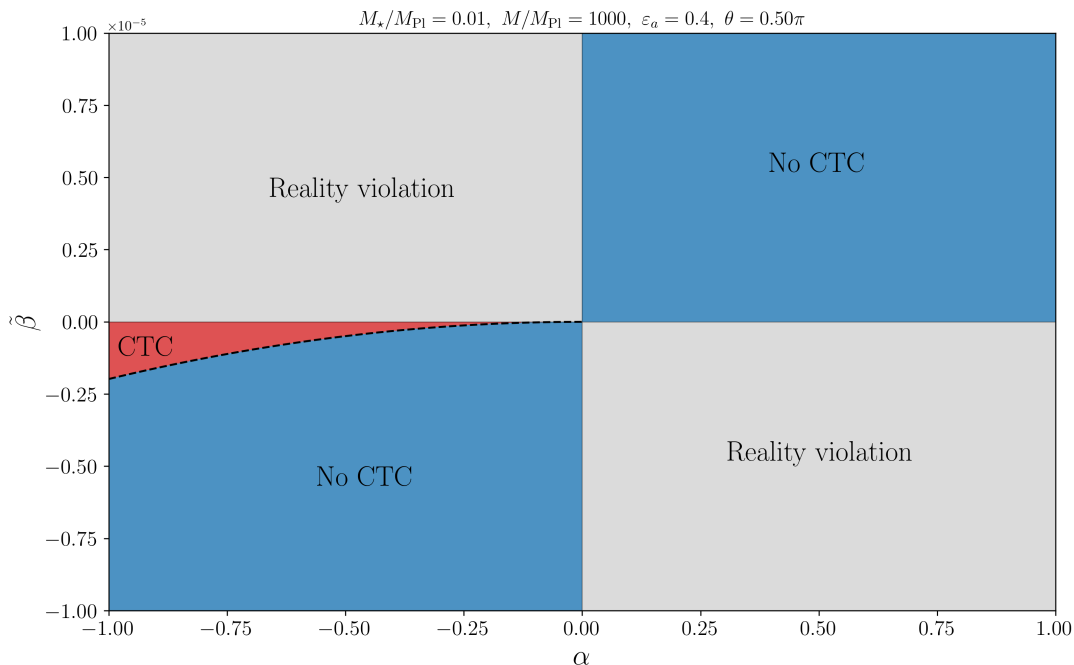


FIG. 3: Causality parameter space for zero-change k-essence. CTCs only appear in the red region in the third quadrant. The dashed line indices the boundary between the causal and acausal region of parameter space, which is shown for different values of M and M_* in Figure 4.

exact Kerr geometry in Boyer-Lindqvist coordinates, solve the resulting partial differential equations using Teukolsky methods, and then take the slow-rotation limit in order to obtain analytically tractable results. This is conceptually appealing but technically involved. Instead, we adopt a formalism which works as follows: the background is Kerr, but expressed through its Hartle-Thorne form up to some order; then, the EdGB corrections (spin-0 and spin-2) are treated as perturbations sourced by the zeroth-order Gauss-Bonnet invariant on the Kerr-HT background. Finally, we expand all equations simultaneously in the EdGB terms and slow rotation, and we can then solve the equations systematically order by order up to the required accuracy in both the metric and scalar sectors. In this way, we do not need to introduce the involved Teukolsky formalism only to expand in slow rotation at the end, and instead work only to the level of precision we require. We work in the standard EdGB small-coupling expansion, in which $\vartheta = \mathcal{O}(\varepsilon)$ and the metric deformation is $\mathcal{O}(\varepsilon^2)$ (defined precisely below). Then

$$e^\vartheta = 1 + \vartheta + \mathcal{O}(\vartheta^2).$$

In the scalar equation in Eq. (2.61), the term $\alpha \mathcal{G}$ provides the leading source, while the nonlinear correction $\alpha \vartheta \mathcal{G}$ is higher order in ε and can be dropped. In the corresponding metric equation, $\mathcal{C}_{\mu\nu}[e^\vartheta]$ depends on $\nabla\nabla e^\vartheta = e^\vartheta(\nabla\nabla\vartheta + \nabla\vartheta\nabla\vartheta)$. The $\nabla\vartheta\nabla\vartheta$ contribution is $\mathcal{O}(\varepsilon^2)$ and is multiplied by α , hence it only enters beyond the $\mathcal{O}(\varepsilon^2)$ metric equation we keep. Therefore, to $\mathcal{O}(\varepsilon^2)$ one may replace

$$e^\vartheta \rightarrow 1 \quad \text{in the scalar equation,} \quad \nabla\nabla e^\vartheta \rightarrow \nabla\nabla\vartheta \quad \text{in the metric equation,} \quad (4.1)$$

which yields the same leading-order scalar and metric structure as the linear-coupling EdGB treatment.

From now on, we distinguish the EFT cutoff M_* from the black-hole mass M : the dimensionless spin parameter ε_a

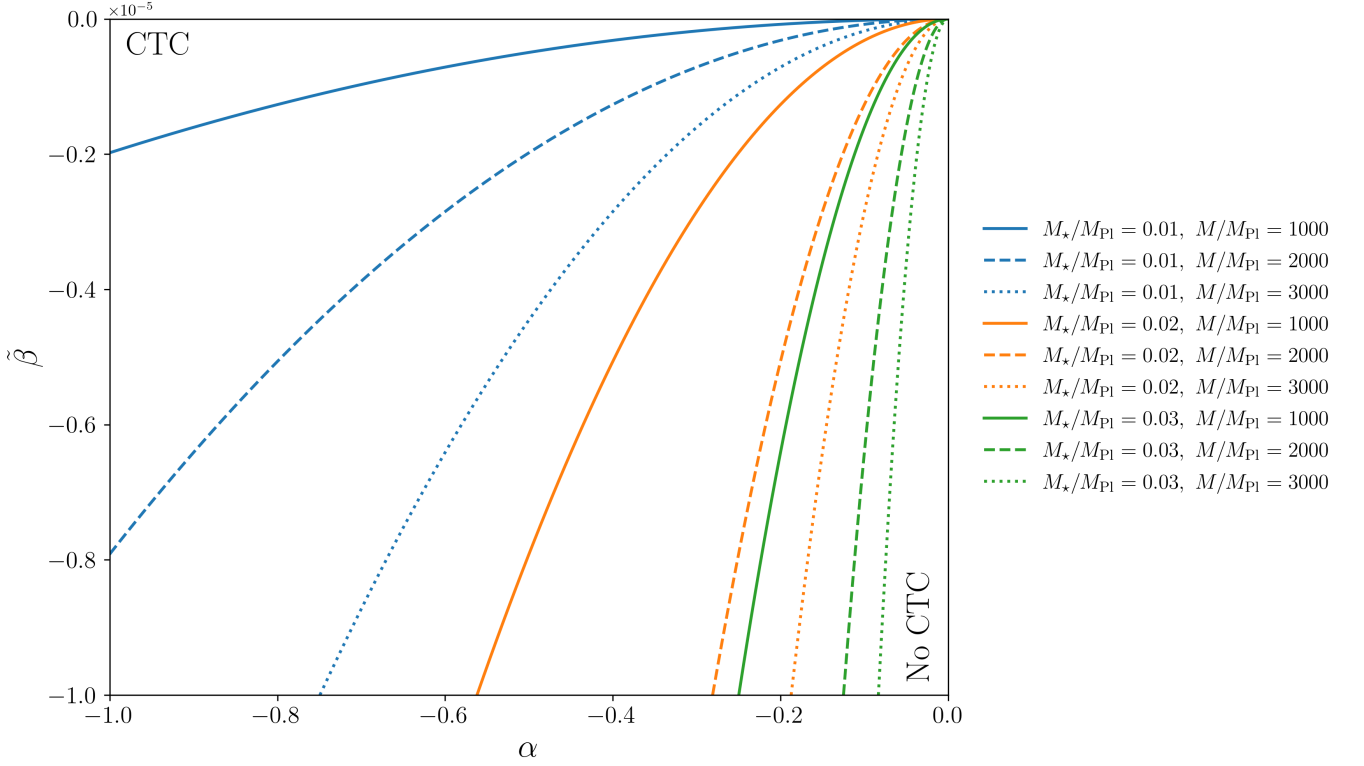


FIG. 4: CTC regions for zero-charge k-essence for different values of M and M_* using $\varepsilon_a = 0.4$ and $\theta = \pi/2$ (third quadrant of Figure 3). CTCs appear to the left of any curve. The region to the right is chronologically safe shrinks with increasing M and M_* in general. The region where α and $\tilde{\beta}$ are both positive is always chronologically safe, and when either α or $\tilde{\beta}$ is negative, there is no real solution for the scalar field.

is defined using the black-hole mass while the decoupling/small-coupling parameter is defined using the EFT cutoff

$$\varepsilon^2 \equiv \frac{\alpha^2}{\beta \kappa}, \quad (4.2)$$

where we note that the couplings have dimension $[\alpha] = 1$ and $[\beta] = M^2$ which is different from the k-essence case. In the regime where the EFT is valid, we should have $M_* > M$, where we can consider M_* as the EFT cut-off scale. In this context, we consider ϑ as $\mathcal{O}(\varepsilon)$ and the metric correction $h_{\mu\nu}$ as $\mathcal{O}(\varepsilon^2)$. The metric and scalar are expanded as

$$g_{\mu\nu} = g_{\mu\nu}^{(0)}(M, \varepsilon_a) + \varepsilon^2 h_{\mu\nu}(M, \varepsilon_a) + \mathcal{O}(\varepsilon^4), \quad (4.3)$$

$$\vartheta = \varepsilon \vartheta^{(1)}(M, \varepsilon_a) + \mathcal{O}(\varepsilon^3), \quad (4.4)$$

where $g_{\mu\nu}^{(0)}$ is the Kerr metric in Hartle–Thorne form to $\mathcal{O}(\varepsilon_a^2)$ and $\vartheta^{(1)}$ is the leading-order scalar; as we will see, higher orders in ε will not be needed. We see that at $\mathcal{O}(\varepsilon)$, Eq. (4.4) becomes

$$\beta \square^{(0)} \vartheta^{(1)} + \alpha \mathcal{G}^{(0)} = 0, \quad (4.5)$$

where $\square^{(0)}$ and $\mathcal{G}^{(0)}$ are computed with $g_{\mu\nu}^{(0)}$. Similarly, but at $\mathcal{O}(\varepsilon^2)$, the metric equation reads

$$G_{\mu\nu}^{(1)}[h] = \kappa (T_{a\mu\nu}^{(\vartheta)}[\vartheta^{(1)}] + D_{\mu\nu}[\vartheta^{(1)}]), \quad (4.6)$$

where $G_{\mu\nu}^{(1)}[h]$ is the linearised Einstein tensor on the Kerr–HT background. All quantities on the right-hand side are

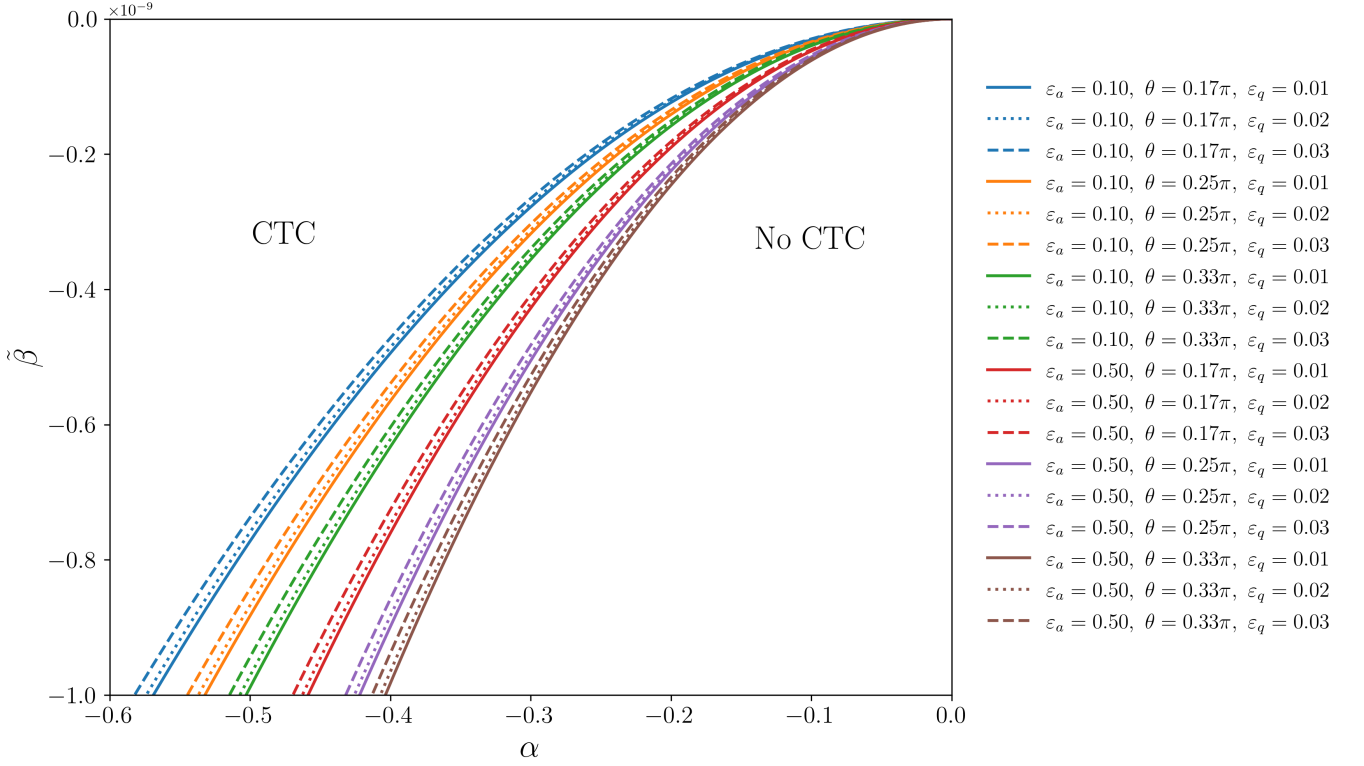


FIG. 5: CTC regions for non zero-charge k-essence for different values of spin ε_a , matter coupling ε_q , and equatorial angle θ when using $M_* = M_{\text{Pl}}/100$ and $M = 1000M_{\text{Pl}}$. CTCs appear in the top left region, and the lower right region is chronologically safe and which shrinks with increasing angular momentum and matter coupling strength. The region $\{\alpha > 0, \beta > 0\}$ is always chronologically safe. In the regions where either α or β is negative, the scalar field has no real solution.

evaluated using $g_{ab}^{(0)}$ and $\vartheta^{(1)}$.

We use Schwarzschild-like coordinates (t, r, θ, φ) and write the slow-rotation expansion

$$ds_0^2 = -f(r) dt^2 + \frac{dr^2}{f(r)} + r^2(d\theta^2 + \sin^2 \theta d\varphi^2) + \varepsilon_a \delta g_{t\varphi}^{(1)} dt d\varphi + \varepsilon_a^2 \delta g_{\mu\nu}^{(2)} dx^\mu dx^\nu, \quad (4.7)$$

where $f(r) = 1 - 2GM/r$ and at $\mathcal{O}(\varepsilon_a)$

$$\delta g_{t\varphi}^{(1)} = -2 \frac{(GM)^2}{r} \sin^2 \theta. \quad (4.8)$$

At $\mathcal{O}(\varepsilon_a^2)$ one may parametrise the even-parity corrections in standard Hartle–Thorne form as

$$\delta g_{tt}^{(2)} = f(r) \left[H_0(r) + H_2(r) P_2(\cos \theta) \right], \quad (4.9)$$

$$\delta g_{rr}^{(2)} = f(r)^{-1} \left[M_0(r) + M_2(r) P_2(\cos \theta) \right], \quad (4.10)$$

$$\delta g_{\theta\theta}^{(2)} = r^2 \left[K_0(r) + K_2(r) P_2(\cos \theta) \right], \quad (4.11)$$

$$\delta g_{\varphi\varphi}^{(2)} = \delta g_{\theta\theta}^{(2)} \sin^2 \theta. \quad (4.12)$$

These functions are fixed (up to trivial second-order coordinate/gauge redefinitions) by matching to Kerr expanded to $\mathcal{O}(\varepsilon_a^2)$ [50]. It is often convenient to use $u \equiv GM/r$, so $f(u) = 1 - 2u$. What matters for our purposes is that all

background curvature invariants admit a multipole expansion of the schematic form

$$\mathcal{I}(r, \theta; \varepsilon_a) = \mathcal{I}^{(0)}(r) + \varepsilon_a^2 [\mathcal{I}^{(20)}(r) + \mathcal{I}^{(22)}(r)P_2(\cos\theta)] + \mathcal{O}(\varepsilon_a^4), \quad (4.13)$$

where the coefficients are rational functions of u . Of particular interest is the Gauss-Bonnet invariant which in vacuum Kerr reads $\mathcal{G} = R_{\mu\nu\rho\sigma}R^{\mu\nu\rho\sigma}$, since $R_{\mu\nu} = 0$. Expanding to $\mathcal{O}(\varepsilon_a^2)$ yields

$$\mathcal{G}^{(0)}(r, \theta; \varepsilon_a) = \frac{48(GM)^2}{r^6} - \frac{1008\varepsilon_a^2(GM)^4}{r^8} \cos^2\theta + \mathcal{O}(\varepsilon_a^4), \quad (4.14)$$

which can be rewritten in $P_2(\cos\theta)$ as

$$\mathcal{G}^{(0)}(r, \theta; \varepsilon_a) = \mathcal{G}_0(r) + \varepsilon_a^2 [\mathcal{G}_{20}^{(0)}(r) + \mathcal{G}_{22}^{(0)}(r)P_2(\cos\theta)] + \mathcal{O}(\varepsilon_a^4), \quad (4.15)$$

with

$$\mathcal{G}_0(r) = \frac{48(GM)^2}{r^6}, \quad (4.16)$$

and coincides with the Schwarzschild Kretschmann scalar, and where $\mathcal{G}_{20}^{(0)}, \mathcal{G}_{22}^{(0)}$ are the spin-dependent monopole and quadrupole corrections at $\mathcal{O}(\varepsilon_a^2)$.¹⁰

A. The EdGB scalar in Kerr-HT

To leading order in the Gauss-Bonnet coupling, the scalar field ϑ satisfies

$$\beta \square^{(0)}\vartheta^{(1)} + \alpha \mathcal{G}^{(0)} = 0, \quad (4.17)$$

where $\square^{(0)}$ and $\mathcal{G}^{(0)}$ are constructed from the Kerr background metric $g_{\mu\nu}^{(0)}$ written in the Hartle-Thorne slow rotation expansion up to $\mathcal{O}(\varepsilon_a^2)$. We restrict attention to stationary, axisymmetric configurations, so that $\vartheta^{(1)}$ depends only on (r, θ) . As in previous sections, we expand in Legendre polynomials on the Schwarzschild background and treat spin corrections as $\mathcal{O}(\varepsilon_a^2)$. Both the monopole and quadrupole sectors therefore acquire spin dependence, and we write

$$\vartheta^{(1)}(r, \theta) = \vartheta_0^{(0)}(r) + \varepsilon_a^2 \vartheta_0^{(2)}(r) + \varepsilon_a^2 P_2(\cos\theta) \vartheta_2(r), \quad (4.18)$$

where $\vartheta_0^{(0)}$ is the spin-independent Schwarzschild monopole, $\vartheta_0^{(2)}$ is the spin-dependent monopole correction, and ϑ_2 is the $\ell = 2$ quadrupole profile. To leading order in ε_a , the Laplacian on a spherically symmetric background acting on a single harmonic $\phi_\ell(r)Y_{\ell 0}(\theta)$ reduces to

$$\square^{(0)}[\phi_\ell(r)Y_{\ell 0}(\theta)] = \left[\frac{1}{r^2} \frac{d}{dr} \left(r^2 f(r) \frac{d}{dr} \right) - \frac{\ell(\ell+1)}{r^2} \right] \phi_\ell(r) Y_{\ell 0}(\theta) + \mathcal{O}(\varepsilon_a^2), \quad (4.19)$$

with $f(r) = 1 - 2GM/r$. Inserting the multipole expansion of $\mathcal{G}^{(0)}$ and the ansatz (4.18) into Eq. (4.17) and projecting onto $\ell = 0, 2$ gives three radial ODEs

$$\beta \frac{1}{r^2} \frac{d}{dr} \left(r^2 f \vartheta_0^{(0)'} \right) = -\alpha \mathcal{G}_0(r), \quad (4.20)$$

$$\beta \frac{1}{r^2} \frac{d}{dr} \left(r^2 f \vartheta_0^{(2)'} \right) = -\alpha \mathcal{S}_0^{(2)}(r), \quad (4.21)$$

¹⁰ This is parity even, so the scalar has no $\mathcal{O}(\varepsilon_a)$ term.

$$\beta \left[\frac{1}{r^2} \frac{d}{dr} \left(r^2 f \vartheta'_2 \right) - \frac{6}{r^2} \vartheta_2 \right] = -\alpha \mathcal{S}_2^{(2)}(r), \quad (4.22)$$

where \mathcal{G}_0 is the Schwarzschild Gauss–Bonnet invariant, and $\mathcal{S}_0^{(2)}, \mathcal{S}_2^{(2)}$ are $\mathcal{O}(\varepsilon_a^2)$ sources built from the spin–corrected Gauss–Bonnet invariant and the $\mathcal{O}(\varepsilon_a^2)$ corrections to $\square^{(0)}$. Concretely, we have

$$\ell = 0, \varepsilon_a^0 : \quad \frac{1}{r^2} \frac{d}{dr} \left(r^2 f \vartheta'_0(r) \right) = -\frac{\alpha}{\beta} \frac{48 (GM)^2}{r^6}, \quad (4.23)$$

$$\ell = 0, \varepsilon_a^2 : \quad \frac{1}{r^2} \frac{d}{dr} \left(r^2 f \vartheta'_{20}(r) \right) = +\frac{\alpha}{\beta} \frac{336 (GM)^4}{r^8}, \quad (4.24)$$

$$\ell = 2, \varepsilon_a^2 : \quad \frac{1}{r^2} \frac{d}{dr} \left(r^2 f \vartheta'_{22}(r) \right) - \frac{6}{r^2} \vartheta_{22}(r) = +\frac{\alpha}{\beta} \frac{672 (GM)^4}{r^8}. \quad (4.25)$$

It is now necessary to pick boundary conditions, which we impose by demanding regularity at the horizon $r = 2GM$ and decay at $r \rightarrow \infty$. Solving Eq. (4.23) gives

$$\vartheta_0(r) = \frac{\alpha}{\beta} \frac{2}{(GM)r} \left(1 + \frac{GM}{r} + \frac{4}{3} \frac{(GM)^2}{r^2} \right) \quad (4.26)$$

$$\vartheta_{20}(r) = -\frac{\alpha}{2\beta} \left[\frac{1}{GMr} + \frac{1}{r^2} + \frac{8}{3} \frac{GM}{r^3} + 6 \frac{(GM)^2}{r^4} + \frac{64}{5} \frac{(GM)^3}{r^5} \right], \quad (4.27)$$

$$\vartheta_{22}(r) = -\frac{\alpha}{2\beta} \left[\frac{56}{15} \frac{GM}{r^3} + \frac{56}{5} \frac{(GM)^2}{r^4} + \frac{128}{5} \frac{(GM)^3}{r^5} \right], \quad (4.28)$$

and at $\mathcal{O}(\varepsilon_a^2)$ the full scalar may be written compactly as

$$\begin{aligned} \vartheta^{(1)}(r, \theta) = & \frac{\alpha}{\beta} \frac{2}{GGMr} \left(1 + \frac{GM}{r} + \frac{4}{3} \frac{(GM)^2}{r^2} \right) - \frac{\alpha \varepsilon_a^2}{2\beta GMr} \left[1 + \frac{GM}{r} + \frac{4}{5} \frac{(GM)^2}{r^2} + \frac{2}{5} \frac{(GM)^3}{r^3} \right. \\ & \left. + \frac{28}{5} \frac{(GM)^2}{r^2} \cos^2 \theta \left(1 + \frac{3GM}{r} + \frac{48}{7} \frac{(GM)^2}{r^2} \right) \right] + \mathcal{O}(\varepsilon_a^4), \end{aligned} \quad (4.29)$$

which we can rewrite in terms of the variable u as

$$\vartheta^{(1)}(u, \theta) = \frac{\alpha}{\beta} 2u \left(1 + u + \frac{4}{3} u^2 \right) - \frac{\alpha \varepsilon_a^2}{\beta} \frac{u}{2} \left[1 + u + \frac{4}{5} u^2 + \frac{2}{5} u^3 + \frac{28}{5} u^2 \cos^2 \theta \left(1 + 3u + \frac{48}{7} u^2 \right) \right] + \mathcal{O}(\varepsilon_a^4). \quad (4.30)$$

By construction, Eq. (4.29) is regular on the future event horizon, decays as $1/r$ at infinity, and agrees with the known EdGB scalar solution on a slowly rotating black hole in the gauge of Ref. [62], while being written in a form that is manifestly adapted to the Kerr–Hartle–Thorne approach we use in this paper.

B. EdGB metric corrections

We now turn to the metric correction $h_{\mu\nu}$ at order ε^2 : starting from the linearised Einstein equations (A4), we adopt a HT-style decomposition for the metric perturbation as $ds^2 = ds_0^2 + \varepsilon^2 ds_1^2$, where ds_0^2 is the Kerr-HT background line element defined in Eq. (4.7) and ds_1^2 is

$$\begin{aligned} ds_1^2 = & -f(r) \left[A_0(r) + A_2(r) P_2(\cos \theta) \right] dt^2 + f(r)^{-1} \left[B_0(r) + B_2(r) P_2(\cos \theta) \right] dr^2 \\ & + r^2 \left[C_0(r) + C_2(r) P_2(\cos \theta) \right] \left(d\theta^2 + \sin^2 \theta d\varphi^2 \right) - 2r^2 \sin^2 \theta \Omega(r) dt d\varphi, \end{aligned} \quad (4.31)$$

where (A_0, B_0, C_0) describe the monopole corrections, (A_2, B_2, C_2) the quadrupole corrections, and $\Omega(r)$ is the correction to frame dragging. Each radial function has an expansion in ε_a of the form

$$X(r; \varepsilon_a) = X^{(0)}(r) + \varepsilon_a^2 X^{(2)}(r) + \mathcal{O}(\varepsilon_a^4), \quad X \in \{A_0, B_0, C_0, A_2, B_2, C_2, \Omega\}. \quad (4.32)$$

We impose a HT gauge (a variant of Lorenz/de Donder gauge) which eliminates redundant components and simplifies the radial equations; the gauge conditions may be chosen so that only the functions in Eq. (4.31) remain.

We now compute the source terms starting with those arising from the scalar sector. The scalar $\vartheta^{(1)}$ obtained in Sec. IV A produces a stress tensor and Gauss–Bonnet corrections, which we decompose as

$$T_{ab}^{(\vartheta)} + D_{ab} = \left(\mathcal{T}_{ab}^{(0)}(r) + \varepsilon_a^2 \mathcal{T}_{ab}^{(20)}(r) \right) + \varepsilon_a^2 \mathcal{T}_{ab}^{(22)}(r) P_2(\cos \theta) + \varepsilon_a \mathcal{T}_{ab}^{(1)}(r) \sin^2 \theta + \mathcal{O}(\varepsilon_a^3), \quad (4.33)$$

where the ε_a -odd piece contributes to the $t\phi$ sector (the frame dragging term), and the $\ell = 0, 2$ pieces contribute to the even-parity metric perturbations. Projecting onto appropriate tensor spherical harmonics yields source terms $S_X(r)$ for each radial function X . The monopole sector involves (A_0, B_0, C_0) , and at $\mathcal{O}(\varepsilon_a^0)$ we recover the purely Schwarzschild EdGB correction, while at $\mathcal{O}(\varepsilon_a^2)$ we find a spin-dependent monopole. These can be written schematically as $\mathcal{E}_0^{(ii)}[A_0, B_0, C_0] = S_0^{(ii)}(r)$, where \mathcal{E}_0 are differential operators derived from $G_{ab}^{(1)}$. These can be combined into a single master equation for, say, C_0 (from which A_0 and B_0 follow)

$$\frac{1}{r^2} \frac{d}{dr} \left(r^2 f \frac{dC_0}{dr} \right) + V_0(r) C_0(r) = S_0(r), \quad (4.34)$$

with $V_0(r)$ a Zerilli-type potential and $S_0(r)$ a source built from $\vartheta_0^{(0)}$ and $\vartheta_0^{(2)}$. The spin-independent and spin-dependent pieces are separated via

$$C_0(r) = C_0^{(0)}(r) + \varepsilon_a^2 C_0^{(2)}(r), \quad S_0(r) = S_0^{(0)}(r) + \varepsilon_a^2 S_0^{(2)}(r), \quad (4.35)$$

with the integral solution given as

$$C_0^{(0)}(r) = \int_r^\infty d\bar{r} G_0(r, \bar{r}) S_0^{(0)}(\bar{r}), \quad C_0^{(2)}(r) = \int_r^\infty d\bar{r} G_0(r, \bar{r}) S_0^{(2)}(\bar{r}), \quad (4.36)$$

where $G_0(r, \bar{r})$ is the Green function for the monopole operator (4.34) with horizon-regular and decaying boundary conditions. Once C_0 is known, the remaining functions A_0, B_0 follow from first-order constraint equations and can be written as single integrals of known combinations of C_0 and the sources. As in the scalar case, the explicit solutions can be expressed as

$$\begin{aligned} A_0(r) &= \varepsilon^2 \left[P_{A_0}^{(0)}(x) + Q_{A_0}^{(0)}(x) \ln \left(1 - \frac{2}{x} \right) + \varepsilon_a^2 \left(P_{A_0}^{(2)}(x) + Q_{A_0}^{(2)}(x) \ln \left(1 - \frac{2}{x} \right) \right) \right], \\ B_0(r) &= \varepsilon^2 \left[P_{B_0}^{(0)}(x) + Q_{B_0}^{(0)}(x) \ln \left(1 - \frac{2}{x} \right) + \varepsilon_a^2 \left(P_{B_0}^{(2)}(x) + Q_{B_0}^{(2)}(x) \ln \left(1 - \frac{2}{x} \right) \right) \right], \\ C_0(r) &= \varepsilon^2 \left[P_{C_0}^{(0)}(x) + Q_{C_0}^{(0)}(x) \ln \left(1 - \frac{2}{x} \right) + \varepsilon_a^2 \left(P_{C_0}^{(2)}(x) + Q_{C_0}^{(2)}(x) \ln \left(1 - \frac{2}{x} \right) \right) \right], \end{aligned} \quad (4.37)$$

with rational functions $P_X^{(0,2)}(x)$, $Q_X^{(0,2)}(x)$; finally, an appropriate choice of boundary conditions ensures that all monopole corrections decay faster than r^{-1} .

Quadrupole metric corrections

The quadrupole sector obeys a similar structure to that of the monopole, with a master equation for C_2 which reads

$$\frac{1}{r^2} \frac{d}{dr} \left(r^2 f \frac{dC_2}{dr} \right) + V_2(r) C_2(r) = S_2(r), \quad (4.38)$$

where $V_2(r)$ is the $\ell = 2$ even-parity potential on the Kerr-HT background and $S_2(r)$ is sourced by ϑ_2 , $\vartheta_0^{(0)}$, and $\vartheta_0^{(2)}$, which are now known. Again we expand the function as

$$C_2(r) = C_2^{(0)}(r) + \varepsilon_a^2 C_2^{(2)}(r), \quad S_2(r) = S_2^{(0)}(r) + \varepsilon_a^2 S_2^{(2)}(r), \quad (4.39)$$

and solve with the Green's function method

$$C_2^{(0)}(r) = \int_r^\infty d\bar{r} G_2(r, \bar{r}) S_2^{(0)}(\bar{r}), \quad C_2^{(2)}(r) = \int_r^\infty d\bar{r} G_2(r, \bar{r}) S_2^{(2)}(\bar{r}), \quad (4.40)$$

with G_2 the appropriate $\ell = 2$ Green function. The horizon-regular and asymptotically decaying solutions again have the structure

$$\begin{aligned} A_2(r) &= \varepsilon^2 \left[P_{A_2}(x) + Q_{A_2}(x) \ln \left(1 - \frac{2}{x} \right) \right], \\ B_2(r) &= \varepsilon^2 \left[P_{B_2}(x) + Q_{B_2}(x) \ln \left(1 - \frac{2}{x} \right) \right], \\ C_2(r) &= \varepsilon^2 \left[P_{C_2}(x) + Q_{C_2}(x) \ln \left(1 - \frac{2}{x} \right) \right], \end{aligned} \quad (4.41)$$

where $\{P_X, Q_X\}$ are rational functions which we display in Appendix D.

Frame-dragging corrections

The $t\varphi$ component yields a first-order equation for $\Omega'(r)$ of the form

$$\frac{d}{dr} \left(r^4 f \frac{d\Omega}{dr} \right) = S_\Omega(r), \quad (4.42)$$

where $S_\Omega(r)$ is sourced by the ε_a -odd pieces of the scalar stress tensor and Gauss–Bonnet corrections. Integrating from the horizon and imposing that $\Omega(r)$ decays at infinity and regularity at the horizon, we obtain

$$\Omega(r) = \int_r^\infty d\bar{r} \frac{1}{\bar{r}^4 f(\bar{r})} \int_{2M}^{\bar{r}} d\tilde{r} S_\Omega(\tilde{r}), \quad (4.43)$$

the solution for which can be written as

$$\Omega(x) = \text{const.} \times \left[\sum_{k=2}^6 \frac{\Omega_k}{x^k} + \left(\sum_{k=2}^4 \frac{\tilde{\Omega}_k}{x^k} \right) \ln \left(1 - \frac{2}{x} \right) \right]. \quad (4.44)$$

In the Hartle-Thorne gauge, the EdGB corrections are parametrised as

$$\begin{aligned} h_{tt} &= \varepsilon^2 \left[A_0(r) + \varepsilon_a^2 P_2(\cos \theta) A_2(r) \right], & h_{rr} &= \varepsilon^2 \left[B_0(r) + \varepsilon_a^2 P_2(\cos \theta) B_2(r) \right], \\ h_{\theta\theta} &= \varepsilon^2 r^2 \left[C_0(r) + \varepsilon_a^2 P_2(\cos \theta) C_2(r) \right], & h_{\varphi\varphi} &= \varepsilon^2 r^2 \sin^2 \theta \left[C_0(r) + \varepsilon_a^2 P_2(\cos \theta) C_2(r) \right], \\ h_{t\varphi} &= \varepsilon^2 \varepsilon_a \sin^2 \theta \Omega(r), \end{aligned} \quad (4.45)$$

with all other components vanishing at $\mathcal{O}(\varepsilon^2, \varepsilon_a^2)$. In order to make contact with the series solutions of Ref. [63], we

rewrite each radial function as a dimensionless polynomial in x as

$$\begin{aligned}
A_0(x) &= -\varepsilon^2 f(x) M^3 \left[p_{A_0}(x) + q_{A_0}(x) \ln f(x) \right], & B_0(x) &= -\varepsilon^2 \frac{M^2}{f(x)^2} \left[p_{B_0}(x) + q_{B_0}(x) \ln f(x) \right], \\
C_0(x) &= -\varepsilon^2 M^3 \left[p_{C_0}(x) + q_{C_0}(x) \ln f(x) \right], & A_2(x) &= -\varepsilon^2 \varepsilon_a^2 M^3 \left[p_{A_2}(x) + q_{A_2}(x) \ln f(x) \right], \\
B_2(x) &= -\varepsilon^2 \varepsilon_a^2 \frac{M^2}{f(x)^2} \left[p_{B_2}(x) + q_{B_2}(x) \ln f(x) \right], & C_2(x) &= -\varepsilon^2 \varepsilon_a^2 M^3 \left[p_{C_2}(x) + q_{C_2}(x) \ln f(x) \right], \\
\Omega(x) &= \varepsilon^2 \varepsilon_a M^5 \left[p_\Omega(x) + q_\Omega(x) \ln f(x) \right].
\end{aligned} \tag{4.46}$$

In the particular gauge that matches the Yunes-Stein [63] solution (up to a choice of units) we may consistently take all logarithmic polynomials to vanish,

$$q_{A_0} = q_{B_0} = q_{C_0} = q_{A_2} = q_{B_2} = q_{C_2} = q_\Omega = 0, \tag{4.47}$$

so that the entire structure is captured by a finite set of dimensionless polynomials $p_X(x)$. Since the spin-independent ($\ell = 0$) EdGB corrections are encoded in the three polynomials

$$\begin{aligned}
p_{A_0}(x) &= x^3 \left(1 + 26x + \frac{66}{5}x^2 + \frac{96}{5}x^3 - 80x^4 \right), \\
p_{B_0}(x) &= x^2 \left(1 + x + \frac{52}{3}x^2 + 2x^3 + \frac{16}{5}x^4 - \frac{368}{3}x^5 \right), \\
p_{C_0}(x) &= x^3 \left(\frac{5}{3}x + \frac{9}{5}x^2 + \frac{2}{5}x^3 - \frac{16}{3}x^4 \right),
\end{aligned} \tag{4.48}$$

we note in particular that $p_{C_0}(x) \neq 0$, so $C_0(r)$ is non-vanishing even in the spin-independent sector. This reproduces the structure of the spin-independent EdGB deformation found in Eq. (45) of Ref. [63], but written in the Kerr-Hartle-Thorne language used in this work. Furthermore, the leading spin-quadrupole deformation ($\ell = 2$) is captured by polynomials $p_{A_2}(x)$, $p_{B_2}(x)$ and $p_{C_2}(x)$. A convenient representation is

$$p_{A_2}(x) = x^3 \left(1 + \frac{10370}{4463}x + \frac{266911}{62482}x^2 + \frac{63365}{13389}x^3 - \frac{309275}{31241}x^4 - \frac{81350}{4463}x^5 - \frac{443800}{13389}x^6 + \frac{210000}{4463}x^7 \right), \tag{4.49}$$

with $p_{B_2}(x)$ and $p_{C_2}(x)$ chosen to describe the same radial behaviour in the rr and angular components. For many applications it is sufficient (and very convenient) to use the relations

$$p_{B_2}(x) \simeq p_{A_2}(x), \quad p_{C_2}(x) \simeq -\frac{1}{2}p_{A_2}(x), \tag{4.50}$$

which reproduces the Yunes solution to the order needed for our slow-rotation analysis. Finally, the EdGB correction to the frame-dragging potential can be expressed as

$$p_\Omega(x) = x^5(2 + 10x + 15x^2), \tag{4.51}$$

so that

$$\Omega(r) = \varepsilon^2 \varepsilon_a (GM)^5 p_\Omega \left(\frac{GM}{r} \right), \tag{4.52}$$

and Eqs (4.46) together with the polynomials (4.48) and (4.51) completes the solution in the Kerr-Hartle-Thorne variables $(\varepsilon, \varepsilon_a, x)$ used in this paper.

C. CTC avoidance

In the Kerr-Hartle-Thorne EdGB background constructed above, the appearance of CTCs provides a non-trivial constraint on the effective coupling ε . We now summarise the azimuthal and helical CTC conditions and combine them with the scalar energy condition, which enforces $\beta > 0$. This mirrors the discussion in Section III C in the notation used for EdGB. The simplest potential CTCs are purely azimuthal orbits at fixed (t, r, θ) , generated by the Killing vector $\xi_{(\varphi)} = \partial_\varphi$. Such curves become timelike when $g_{\varphi\varphi}(r, \theta; \varepsilon_a, \varepsilon^2) < 0$, which in our Hartle-Thorne gauge can be written as

$$g_{\varphi\varphi}(r, \theta; \varepsilon_a, \varepsilon^2) = g_{\varphi\varphi}^{\text{Kerr}}(r, \theta; \varepsilon_a) + \varepsilon^2 \delta g_{\varphi\varphi}(r, \theta; \varepsilon_a), \quad (4.53)$$

where $g_{\varphi\varphi}^{\text{Kerr}} > 0$ outside the Kerr horizon and $\delta g_{\varphi\varphi}$ is the EdGB correction built from $\{A_0, B_0, C_0, A_2, B_2, C_2\}$ defined in Eq. (4.46). For fixed spin ε_a we define the azimuthal CTC threshold $\varepsilon_{\text{crit}}^{(\varphi)}(\varepsilon_a)$ as the smallest nonzero value of ε for which $g_{\varphi\varphi}$ vanishes somewhere outside the horizon as

$$\exists (r_*, \theta_*): \quad g_{\varphi\varphi}(r_*, \theta_*; \varepsilon_a, (\varepsilon_{\text{crit}}^{(\varphi)})^2) = 0, \quad r_* > r_+(\varepsilon_a), \quad (4.54)$$

and demanding the absence of azimuthal CTCs then yields the bound

$$0 \leq \varepsilon^2 \leq (\varepsilon_{\text{crit}}^{(\varphi)})^2(\varepsilon_a). \quad (4.55)$$

More general CTCs may be generated by helical combinations of the stationary and axial Killing vectors as discussed in Section II A.

Following that discussion, we find that helical CTCs are avoided whenever $g_{tt}(r, \theta; \varepsilon_a, \varepsilon^2) g_{\varphi\varphi}(r, \theta; \varepsilon_a, \varepsilon^2) - g_{t\varphi}^2(r, \theta; \varepsilon_a, \varepsilon^2) \leq 0$ for all $r \geq r_+(\varepsilon_a)$ and all θ . As for the azimuthal case, this condition defines a critical value $\varepsilon_{\text{crit}}^{(\text{hel})}(\varepsilon_a)$ via

$$\exists (r_*, \theta_*): \quad g_{tt} g_{\varphi\varphi} - g_{t\varphi}^2 \Big|_{(r_*, \theta_*; \varepsilon_a, \varepsilon_{\text{crit}}^{(\text{hel})2})} = 0, \quad r_* > r_+(\varepsilon_a), \quad (4.56)$$

and demanding the absence of helical CTCs similarly implies $0 \leq \varepsilon^2 \leq (\varepsilon_{\text{crit}}^{(\text{hel})})^2(\varepsilon_a)$. Imposing that neither azimuthal nor helical CTCs appear outside the horizon leads to the combined CTC constraint

$$\varepsilon^2 \leq \varepsilon_{\text{CTC}}^2(\varepsilon_a), \quad \varepsilon_{\text{CTC}}^2(\varepsilon_a) \equiv \min \left((\varepsilon_{\text{crit}}^{(\varphi)})^2(\varepsilon_a), (\varepsilon_{\text{crit}}^{(\text{hel})})^2(\varepsilon_a) \right), \quad (4.57)$$

and using the definition of ε , this inequality can be rewritten as a bound on (α, β)

$$\frac{\alpha^2}{\tilde{\beta} \kappa M_*^2} \leq \varepsilon_{\text{CTC}}^2(\varepsilon_a). \quad (4.58)$$

For a canonical scalar with positive kinetic energy we require $\beta > 0$, so the allowed region in the (α, β) plane is

$$\beta > 0, \quad |\alpha| \leq \sqrt{\tilde{\beta} \kappa M_*^2 \varepsilon_{\text{CTC}}^2(\varepsilon_a)}, \quad (4.59)$$

which (for fixed mass and spin) restricts α to lie inside a wedge $|\alpha| \leq \alpha_{\text{max}}(\beta; \varepsilon_a)$ whose slope is controlled by $\varepsilon_{\text{CTC}}(\varepsilon_a)$, while the energy condition excludes the half-plane $\beta \leq 0$. We evaluate Eq. (4.59) numerically and show the result in Figure 6 for fixed black-hole mass $M/M_{\text{Pl}} = 10^3$ and when varying the equatorial angle, spin parameter, and EFT cutoff scale M_* . Since the bound is quadratic in α , we naturally obtain a parabolic shape of the allowed region, and the region inside the parabola is chronologically safe with no CTC formation. As in the case of the zero-charge

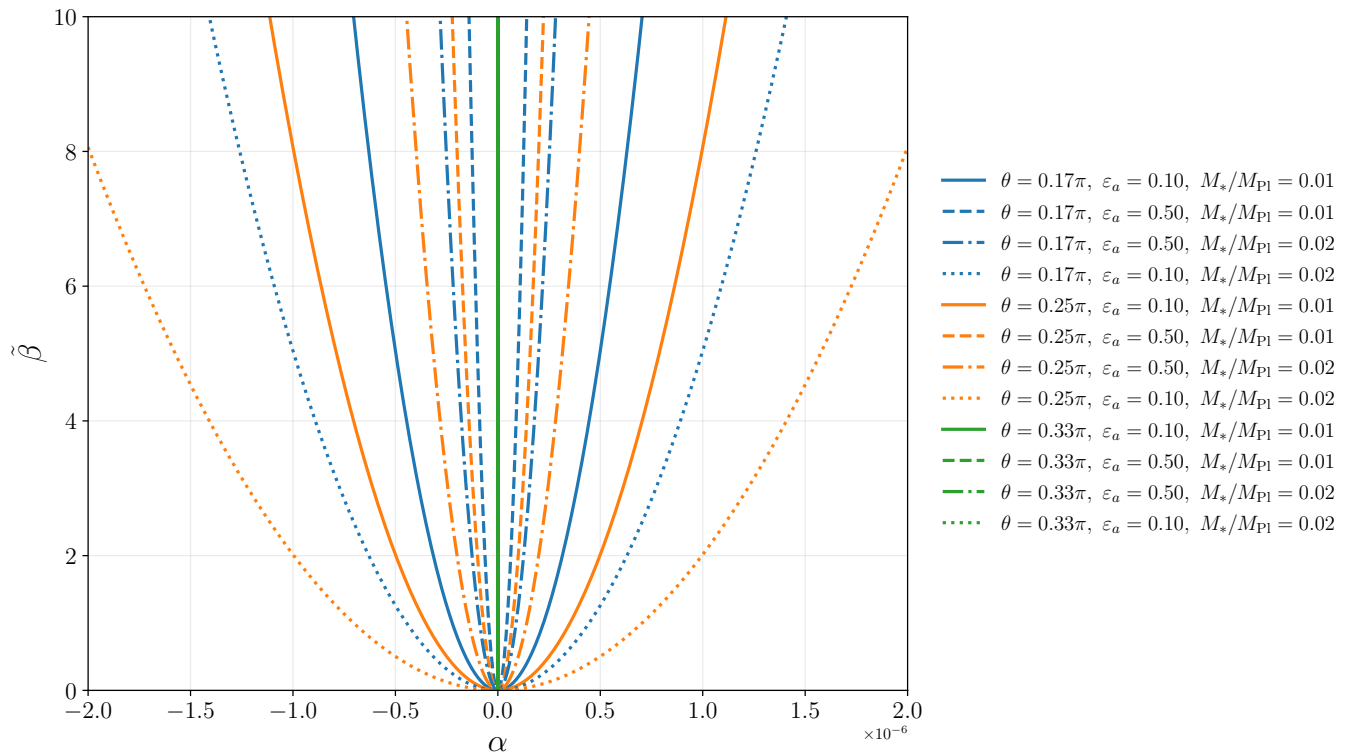


FIG. 6: CTC regions for non the EDGB model for different values of spin ε_a , equatorial angle θ and M_* when using $M = 1000M_{\text{Pl}}$. The region inside each described parabola is chronologically safe and shows no CTC.

k-essence case in Figure 4, the regions overlap for some choice of parameters, the dependence of the equatorial angle is strong; indeed, for $\theta = \pi/3$, the chronologically safe region is not resolvable in the Figure. Interestingly, the largest allowed region does not occur for the smallest θ ; instead, it occurs for $\theta = \pi/4$ and for the case of $M_*/M_{\text{Pl}} = 0.02$, the largest value we consider. Outside the allowed region, CTCs can form and the EFT is sick, which can leave an imprint in the quasinormal mode ringdown, as we show in the next section.

V. GRAVITATIONAL-WAVE ECHOES AS PROBES OF CAUSALITY

Gravitational-wave astronomy has provided a direct probe of the strong-field regime of gravity. Following a binary black hole merger, the remnant spacetime settles down to equilibrium through a sequence of damped oscillations known as quasi-normal modes (QNMs) [64–68]. These modes constitute the ringdown phase of the gravitational waveform and are determined entirely by the mass and spin of the final rotating black hole. In general relativity, the event horizon is perfectly absorbing: perturbations crossing it are lost, leading to a single, exponentially decaying signal with no delayed features. If, however, the near-horizon region is modified by new physics, such as quantum-gravitational effects or higher-derivative terms arising effective field theory (EFT) of gravity, the inner boundary condition may deviate from perfect absorption and become at least slightly reflective. In that case, part of the perturbation may reflect off some microscopic structure just outside the would-be horizon, forming a resonant cavity between the photon-sphere potential barrier and this reflective surface. Successive reflections within this cavity would then produce a train of gravitational-wave *echoes* which follow the primary ringdown, as was first investigated in for example [64, 69–71] in various contexts. The detection of gravitational-wave echoes remains an open but promising observational frontier.

Current LIGO-Virgo-KAGRA searches have uncovered no statistically significant evidence for echoes, with recent

upper limits on the time-domain amplitude set around 10^{-24} at 90% certainty [72]; however, several post-merger events show low-significance excess power consistent with echo-like residuals [68, 70, 73]. Echoes are intrinsically challenging to detect since they produce quasi-periodic, slowly damped signals with amplitudes which typically make up $\lesssim 10\text{--}20\%$ of the main ringdown, requiring matched-filtering templates that incorporate spin-dependent phase shifts and possible mode mixing [74, 75]. Nevertheless, next-generation detectors such as the Einstein Telescope, Cosmic Explorer, and LISA are expected to push echo sensitivity well into the theoretically interesting regime, with the capability to detect echo time delays and angular modulations with percent-level precision [76, 77]. Such observations would provide a direct probe of near-horizon structure, quantum-gravity corrections, and the causal properties of modified-gravity EFTs. Each echo represents a round trip of the tensor perturbation inside the cavity formed between the reflective surface and the photon sphere. The approximate time interval between successive echoes is

$$t_{\text{echo}} \simeq \frac{r_+^2 + a^2}{\kappa_s} \ln\left(\frac{r_+}{\delta}\right), \quad (5.1)$$

where r_+ is the outer horizon radius, κ_s is the surface gravity, and δ is the proper distance between the reflective surface and the classical horizon. In the GR limit we have $\delta \rightarrow 0$, and the horizon becomes perfectly absorbing, $t_{\text{echo}} \rightarrow \infty$, and the echo sequence disappears, recovering the pure Kerr QNM ringdown. In the frequency domain, repeated reflections generate a discrete comb structure in the power spectral density (PSD) with characteristic spacing

$$\Delta\omega \simeq \frac{2\pi}{t_{\text{echo}}}, \quad (5.2)$$

so the echo delay and the spectral spacing both encode information about the microscopic properties of the near-horizon region, including the causal structure.

In an EFT extension of GR, higher-curvature and higher-derivative operators modify the geometry and the effective potential governing perturbations; typical examples include terms such as R^2 , $R_{\mu\nu}R^{\mu\nu}$, $R\Box R$, as well as scalar–tensor couplings. To first order in the EFT couplings λ_i , these corrections alter the tortoise coordinate near the horizon as

$$r_* = r_*^{(\text{Kerr})} + \Delta r_*^{(\text{EFT})}(\lambda_i), \quad (5.3)$$

thereby shifting the echo delay,

$$t_{\text{echo}} = t_{\text{echo}}^{(\text{Kerr})} + 2\Delta r_*^{(\text{EFT})}. \quad (5.4)$$

Consistency of the EFT requires that perturbations remain hyperbolic and causal [78, 79]

$$v_{\text{signal}}^2 \leq 1, \quad \mathcal{N}(r, \theta; \lambda_i) > 0, \quad (5.5)$$

where \mathcal{N} ensures the absence of CTCs. If the inequalities (5.5) are violated, the tortoise coordinate becomes ill-defined, t_{echo} diverges, and the echo pattern is destroyed. In scalar–tensor EFTs, the propagation of perturbations is controlled not only by the background metric $g_{\mu\nu}$ but by the effective metric for perturbations which depends on the linearised equations of motion. In the high–frequency (WKB) limit any perturbation Ψ behaves as $\Psi \sim e^{i\theta}$, with wave–vector $k_\mu = \nabla_\mu \theta$, and the highest–derivative part of the field equation defines a characteristic condition of the form $P^{\mu\nu}(x)k_\mu k_\nu = 0$. When $P^{\mu\nu}$ can be interpreted as an effective inverse metric $g_{\text{eff}}^{\mu\nu}$, the perturbation propagates along null cones defined through $g_{\text{eff}}^{\mu\nu}$. The signal velocity measured by a local observer is then the speed of these null rays in the observer’s orthonormal frame, and provides the covariant definition of the group velocity in any curved background. For quadratic k–essence with $K(X) \sim X + \beta X^2$, the scalar sector has an effective metric $Z^{\mu\nu} = K_X g^{\mu\nu} + K_{XX} \partial^\mu \phi \partial^\nu \phi$, so the scalar mode propagates with a sound speed c_s determined by the local value of $X = -(\nabla\phi)^2/2$. In the EdGB model, the Gauss-Bonnet coupling similarly modifies the effective metric of the spin–2

sector, so gravitons propagate on a tensor effective metric $g_{\text{eff}}^{\mu\nu} = g^{\mu\nu} + \delta g^{\mu\nu}(\phi, \nabla\phi, R)$. Our causality condition $v_{\text{signal}}^2 \leq 1$ is therefore a coordinate-independent constraint on the opening of these EFT light cones.

In the rest of this section, we present the formation of echoes in a systematic way: starting with the quasinormal-mode ringdown for the Kerr system with a probe scalar, we introduce the notion of echoes by placing an artificial boundary near the outer horizon, showing the formation of the echo cavity for a deformed Kerr system. Following this, we show the echo formation in the k-essence model in the presence of CTCs. Qualitatively, the chronological horizon for both the zero charge (stealth solution) and the non-zero charge case have similar behaviour except from the small deformation due to the charge parameter. For brevity and simplicity, we consider only the zero-charge case. Finally, we discuss echo formation in the EdGB model and show explicitly how the presence of a chronological horizon modifies the structure of the QNM ringdown due to the presence of a cavity. When all causality conditions are satisfied, the chronology horizon ceases to exist and we reobtain standard QNM ringdown. The key distinctions between standard Kerr ringdown and the echo response in EFT-modified gravity can be categorised as tabulated in Table II.

Scenario	Boundary condition	Signal type	Causality
Kerr (GR)	Perfect absorption ($\delta = 0$)	Single QNM ringdown	Fully causal
Modified near-horizon (EFT)	Partial reflection	Echo train with shifted delay	Causal within bounds
EFT beyond causal bound	CTC region exists	Echoes diverge or vanish	Acausal

TABLE II: Scenarios under consideration, their causality, and their expected ringdown signals.

A. Kerr ringdown with an artificial boundary

Before introducing more complicated scalar-tensor theory, it is useful to recall the case of a minimally coupled scalar field on a Kerr black hole background without backreaction. In this subsection, we derive the scalar master equation in the Kerr geometry, identify the corresponding one-dimensional potential, and show how the ringdown waveform is determined by the QNMs of this potential. The Kerr metric in Boyer-Lindquist coordinates (t, r, θ, φ) can be written as

$$ds^2 = -\frac{\Delta}{\rho^2} (dt - a \sin^2 \theta d\varphi)^2 + \frac{\rho^2}{\Delta} dr^2 + \rho^2 d\theta^2 + \frac{\sin^2 \theta}{\rho^2} ((r^2 + a^2) d\varphi - a dt)^2, \quad (5.6)$$

where $\Delta = r^2 - 2GMr + a^2$, $\rho^2 = r^2 + a^2 \cos^2 \theta$. Moreover, a minimally coupled scalar field obeys the Klein-Gordon equation which we write as

$$\square_g \Phi = \frac{1}{\sqrt{-g}} \partial_\mu (\sqrt{-g} g^{\mu\nu} \partial_\nu \Phi) = 0, \quad \sqrt{-g} = \rho^2 \sin \theta, \quad (5.7)$$

on the Kerr background. For the scalar, we use a separable ansatz of the form

$$\Phi(t, r, \theta, \varphi) = e^{-i\omega t} e^{im\varphi} S_{lm}(\theta) R_{lm\omega}(r), \quad (5.8)$$

which we plug in to Eq. (5.7). For the Kerr metric, the angular and radial dependence separate, and we obtain the following system of equations

$$\frac{1}{\sin \theta} \frac{d}{d\theta} \left(\sin \theta \frac{dS_{lm}}{d\theta} \right) + (a^2 \omega^2 \cos^2 \theta - m^2 / \sin^2 \theta + \lambda_{lm}) S_{lm} = 0, \quad (5.9)$$

$$\frac{d}{dr} \left(\Delta \frac{dR_{lm\omega}}{dr} \right) + \left(\frac{K^2}{\Delta} - a^2 \omega^2 - \lambda_{lm} \right) R_{lm\omega} = 0, \quad (5.10)$$

where we have defined $K(r) = (r^2 + a^2)\omega - am$, and where λ_{lm} is the separation constant associated with the scalar spheroidal harmonics S_{lm} . We note specifically that Eq. (5.10) is the scalar ($s = 0$) radial Teukolsky equation of the Kerr geometry. It is useful to work in tortoise coordinates r_* defined as

$$\frac{dr_*}{dr} = \frac{r^2 + a^2}{\Delta}, \quad (5.11)$$

which maps the outer horizon $r \rightarrow r_+$ to $r_* \rightarrow -\infty$ and spatial infinity $r \rightarrow \infty$ to $r_* \rightarrow +\infty$. We also remove the first derivative from the radial equation by the field redefinition $R_{lm\omega}(r) = f(r) \Psi_{lm\omega}(r_*)$, with $f(r)$ chosen such that the coefficient of $d\Psi/dr_*$ vanishes. Then, by using the identity

$$\frac{d}{dr} = \frac{\Delta}{r^2 + a^2} \frac{d}{dr_*}, \quad (5.12)$$

and substituting it into Eq. (5.10), we find an equation of the form

$$\frac{d^2 \Psi_{lm\omega}}{dr_*^2} + [\omega^2 - V_{\text{Kerr}}(r; \omega, l, m)] \Psi_{lm\omega} = 0, \quad (5.13)$$

where the effective Kerr potential V_{Kerr} is given by

$$V_{\text{Kerr}}(r; \omega, l, m) = \omega^2 - \frac{\Delta f'' + A(r)f' + Q(r)f}{\Delta f}, \quad (5.14)$$

with $A(r)$ and $Q(r)$ determined by the metric functions and the original coefficient $Q_{\text{orig}}(r) = K^2/\Delta - a^2\omega^2 - \lambda_{lm}$, which is generally lengthy. Crucially, V_{Kerr} depends on (ω, l, m) and is not a simple Regge–Wheeler potential, reflecting the well-known structure of scalar perturbations in the Kerr geometry.¹¹

The physical quasinormal modes are defined by solutions of Eq. (5.13) which are purely ingoing at the horizon, and purely outgoing at infinity, i.e. we look for solutions of the form

$$\Psi_{lm\omega} \sim e^{-i\omega r_*}, \quad r_* \rightarrow -\infty; \quad \Psi_{lm\omega} \sim e^{+i\omega r_*}, \quad r_* \rightarrow +\infty, \quad (5.15)$$

which is satisfied only for certain discrete complex frequencies $\omega = \omega_{nlm}$ (where n labels the overtone); the set $\{\omega_{nlm}\}$ are the scalar quasinormal-mode frequencies of the Kerr black hole. A perturbation Φ with compact support will, at late times, be dominated by the fundamental QNM for each (l, m) ; therefore, the observed ringdown signal can be written as

$$h_{\text{Kerr}}(t) \simeq \sum_n A_n e^{-i\omega_{nlm}t} = \sum_n A_n e^{-\text{Im}\omega_{nlm}t} \cos(\text{Re}\omega_{nlm}t + \varphi_n), \quad (5.16)$$

where A_n and φ_n depend on the initial data. In practice, the sum is often truncated to the fundamental mode ($n = 0$), yielding the familiar damped sinusoid of the form

$$h_{\text{Kerr}}(t) \approx A_0 e^{-\gamma t} \sin(\omega_0 t + \phi_0), \quad \omega_0 \equiv \text{Re}(\omega_{0lm}), \quad \gamma \equiv -\text{Im}(\omega_{0lm}), \quad (5.17)$$

which is precisely what we use as the pure Kerr ringdown in the k -essence analysis; in the dS and AdS causal branches (no CTC, no reflective boundary conditions), the scalar field sees the same Kerr ringdown governed by the potential V_{Kerr} and the late-time waveform is still well approximated by the fundamental QNM above.

¹¹ For the purpose of illustrating the effect of a CTC-induced or EFT-induced reflective surface, we use the standard single-mode phenomenological ringdown model in which the dominant Kerr QNM is represented as a damped sinusoid with frequency and damping time given by the Echeverria fits [80, 81]. The echo waveform is constructed from the canonical geometric series of delayed and attenuated copies of this mode. This model has been widely used in the echo literature and captures the essential physics of near-horizon modifications.

B. Introducing echoes

We now introduce a deviation from the Kerr case in the previous subsection in a manner that mimics the effect of a k -essence CTC surface, or in fact any EFT-induced departure from perfect absorption at the horizon. Instead of imposing the standard boundary condition (5.15) at $r = r_+$, we place a partially reflective boundary at a proper distance δr such that $(\delta r - r)/r \ll 1$ outside the outer horizon. Concretely, we introduce a surface at

$$r_0 = r_+(1 + \epsilon), \quad \epsilon \ll 1, \quad (5.18)$$

and impose a mixed (Robin-type) boundary condition on the master field $\Psi_{lm\omega}$ at the corresponding tortoise coordinate position $r_{*0} = r_*(r_0)$. When $r \rightarrow r_+$ (or equivalently $r_* \rightarrow -\infty$), the effective potential for the scalar field satisfies $V_{\text{Kerr}}(r) \rightarrow 0$, and the master field behaves as a superposition of ingoing and outgoing plane waves as

$$\Psi_{lm\omega}(r_*) \simeq A_{\text{in}} e^{-i\omega r_*} + A_{\text{out}} e^{+i\omega r_*}, \quad (5.19)$$

where in the pure Kerr case one enforces purely ingoing behaviour ($A_{\text{out}} = 0$). Here, the modified inner boundary partially reflects the wave and we have

$$A_{\text{out}} = \mathcal{R} A_{\text{in}}, \quad \mathcal{R} = R e^{i\phi_R}, \quad 0 < R \leq 1, \quad (5.20)$$

where the reflection coefficient R and the phase shift ϕ_R encode the properties of the effective wall. In the limit $R \rightarrow 0$ we recover the Kerr horizon, and in the limit $R \rightarrow 1$ the wall becomes perfectly reflecting.

The scalar potential $V_{\text{Kerr}}(r)$ contains a barrier associated with the unstable photon orbit at $r = r_{\text{ph}}$. The region between the barrier peak and the reflective wall forms a cavity with partially reflecting walls in which waves can bounce multiple times before escaping to infinity. Let $r_*(r_{\text{ph}})$ denote the tortoise coordinate location of the barrier peak: the one-way travel time for a wavepacket between the barrier and the wall is approximately $r_*(r_{\text{ph}}) - r_*(r_0)$, where $r_*(r)$ is the radial tortoise coordinate defined in Eq. (5.11) with $\Delta = \Delta_r(r; \Lambda_{\text{eff}})$. In the tortoise coordinate, defined as

$$r_*(R) = \int^R dr \frac{r^2 + a^2}{\Delta_r(r; \Lambda_{\text{eff}})}, \quad (5.21)$$

the photon sphere and the reflective wall are located at $r_*(r_{\text{ph}})$ and $r_*(r_0)$, respectively; in the EFT interpretation, the wall is provided by the onset of the CTC region, so that we may set $r_0 \equiv r_{\text{CTC}}$, $r_*(r_0) \equiv r_*(r_{\text{CTC}})$. The region between these two radii in r_* is the echo cavity

$$\Delta t \simeq 2 [r_*(r_{\text{ph}}) - r_*(r_0)]. \quad (5.22)$$

Because $r_*(r_0)$ diverges logarithmically as $r_0 \rightarrow r_+$, the delay Δt depends on the microscopic displacement ϵ and can be macroscopic even when the boundary lies Planck distances outside of the horizon. At spatial infinity ($r_* \rightarrow +\infty$) the scalar potential also vanishes and the outgoing-wave condition remains unchanged

$$\Psi_{lm\omega}(r_*) \sim B_{\text{out}} e^{+i\omega r_*}, \quad (5.23)$$

and the only departure from the pure Kerr problem in this case therefore lies in replacing the ingoing horizon condition by the partially reflective condition at r_0 .

Echo waveform in the time domain

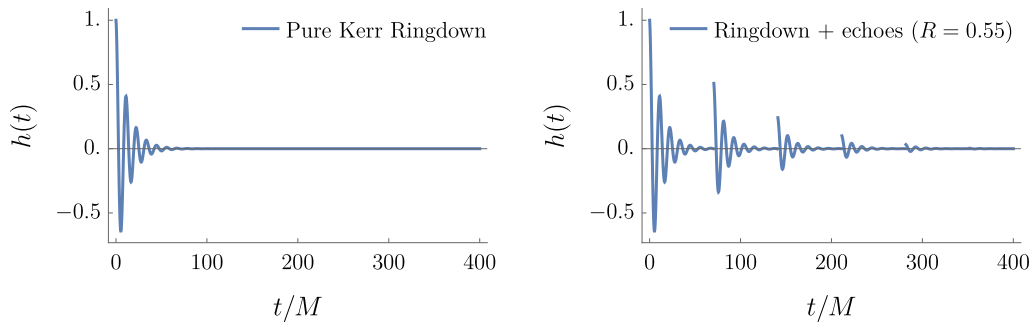


FIG. 7: Comparison between the pure Kerr ringdown (left) and echo-modification with reflectivity $R = 0.55$ (right).

Let $h_{\text{Kerr}}(t)$ denote the pure Kerr ringdown associated with the fundamental QNM. The presence of the wall leads to repeated reflections, each producing a delayed and attenuated copy of the primary pulse. The resulting time-domain signal takes the schematic form

$$h_{\text{echo}}(t) = h_{\text{Kerr}}(t) + \sum_{n=1}^{\infty} R^n e^{in\phi_R} h_{\text{Kerr}}(t - n \Delta t), \quad (5.24)$$

with Δt given by Eq. (5.22). The integer n labels the number of round trips inside the cavity, and the factor R^n encodes the geometric suppression associated with partial reflection. The detailed shape of each echo inherits the structure of the Kerr potential barrier, while the spacing and relative phase encode the physics of the near-horizon boundary. In the k -essence and EdGB models, the wall position and phase receive explicit (α, β) -dependent corrections, modifying the echo timing and amplitude.

We now compare waveforms obtained from the scalar master equation (5.16) for the following cases

(i) pure Kerr ringdown, corresponding to a perfectly absorbing horizon, and

(ii) echo signal, obtained when a partially reflective surface is placed just outside the horizon;

for these examples, we use parameters to match the dominant $(\ell, m, n) = (2, 2, 0)$ mode of a Kerr black hole with spin $\varepsilon_a = 0.7$, in order to obtain effects which can be clearly seen by eye.

(i) Pure Kerr ringdown

The reference signal is the late-time response of a minimally coupled scalar perturbation in a pure Kerr geometry. The dominant mode is governed by the complex quasinormal frequency $\omega = \omega_R - i\omega_I$, for which we adopt the Echeverria fits [80, 81]

$$f = \frac{1 - 0.63(1 - \varepsilon_a)^{0.3}}{2\pi GM}, \quad Q = 2(1 - \varepsilon_a)^{-0.45}, \quad (5.25)$$

where $f = \omega_R/(2\pi)$ is the oscillation frequency and $Q = \omega_R/(2\omega_I)$ is the quality factor. For $a/(GM) = 0.7$ these yield

$$\omega_R GM \simeq 0.561, \quad \omega_I GM \simeq 0.081, \quad \tau/(GM) = \frac{1}{\omega_I} \simeq 12.3, \quad (5.26)$$

and the pure Kerr ringdown is therefore well approximated by the damped sinusoid

$$h_{\text{Kerr}}(t) = A_0 e^{-t/\tau} \cos(\omega_R t + \phi_0), \quad (5.27)$$

where A_0 and ϕ_0 encode the initial data. The first panel of Figure 7 shows this exponentially decaying sinusoidal signal, which we use to compare the modifications coming from the reflective boundary.

(ii) Artificial reflective boundary and echo formation

To model possible near-horizon structures arising from k -essence, EdGB, quantum-gravity effects, or CTC-induced walls, we replace the usual ingoing boundary condition at $r = r_+$ by a partially reflective surface as described in Eq. (5.18). The reflection is then characterised by a complex coefficient $\mathcal{R} = R e^{i\phi_R}$, $0 < R < 1$, as defined in Eq. (5.20). As such, waves travel between the photon-sphere barrier at $r = r_{\text{ph}}$ and the wall at r_0 which forms a cavity. The round-trip travel time in Eq. (5.22) then reads

$$\Delta t = 2[r_*(r_{\text{ph}}) - r_*(r_0)] \simeq 70.4 GM, \quad (5.28)$$

which we evaluated using the Kerr tortoise coordinate for $a/(GM) = 0.7$ and $\varepsilon \ll 1$. Each cavity traversal produces a delayed and attenuated copy of the primary Kerr pulse, and the resulting waveform is the echo series defined in Eq. (5.24). In Figure 7, we display the pure Kerr case (left panel) alongside the echo signals obtained from choosing $R = 0.55$, $\phi_R = 0.3$, $N = 7$ (right panel), which have been tuned to ensure visibility. The second panel shows the echo-modified signal: after the initial Kerr-like pulse, the waveform features a series of secondary pulses separated by $\Delta t \simeq 70 GM$, each with an amplitude smaller than the previous by a factor of $R^n e^{-n\Delta t/\tau}$. These echoes encode the location, reflectivity, and phase structure of the near-horizon boundary, which in the case of the EFT models discussed later become functions of the model parameters. Therefore, echo formation is a sensitive probe of horizon-scale microphysics.

Zero-charge k -essence and Kerr-(A)dS Geometry

We consider the shift-symmetric k -essence model defined in Eq. (3.3) and consider the zero-charge branch defined by $P_X(X_0) = \alpha + 2\beta X_0 = 0$, $X = X_0 = \text{constant}$. Since the scalar equation of motion is automatically satisfied on this branch and the Einstein equations becomes that of Eq. (3.24), the background geometry is *exactly* Kerr-(A)dS (3.25). We note that the sign of (α, β) determines the branch of the solution; in fact, we have three options

- dS branch: $\beta > 0$, $\alpha > 0 \Rightarrow \Lambda_{\text{eff}} > 0$. Satisfies WEC/DEC; no CTCs appear.
- AdS causal branch: $\beta < 0$, $\alpha < 0$ and $|\alpha^2/\beta| < |\alpha^2/\beta|_{\text{crit}}$. No CTC surface outside the horizon.
- AdS acausal branch: $\beta < 0$, $\alpha < 0$ and $|\alpha^2/\beta| > |\alpha^2/\beta|_{\text{crit}}$. A CTC surface forms at $r_{\text{CTC}} > r_+$,

which are expressed in a different way in Table I; only the AdS acausal branch generates echoes.

As discussed previously, azimuthal CTCs appear when the azimuthal metric component becomes negative¹² $g_{\varphi\varphi}(r, \theta) < 0$, which we express through Eq. (3.25) as

$$g_{\varphi\varphi} = \frac{\sin^2 \theta}{\rho^2 \Xi^2} [\Delta_\theta (r^2 + a^2)^2 - a^2 \sin^2 \theta \Delta_r] \equiv \frac{\sin^2 \theta}{\rho^2 \Xi^2} \mathcal{N}(r, \theta; \Lambda_{\text{eff}}), \quad (5.29)$$

and the CTC condition becomes $\mathcal{N}(r, \theta; \Lambda_{\text{eff}}) < 0$. Therefore, the CTC surface r_{CTC} can be defined from the condition that $\mathcal{N}(r_{\text{CTC}}, \theta; \Lambda_{\text{eff}}) = 0$ for $r_{\text{CTC}} > r_+$. In the acausal AdS branch, r_{CTC} acts as a reflective inner wall such that the probe scalar has the property $\Psi(r_*) = 0$ for $r_* \leq r_*(r_{\text{CTC}})$, which creates the partially reflective trapping region. Since $P_X(X_0) = 0$, perturbations of the k -essence scalar are strongly coupled and do not propagate. To probe the

¹² For simplicity, we consider only azimuthal CTCs and leave the helical case for future work.

geometry, we instead consider a minimally coupled test scalar Φ on top of the acausal background such that

$$\square_g \Phi = 0. \quad (5.30)$$

We solve the equation of motion by considering the separable form $\Phi = e^{-i\omega t} e^{im\varphi} S(\theta) R(r)$, after which the radial equation becomes

$$\frac{d}{dr} \left(\Delta_r \frac{dR}{dr} \right) + \left(\frac{K^2}{\Delta_r} - \lambda - a^2 \omega^2 \right) R = 0, \quad K(r) = (r^2 + a^2) \omega - am. \quad (5.31)$$

After transforming to the tortoise coordinate and removing first derivatives as in previous sections, we obtain the Schrödinger-type master equation which reads

$$\frac{d^2 \Psi}{dr_*^2} + (\omega^2 - V_{\text{eff}}(r)) \Psi = 0, \quad (5.32)$$

and since echo formation only depends on the photon-sphere barrier and the presence or absence of the inner wall, a Kerr-like phenomenological potential reproduces the correct qualitative behaviour. The echo cavity is the region between the photon sphere and the CTC surface, the radial size of which can be written as $L_{\text{cav}} = r_*(r_{\text{ph}}) - r_*(r_{\text{CTC}})$, and the echo spacing is therefore equal to the period $\Delta t_{\text{echo}} = 2L_{\text{cav}}$. Physically, echoes arise because the wave is trapped between two partially reflecting structures: the photon-sphere barrier and an inner wall. The photon-sphere radius r_{ph} is defined geometrically as the radius of an unstable circular null orbit. In the one-dimensional Schrödinger-type radial problem, the relevant scattering barrier is set by the maximum of the effective potential, located at $r = r_{\text{peak}}$ (typically close to r_{ph}), defined by

$$V'_{\text{eff}}(r_{\text{peak}}) = 0, \quad V''_{\text{eff}}(r_{\text{peak}}) < 0. \quad (5.33)$$

In the eikonal (large- ℓ) limit one has $r_{\text{peak}} \simeq r_{\text{ph}}$. The tortoise location $r_*(r_{\text{peak}})$ therefore sets the outer edge of the echo cavity. The inner edge is provided by the EFT-induced onset of CTCs, which we model as a partially reflective wall at $r_0 \equiv r_{\text{CTC}}$ placed just outside the horizon,

$$r_{\text{CTC}} = r_+(1 + \epsilon), \quad \epsilon \ll 1. \quad (5.34)$$

The cavity is thus the interval $r_*(r_{\text{CTC}}) < r_* < r_*(r_{\text{peak}})$, and the corresponding echo delay is approximately twice the one-way travel time across it as in the case of the artificial barrier. Moreover, since the effective cosmological constant Λ_{eff} is a combination of α and β , an observed echo spacing determines the k-essence parameter combination

$$\frac{\alpha^2}{\beta} = \frac{4}{\kappa} \Lambda_{\text{eff}}(\Delta t_{\text{echo}}; a, \theta). \quad (5.35)$$

Since Λ_{eff} appears explicitly in the metric functions, it can be said to be an implicit function of an observed gravitational-wave echo $\Delta t_{\text{echo}} \neq 0$; therefore, in order to infer Λ_{eff} from Δt_{echo} , we first construct the expression for the time delay below and invert it numerically in our numerical analysis. On the other hand, for sufficiently negative Λ_{eff} , the metric develops closed timelike curves outside the horizon. As discussed previously, the azimuthal CTC condition is encoded in

$$\mathcal{N}(r, \theta; \Lambda_{\text{eff}}) = \Delta_\theta (r^2 + a^2)^2 - a^2 \sin^2 \theta \Delta_r(r; \Lambda_{\text{eff}}), \quad (5.36)$$

with CTCs arising wherever $\mathcal{N} < 0$. The outermost CTC surface at a given polar angle θ is defined by $\mathcal{N}(r_{\text{CTC}}, \theta; \Lambda_{\text{eff}}) = 0$, $r_{\text{CTC}} > r_+$. Inside this radius the azimuthal (and helical) Killing directions become timelike, and the spacetime is

causally pathological. From the point of view of the wave equation (5.32), this surface must therefore be treated as an inner reflecting boundary, and classical waves cannot be continued into the CTC region.

To compute the echo time delay, we work in the geometric-optics limit of the master equation (5.32). Locally, the wave behaves as a superposition of ingoing and outgoing WKB rays as

$$\Psi(r_*) \sim A_{\pm}(r_*) \exp[\pm i\omega r_*], \quad (5.37)$$

for which the radial phase is $S(r_*) = \pm\omega r_*$ and the WKB dispersion relation reads

$$k_{r_*}^2 = \omega^2 - V_{\text{eff}}(r_*). \quad (5.38)$$

In the high-frequency limit, or in regions where V_{eff} varies slowly, the wave packets propagate along characteristics which satisfy

$$\frac{dr_*}{dt} = \pm 1, \quad (5.39)$$

corresponding to null characteristics in the (t, r_*) plane. This relation simply states that in tortoise coordinates, the group velocity of the ingoing and outgoing modes is ± 1 . Furthermore, the coordinate time Δt_{in} for a one-way trip from r_{ph} to r_{CTC} is obtained by integrating (5.39):

$$\Delta t_{\text{in}} = \int_{r_*(r_{\text{ph}})}^{r_*(r_{\text{CTC}})} dt = \int_{r_*(r_{\text{ph}})}^{r_*(r_{\text{CTC}})} \frac{dr_*}{dr_*} = r_*(r_{\text{ph}}) - r_*(r_{\text{CTC}}). \quad (5.40)$$

Consider now a wave packet localized near the photon sphere r_{ph} that propagates inward, reflects off the CTC surface at r_{CTC} , and returns to the photon sphere region. The same time is required for the return trip (from the CTC wall back to the photon sphere). Thus, the *round-trip* time takes the same form as for the Kerr case and we again define the echo cavity length in tortoise coordinate as $L_{\text{cav}} \equiv r_*(r_{\text{ph}}) - r_*(r_{\text{CTC}})$, so that $\Delta t_{\text{echo}} = 2L_{\text{cav}}$. Therefore, the echo spacing is

$$\Delta t_{\text{echo}} = 2 \int_{r_{\text{CTC}}}^{r_{\text{ph}}} \frac{r^2 + a^2}{\Delta_r(r; \Lambda_{\text{eff}})} dr, \quad (5.41)$$

where the integration limits are determined by the geometry through $\mathcal{N}(r_{\text{CTC}}, \theta; \Lambda_{\text{eff}}) = 0$, $V'_{\text{eff}}(r_{\text{ph}}) = 0$, where it should be understood that the dependence on the k -essence parameters (α, β) enters only through Λ_{eff} . Given an observed non-zero Δt_{echo} , this expression can be numerically inverted to find Λ_{eff} .

The physically allowed region must also respect hyperbolicity and CTC absence; typically, one requires $P_X > 0$ and $P_X + 2XP_{XX} > 0$, and the no-CTC condition $\mathcal{N}(r, \theta; \Lambda_{\text{eff}}) \geq 0$ outside the horizon (see Section III). If the inferred α/β ratio violates these theoretical bounds, the EFT breaks down at that point. We show this behaviour in Figure 8 for two cases: with and without CTCs.

C. Echoes in EdGB

We outline now how to obtain the echo waveforms used in the numerical solutions for the EdGB model, using the Kerr-HT solution in Sec. IV. This parallels the discussion of Sec. V (and our k -essence analysis), but now the location of the reflective surface is determined dynamically by the EdGB CTC conditions in the backreacted geometry. We work with the perturbative EdGB expansion (4.3) as before. Throughout this section, we enforce the scalar energy condition $\beta > 0$. As discussed in Sec. IV C, the onset of CTCs outside the outer horizon constitutes a consistency constraint on ε^2 . At fixed (ε_a, θ) we define the critical couplings $\varepsilon_{\text{crit}}^{(\varphi)}(\varepsilon_a, \theta)$ and $\varepsilon_{\text{crit}}^{(\text{hel})}(\varepsilon_a, \theta)$ by the first appearance of

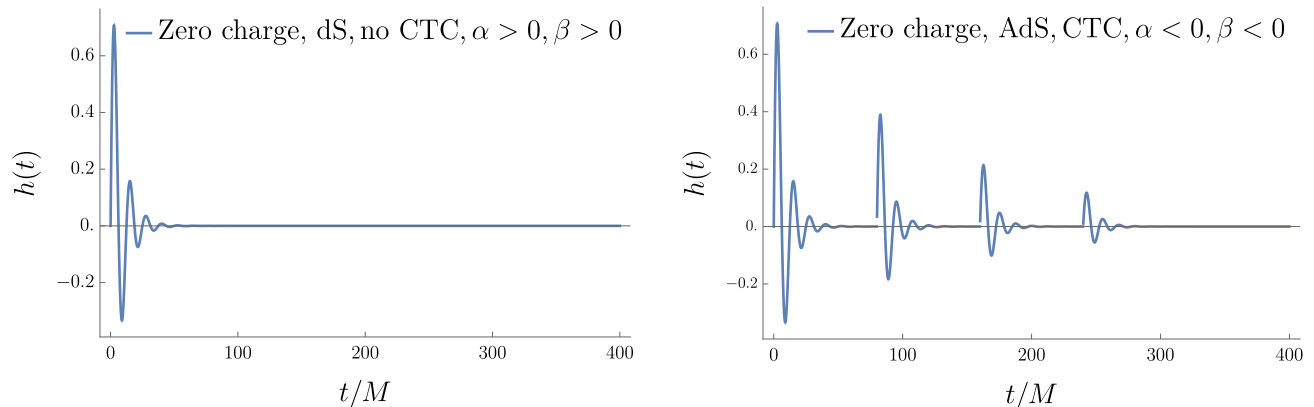


FIG. 8: Qualitative comparison of the zero-charge k-essence model. Left panel: Kerr-dS branch. This case has $\Lambda_{\text{crit}}(GM)^2 \ll 1$, satisfies the WEC and DEC and shows no CTC region.. Right panel: Kerr-AdS branch with CTC bound violated.

azimuthal or helical CTCs as defined for EdGB in Eq. (4.57).

For ε^2 smaller than this critical value, the geometry is causally well behaved outside the horizon and the ringdown is Kerr-like (up to perturbative EdGB corrections). For ε^2 larger than this value, CTC surface forms at some radius $r_{\text{CTC}}(\varepsilon_a, \theta)$ outside r_+ , and the wave problem must be modified accordingly. When the combined constraint (4.57) is violated, the spacetime region $r < r_{\text{CTC}}$ is causally pathological and the classical initial value problem for perturbations ceases to be well posed. In our phenomenological treatment, this is implemented by excising the CTC region and imposing an inner boundary condition at $r = r_{\text{CTC}}$. Equivalently, the CTC surface behaves as an effective “wall” which reflects perturbations back toward the photon-sphere barrier. This is the precise analogue of the near-horizon reflective surface introduced in Sec. V A for modelling generic EFT/quantum modifications, except that here the wall location is fixed by the EdGB causal structure.

Echo cavity and echo time delay

To estimate the echo spacing, we work in the geometric-optics limit of the master equation. The echo cavity is the region between the photon-sphere barrier and the inner wall at r_{CTC} . Denoting by $r_{\text{ph}}(\varepsilon_a)$ the (prograde) equatorial photon orbit radius of Kerr, the round-trip echo time delay is approximated by twice the tortoise-coordinate separation between r_{ph} and r_{CTC} , defined as in Eq. (5.22) with $r_*(r_0) \rightarrow r_*(r_{\text{CTC}})$, and we use the tortoise coordinate as in Eq. (5.11) so that

$$\Delta t_{\text{echo}} \simeq 2 \int_{r_{\text{CTC}}}^{r_{\text{ph}}} \frac{r^2 + a^2}{\Delta(r)} dr. \quad (5.42)$$

This describes the dominant logarithmic sensitivity to the wall location whenever r_{CTC} lies close to the outer horizon. Using the Kerr tortoise coordinate is conservative in the sense that it isolates the echo physics to the presence or absence of the CTC wall, while treating EdGB corrections to the propagation potential as subleading in our phenomenological waveform model.¹³

Ringdown model and echo waveform

We model the primary ringdown as the dominant Kerr QNM represented by the damped sinusoid in Eq. (5.17) with

¹³ A more complete treatment would solve the spin-2 Teukolsky problem on the EdGB-corrected background and extract the modified barrier and phase shifts; this is beyond our present scope.

$\gamma \rightarrow \tau^{-1}$ where (ω_R, τ) are determined by standard fitting formulae for the fundamental $(\ell, m, n) = (2, 2, 0)$ mode as functions of ε_a (e.g. the Echeverria fits used in Sec. V A). When the causal bound (4.57) is satisfied, we take the waveform to be pure ringdown (up to small EdGB corrections to the QNM parameters) as

$$\varepsilon^2 \leq \varepsilon_{\text{CTC}}^2(\varepsilon_a, \theta) \quad \Rightarrow \quad h(t) \simeq h_{\text{Kerr}}(t). \quad (5.43)$$

When the bound is violated and a wall forms at r_{CTC} , part of the outgoing radiation trapped between the photon-sphere barrier and the wall returns to infinity after each round trip, producing an echo train. We model this by the standard geometric series of delayed, attenuated copies of the primary ringdown defined in Eq. (5.24). In practice the sum is truncated at some $n = N$ when the amplitude becomes negligible:

$$h_{\text{echo}}(t) \approx h_{\text{Kerr}}(t) + \sum_{n=1}^N R^n h_{\text{Kerr}}(t - n\Delta t_{\text{echo}}). \quad (5.44)$$

Thus the EdGB parameters (α, β) enter the echo waveform through $\varepsilon^2 = \alpha^2/(\tilde{\beta}\kappa M_*^2)$, $r_{\text{CTC}}(\varepsilon_a, \theta; \varepsilon^2)$, and $\Delta t_{\text{echo}}(\varepsilon_a, \theta; \varepsilon^2)$, through which upper limits on echoes from gravitational-wave measurements of the ringdown can provide constraints on the model parameters, as well as the causal behaviour of the geometry. In Eq. (5.44), R is an effective reflection coefficient for the CTC wall (and phase shifts can be included by $R^n \rightarrow R^n e^{in\phi_R}$). In this model, the time-domain features include initial exponentially damped oscillation at the Kerr QNM frequency ω_R with damping time τ , followed by a sequence of pulses centered near $t \simeq n\Delta t_{\text{echo}}$ that carry the same characteristic QNM oscillations but with amplitudes suppressed as R^n . Thus the EdGB parameters (α, β) enter the echo waveform through the effective coupling ε and the induced cavity scale, i.e. through $r_{\text{CTC}}(\varepsilon_a, \theta; \varepsilon^2)$ and the corresponding round-trip delay $\Delta t_{\text{echo}}(\varepsilon_a, \theta; \varepsilon^2)$. Figure 9 illustrates the resulting transition. When CTCs are absent (blue dashed), the waveform is a single Kerr-like ringdown which decays smoothly to zero with no late-time structure. When CTCs are present (red solid), the early-time signal is still governed by the primary Kerr mode, but after a delay of order Δt_{echo} the first echo appears, followed by subsequent echoes at approximately regular intervals and with progressively decreasing amplitudes, consistent with the geometric-series suppression $\propto R^n$. Increasing ε^2 past the causal threshold triggers the formation of the effective wall at r_{CTC} and reduces the separation between the wall and the photon-sphere barrier at r_{ph} , thereby modifying Δt_{echo} and turning on the echo contribution itself.

VI. DISCUSSION & OUTLOOK

The analysis presented here is based on the idea of geometric causality where the causal structure encoded directly in the spacetime metric, and we diagnosed the spacetime by considering the signs of the azimuthal metric component $g_{\varphi\varphi}$, with $g_{\varphi\varphi} < 0$ signalling the emergence of closed timelike curves, and we further used a gauge-invariant criterion defined in Sec. II A. This approach examines how backreaction from different scalar sectors modifies the metric itself and, consequently, the location of the chronology horizon. As discussed in the Introduction, the Raychaudhuri equation implies that as long as the standard energy conditions hold, the null generators which form the chronology horizon typically develop strong focusing, making the boundary unstable. The same effect appears in geodesic deviation as exponential separation of nearby trajectories, making the effective Lyapunov exponent grow close to the CTC boundary.¹⁴ Causality in this sense is a global, coordinate-invariant property of the geometry and does not depend on the microscopic propagation of specific fields. By contrast, in the de Rham–Gabadadze–Tolley (dRGT) (see for example [17, 22, 32]) and more general effective-field-theory (EFT) frameworks [16, 21, 26, 27], causality is defined at

¹⁴ This does not automatically violate the Maldacena–Shenker–Stanford (MSS) bound [82]; instead, the analyticity assumptions used to derive it generally does not hold and so the bound itself does not apply. However, if the CTC pathology is hidden by a horizon and the boundary thermal state is causal, the MSS bound should still hold; this represents another possible diagnostic of causality.

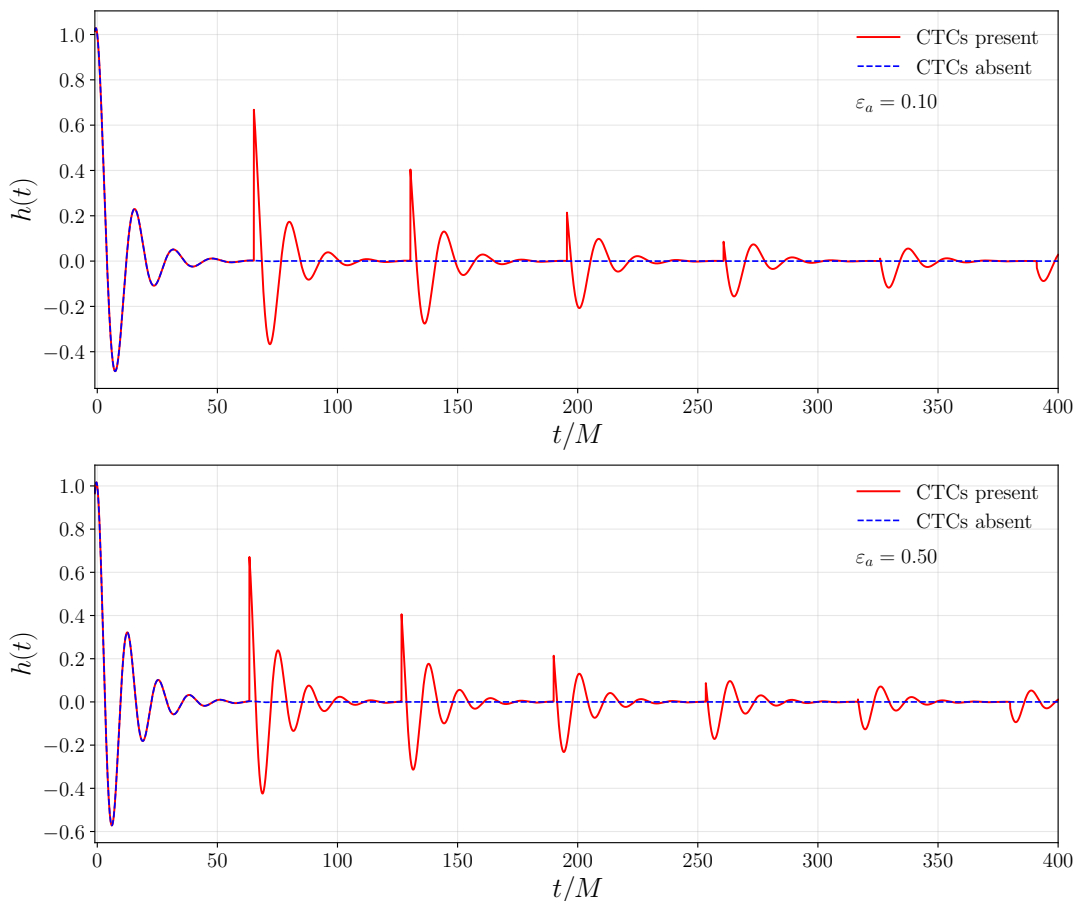


FIG. 9: Echo pattern for the EDGB model with and without CTCs.

the field-theoretic level through the principal component of the equations of motion for perturbations. In this approach, the causal cones governing signal propagation are determined not by $g_{\mu\nu}$ but by an effective metric constructed from the background fields and their derivatives. Violations of causality in this language appear as loss of hyperbolicity, superluminal propagation with respect to the effective Minkowski lightcone, or nonlinear shock formation. The causal structure of the field equations therefore need not coincide with the geometric light cones of the background spacetime.

The approach developed in this work bridges these two notions: by treating scalar backreaction perturbatively, we explicitly show how changes in the underlying geometry through the metric component $g_{\varphi\varphi}$ translate into deformations of the causal domains that would, in a field-theoretic setting, correspond to shifts in the effective cone. In the case of a minimally coupled scalar, the correction to $g_{\varphi\varphi}$ is geometric and isotropic, which offers partial chronology protection without altering the characteristics of the field. In the k-essence and EdGB extensions, the same perturbative framework lets us describe both geometric deformation of the metric as well as modification of the effective propagation cones through higher-derivative terms. In this sense, the present method provides a geometric counterpart to the principal component analysis. The main novelty of this approach is that it offers a perturbative and analytic treatment of causality diagnosis which remains geometric while being applicable across different scalar-tensor theories beyond the examples considered here. Unlike previous studies based on field-theoretic hyperbolicity, this method takes to account how backreaction alters the spacetime metric and the global causal structure. Furthermore, it can be considered a classical counterpart of the de Rham causality analysis, in which the effective cone deformation is encoded geometrically through $g_{\varphi\varphi}$ rather than through a field-dependent principal symbol.

Despite the fact that our approach remains perturbative and classical, one may encounter large scalar amplitudes or theories with higher-order corrections, nonlinearities, or strong coupling which invalidate the linear expansion consid-

ered here. Furthermore, because the analysis focuses on the metric sector, it cannot capture microcausality violations that arise purely from field-derivative interactions in dRGT or Horndeski theories. Finally, the infinite-cylinder geometry used as an example also restricts the discussion to an idealized, non-asymptotically flat configuration. Despite these limitations, the present analysis connects geometric and field-theoretic causality, and where geometric $g_{\phi\phi}$ criterion directly determines the background chronology horizon, the de Rham principal-component criterion governs the characteristics of perturbations on that same background. In the small-backreaction limit, both approaches reduce to the same light-cone structure, but as nonlinearities grow the two notions of causality can diverge. Nevertheless, the results presented here can be used to understand how modifications of the geometry affect the causal structure of the effective field theory, which may be used to construct a notion of causality and chronology protection which incorporates both geometric and microcausal effects. However, we have summarily ignored potential ghost modes in our example models.

To offer a more precise relation between the scattering-amplitude and geometric approach, we note that causality, analyticity, and unitarity in any Lorentz-invariant UV completion of gravity manifests itself through precise positivity constraints on the Wilson coefficients of the low-energy EFT. In the forward limit of the $2 \rightarrow 2$ scattering amplitude, these constraints reduce to the requirement that high-frequency gravitons experience a positive Shapiro time delay when propagating in a curved background. This fundamental relation may be summarised as

$$\text{microcausality} \Leftrightarrow \Delta t_{\text{Shapiro}} \geq 0 \Leftrightarrow \text{positivity of EFT Wilson coefficients},$$

and it is clear that the Shapiro time delay plays a dual role: it is simultaneously the eikonal-limit observable of the scattering amplitude and the geometric diagnostic of causal propagation in a curved background. In the following discussion we show how this microscopic requirement translates into the strong-gravity regime and determines the detailed structure of gravitational perturbations near black holes. In particular, we show that the same Wilson coefficient combinations which ensure (or violate) positivity appear explicitly in the deformation of the tortoise coordinate, the formation of CTCs, and the appearance of gravitational-wave echoes. For any graviton or scalar perturbation of spin s , the propagation is governed by a master wave equation of the Schrödinger form,

$$\frac{d^2\Psi}{dr_*^2} + [\omega^2 - V_{\text{eff}}(r)] \Psi = 0,$$

where the tortoise coordinate r_* is defined by $dr_* dr = \sqrt{f_{\text{eff}}(r) g_{\text{eff}}(r)}$, where $f_{\text{eff}}(r)$ and $g_{\text{eff}}(r)$ encode the kinetic structure of the effective theory. Their product, $f_{\text{eff}} g_{\text{eff}}$, receives corrections from higher-derivative interactions with Wilson coefficients C_i of the form $f_{\text{eff}} g_{\text{eff}} = f_0(r) g_0(r) + C_{\text{eff}} \delta(fg) + \dots$, where C_{eff} is the particular linear combination that controls the high-energy (eikonal) scattering amplitude. The Shapiro time delay for a nearly radial null geodesic is

$$\Delta t_{\text{Shapiro}} = \int_{r_1}^{r_2} \left[\frac{1}{\sqrt{f_{\text{eff}} g_{\text{eff}}}} - 1 \right] dr,$$

and positivity of the EFT requires $\Delta t_{\text{Shapiro}} \geq 0$, implying that the effective propagation cone must remain subluminal, or at least that the propagator does not have support outside of the local Minkowski lightcone. Geometrically, this requires that $f_{\text{eff}} g_{\text{eff}} \rightarrow 0$ as $r \rightarrow r_h$, so that the tortoise coordinate satisfies $r_* \rightarrow -\infty$, which enforces the standard purely ingoing boundary condition. In this regime, the near-horizon geometry is chronologically safe and CTCs cannot form, which equates to standard Kerr-like ringdown. If the Wilson coefficients violate positivity, the high-frequency propagation cone expands, corresponding to a negative Shapiro time delay, which in fact becomes a time *advance*, and certain modes may overtake others. This modifies the tortoise mapping such that $f_{\text{eff}} g_{\text{eff}}$ does not vanish at the would-be horizon $f_{\text{eff}}(r_h) g_{\text{eff}}(r_h) \neq 0$, and the tortoise coordinate fails to diverge $r_*(r_h) = r_*^{\text{wall}} > -\infty$; physically, this finite value plays the role of an inner reflective surface, signalling a breakdown of the usual near-horizon ingoing

boundary condition. In precisely the same region of Wilson-coefficient space, the metric component $g_{\varphi\varphi}$ (or the helical combinations $g_{\varphi\varphi} \pm \Omega g_{t\varphi}$) may turn negative, corresponding to the formation of azimuthal or helical CTCs; we show this below with a concrete example. In the zero-charge branch of quadratic k -essence the background geometry takes the Kerr-(A)dS-like form where the effective cosmological constant Λ_{eff} enter into the metric functions. Therefore, the EFT deformation of the geometry is governed by the single combination $\sim \alpha^2/\beta$ which is analogous to a Wilson coefficient multiplying the leading higher-derivative operator. In this case, the Shapiro delay between the inner reflective surface $r_w = r_+^{Ke} + \epsilon$ and the photon-sphere radius r_{ph} is

$$\Delta t_{\text{Sh}}^{Ke} = \int_{r_w}^{r_{\text{ph}}} \left[\frac{1}{f(r)} - 1 \right] dr,$$

since the metric is homogeneous, and the echo time delay is the round-trip null travel time in the same cavity $T_{\text{echo}}^{Ke} = 2[(r_{\text{ph}} - r_w) + \Delta t_{\text{Sh}}^{Ke}]$, analogous to Eq. (5.22). Near the horizon, we can expand the inverse of the k -essence metric function as in the Shapiro time delay as

$$\frac{1}{f_{Ke}(r)} = \frac{1}{f_0(r)} + \frac{\Lambda_{\text{eff}}}{3} \frac{r^2}{f_0(r)^2} + \dots,$$

and subtracting the corresponding Kerr expression we obtain

$$\Delta T_{\text{echo}} = \frac{2\Lambda_{\text{eff}}}{3} \int_{r_w}^{r_{\text{ph}}} \frac{r^2}{f_0(r)^2} dr + \mathcal{O}(\Lambda_{\text{eff}}^2).$$

We can then define the quantity

$$K(M, a) = \frac{2}{3} \int_{r_w}^{r_{\text{ph}}(M, a)} \frac{r^2}{f_0(r; M, a)^2} dr$$

which we call the cavity response functional and which depends only on the Kerr geometry. ΔT_{echo} can therefore be written in the form $\Delta T_{\text{echo}} = K(M, a) \Lambda_{\text{eff}}$. For Schwarzschild ($a = 0$), $r_w = 2GM(1 + \epsilon)$ with $\epsilon \ll 1$ (where r_w is the photon ring), we obtain that $K(M, 0) \simeq 8GM/3 |\ln \epsilon| + \mathcal{O}(M)$, which shows the near-horizon logarithmic enhancement characteristic of null propagation. Combining these results, we can write

$$\text{Wilson coefficients violate positivity} \Leftrightarrow \Delta t_{\text{Shapiro}} < 0 \Leftrightarrow r_*^{\text{wall}} > -\infty \Leftrightarrow \text{CTCs} + \text{echoes}$$

while the causal region satisfies

$$\Delta t_{\text{Shapiro}} \geq 0 \Rightarrow r_* \rightarrow -\infty \Rightarrow \text{no CTCs, no echoes.}$$

It is therefore clear that the EFT Wilson coefficients which guarantee analyticity and microcausality at high energies govern the emergence of echoes and CTCs in the strong-field region. A more general analysis including higher-order operators in more general scalar-tensor as well as extensions to non-zero charge sectors will be presented in an upcoming work [83].

ACKNOWLEDGMENTS

The authors thank Pavel Petrov and Theodoros Nakas for useful discussions. B.H.L is supported by the National Research Foundation of Korea (NRF) grant RS-2020-NR049598, and Overseas Visiting Fellow Program of Shanghai University. B.H.L thanks Asia Pacific Center for Theoretical Physics, Korea for the hospitality during his visit, where a part of this project was done. N.A.N was supported by the Institute for Basic Science under the project code IBS-

R018-D3 and acknowledges support from PSL/Observatoire de Paris. S.T thanks CQeST for support during this work, as well IIT-BHU for the hospitality during his visit, where a preliminary version of this paper was presented.

APPENDICES

Appendix A: Rotating-cylinder backreaction

In coordinates (t, r, φ, z) we take the stationary background metric

$$ds_0^2 = -dt^2 + 2\omega dt d\varphi + (r^2 - \omega^2) d\varphi^2 + dr^2 + dz^2, \quad (\text{A1})$$

and we introduce the (non-orthonormal) coframe

$$\theta^0 = dt - \omega d\varphi, \quad \theta^1 = dr, \quad \theta^2 = d\varphi, \quad \theta^3 = dz, \quad (\text{A2})$$

using which we can write the metric as

$$ds_0^2 = -(\theta^0)^2 + (\theta^1)^2 + r^2(\theta^2)^2 + (\theta^3)^2. \quad (\text{A3})$$

We perturb the metric as

$$ds^2 = ds_0^2 + \varepsilon ds_{\text{pert}}^2, \quad (\text{A4})$$

with the one-form ansatz

$$ds_{\text{pert}}^2 = -a(r) (\theta^0)^2 + 2b(r) \theta^0 \theta^2 + c(r) (\theta^2)^2 + s(r) (\theta^3)^2. \quad (\text{A5})$$

In the coordinate basis, the nonzero perturbation components are

$$h_{tt} = -a, \quad h_{t\varphi} = \omega a + b, \quad h_{\varphi\varphi} = c - 2\omega b - \omega^2 a, \quad h_{zz} = s, \quad h_{rr} = 0. \quad (\text{A6})$$

By subtracting Eq. (2.15) from Eq. (2.18) we obtain

$$w'' + \frac{1}{r} w' = 0, \quad (\text{A7})$$

and from (2.15) we find the following equation

$$\frac{c''}{2r^2} - \frac{c'}{r^3} + \frac{c}{r^4} = -\Sigma(r) - \frac{1}{2} \left(s'' + \frac{s'}{r} \right). \quad (\text{A8})$$

Substituting now $s = (u + w)/2$ and using Eq. (A7) gives

$$\frac{c''}{2r^2} - \frac{c'}{r^3} + \frac{c}{r^4} = -\Sigma(r) - \frac{1}{4} \left(u'' + \frac{u'}{r} \right), \quad (\text{A9})$$

and we use that $u' = 2r\Sigma$ and $\Sigma = r^2/[2(r^2 + r_0^2)^2]$ to finally find

$$u'' + \frac{u'}{r} = \frac{4r^2 r_0^2}{(r^2 + r_0^2)^3}. \quad (\text{A10})$$

Therefore the decoupled equation becomes

$$c'' - \frac{2}{r} c' + \frac{2}{r^2} c = -\frac{r^4 (r^2 + 3r_0^2)}{(r^2 + r_0^2)^3}. \quad (\text{A11})$$

The homogeneous equation admits power-law solutions $c \sim r^m$, giving $m(m-1) - 2m + 2 = 0$ and therefore $c_h(r) = C_1 r + C_2 r^2$. A convenient particular solution is

$$c_p(r) = \frac{r^2 (4r^2 + 3r_0^2)}{4(r^2 + r_0^2)} - \frac{1}{4} \left(3rr_0 \arctan \frac{r}{r_0} + 2r^2 \ln \left(\frac{r^2 + r_0^2}{b^2} \right) \right), \quad (\text{A12})$$

and the solution is

$$c(r) = C_1 r + C_2 r^2 + \frac{r^2 (4r^2 + 3r_0^2)}{4(r^2 + r_0^2)} - \frac{1}{4} \left(3rr_0 \arctan \frac{r}{r_0} + 2r^2 \ln \left(\frac{r^2 + r_0^2}{b^2} \right) \right), \quad (\text{A13})$$

here b is an integration constant which we fix by boundary condition and the final solution is presented in (2.29).

It is convenient to work with

$$X(r) \equiv \frac{c''}{2r^2} - \frac{c'}{r^3} + \frac{c}{r^4}. \quad (\text{A14})$$

With $s(r) \neq 0$ kept, the relevant linearized Einstein components are

$$\delta G_{tt} = - \left[\frac{1}{2} s'' + \frac{1}{2r} s' + X(r) \right], \quad (\text{A15})$$

$$\delta G_{zz} = \frac{1}{2} a'' + \frac{1}{2r} a' + X(r). \quad (\text{A16})$$

For the scalar source considered here one has $T_{zz} = -T_{tt}$, i.e.

$$T_{tt} = \kappa S(r), \quad T_{zz} = -\kappa S(r), \quad (\text{A17})$$

and the (tt) and (zz) component equations are

$$-\frac{1}{2} s'' - \frac{1}{2r} s' - X = \kappa S, \quad (\text{A18})$$

$$\frac{1}{2} a'' + \frac{1}{2r} a' + X = -\kappa S. \quad (\text{A19})$$

From (A18) we solve for X ,

$$X = -\kappa S - \frac{1}{2} s'' - \frac{1}{2r} s'. \quad (\text{A20})$$

Substituting (A20) into (A19) gives

$$\frac{1}{2} a'' + \frac{1}{2r} a' - \kappa S - \frac{1}{2} s'' - \frac{1}{2r} s' = -\kappa S. \quad (\text{A21})$$

The source cancels on both sides, leaving

$$\frac{1}{2} (a'' - s'') + \frac{1}{2r} (a' - s') = 0. \quad (\text{A22})$$

Multiplying by 2 yields

$$a'' - s'' + \frac{1}{r} (a' - s') = 0 \quad \iff \quad (a - s)'' + \frac{1}{r} (a - s)' = 0. \quad (\text{A23})$$

Defining the difference mode $w(r) \equiv s(r) - a(r)$, this is equivalently

$$w'' + \frac{1}{r}w' = 0, \quad w(r) \equiv s(r) - a(r). \quad (\text{A24})$$

Appendix B: Gauge invariance of the CTC criterion under radial shifts

We verify that the gauge-invariant no-CTC criterion

$$g_{\varphi\varphi} > 0, \quad \Delta \equiv g_{tt}g_{\varphi\varphi} - g_{t\varphi}^2 < 0, \quad (\text{B1})$$

remains unchanged under infinitesimal Hartle-Thorne type radial shifts that preserve stationarity and axisymmetry. Consider the coordinate transformation

$$t' = t, \quad \varphi' = \varphi, \quad \theta' = \theta, \quad r' = r + \varepsilon \xi(r, \theta), \quad 0 < \varepsilon \ll 1, \quad (\text{B2})$$

generated by the vector field

$$X^\mu = (0, \xi(r, \theta), 0, 0), \quad X^\mu \partial_\mu = \xi(r, \theta) \partial_r. \quad (\text{B3})$$

Such a transformation preserves both Killing directions ∂_t and ∂_φ and thus represents a legitimate gauge transformation within the slow-rotation expansion. Under this diffeomorphism, the metric changes according to the Lie derivative

$$\delta g_{\mu\nu} = \mathcal{L}_X g_{\mu\nu} = \nabla_\mu X_\nu + \nabla_\nu X_\mu. \quad (\text{B4})$$

For the Killing subspace indices $A, B \in \{t, \varphi\}$ we have that

$$\delta g_{AB} = \mathcal{L}_X g_{AB} = X^\sigma \partial_\sigma g_{AB} + g_{\sigma B} \partial_A X^\sigma + g_{A\sigma} \partial_B X^\sigma, \quad (\text{B5})$$

and since X^σ depends only on (r, θ) and the metric is stationary and axisymmetric, $\partial_t X^\sigma = \partial_\varphi X^\sigma = 0$, giving

$$\delta g_{AB} = X^i \partial_i g_{AB} = \xi(r, \theta) \partial_r g_{AB}, \quad i \in \{r, \theta\}. \quad (\text{B6})$$

Hence, to $\mathcal{O}(\varepsilon)$ we have that

$$g'_{AB}(r, \theta) = g_{AB}(r, \theta) + \varepsilon \xi \partial_r g_{AB} = g_{AB}(r + \varepsilon \xi(r, \theta), \theta). \quad (\text{B7})$$

Equation (B7) shows that both $g_{\varphi\varphi}$ and the determinant $\Delta \equiv g_{tt}g_{\varphi\varphi} - g_{t\varphi}^2$ transform as scalar functions under the (r, θ) reparametrisation

$$g'_{\varphi\varphi}(r, \theta) = g_{\varphi\varphi}(r + \varepsilon \xi(r, \theta), \theta), \quad \Delta'(r, \theta) = \Delta(r + \varepsilon \xi(r, \theta), \theta). \quad (\text{B8})$$

Their signs and zeros are therefore unchanged and the roots $g_{\varphi\varphi} = 0$ and $\Delta = 0$ are simply dragged along the coordinate map $(r, \theta) \rightarrow (r + \varepsilon \xi, \theta)$. Under such symmetry-preserving transformations,

$$\boxed{g_{\varphi\varphi} > 0, \quad \Delta < 0 \iff g'_{\varphi\varphi} > 0, \quad \Delta' < 0,} \quad (\text{B9})$$

which shows that the no-CTC criterion in Eq. (B1) is fully gauge invariant under Hartle-Thorne type radial shifts. More general reparametrizations of the form $X = \xi(r, \theta)\partial_r + \eta(r, \theta)\partial_\theta$ preserve this property identically. Only coordinate transformations that mix the Killing directions (t, φ) alter the individual components, although the causal character of the Killing subspace with one timelike and one spacelike direction remains invariant.

Appendix C: Vacuum $\ell = 2$ Kerr-(A)dS Hartle-Thorne treatment

In dimensionless variables

$$x \equiv \frac{r}{GM}, \quad \lambda \equiv \Lambda_{\text{eff}}(GM)^2, \quad N^2(x) = 1 - \frac{2}{x} - \frac{\lambda}{3}x^2, \quad (\text{C1})$$

the vacuum basis used in the numerical implementation is

$$h_{2,0}(x; \lambda) = \frac{1+x}{x^4} - \frac{\lambda}{3x}, \quad k_{2,0}(x; \lambda) = -\frac{2+x}{x^4} - \frac{\lambda}{3x}, \quad m_{2,0}(x; \lambda) = \frac{5-x}{x^4} + \frac{\lambda}{3x}. \quad (\text{C2})$$

These reduce smoothly to the Kerr limit as $\lambda \rightarrow 0$. Let x_h be the (outer) black-hole horizon in the static patch, i.e. a simple root of $N^2(x)$:

$$N^2(x) = N_1(x - x_h) + \mathcal{O}((x - x_h)^2), \quad N_1 \equiv \left. \frac{dN^2}{dx} \right|_{x_h}. \quad (\text{C3})$$

Assume regular Taylor expansions

$$H_2(x) = H_h + H_1(x - x_h) + \dots, \quad K_2(x) = K_h + K_1(x - x_h) + \dots. \quad (\text{C4})$$

Inserting Eq. (C4) into the first-order system (3.64) and demanding finiteness fixes (H_1, K_1) in terms of (H_h, K_h) yields one linear regularity constraint which removes the would-be divergent mode. Equivalently, one may use K_h as a shooting parameter, determine H_h from the regularity constraint, and start integration from $x_0 = x_h + \varepsilon$ with $\varepsilon \ll 1$. For $\lambda > 0$ (dS static patch), the same analysis applies at the cosmological horizon x_c (the largest root of $N^2(x) = 0$).

Zero-flux scalar integral $S_r(r)$

With $S'_r(r) = \pm\sqrt{C}/N(r)$ we have that

$$S_r(r) = S_r(r_\infty) \pm \sqrt{C} \int_{r_\infty}^r \frac{dr'}{N(r')}. \quad (\text{C5})$$

For $\Lambda_{\text{eff}} = 0$ this integral is elementary; for $\Lambda_{\text{eff}} \neq 0$ it involves

$$\Delta_0(r) \equiv r^2 N^2(r) = r^2 - 2GMr - \frac{\Lambda_{\text{eff}}}{3}r^4, \quad (\text{C6})$$

and can be expressed in terms of incomplete elliptic integrals.

Constant X and small- λ limit of Φ_0

In the constant- X monopole sub-branch (main text),

$$\frac{d\Phi_0}{dx} = \frac{1}{2\sqrt{C}} \frac{1}{N^3(x)}, \quad N^2(x) = 1 - \frac{2}{x} - \frac{\lambda}{3}x^2. \quad (\text{C7})$$

For $|\lambda| \ll 1$, it is convenient to expand N^{-3} around the Schwarzschild factor

$$u(x) \equiv \sqrt{1 - \frac{2}{x}},$$

which leads to integrals of the form $\int dx/u^3$ and $\int x^2 dx/u^5$. A useful identity is

$$\int \frac{dx}{u^3} = \frac{6u^2 - 4}{u(1 - u^2)} + 3 \ln\left(\frac{1+u}{1-u}\right) + \text{const.} \quad (\text{C8})$$

(understood with absolute values appropriate for $0 < u < 1$ outside the horizon). We also have

$$\int \frac{x^2 dx}{u^5} = \frac{-315u^8 + 840u^6 - 693u^4 + 144u^2 + 16}{3u^3(u^2 - 1)^3} + \frac{105}{2} \ln\left(\frac{1+u}{1-u}\right) + \text{const.} \quad (\text{C9})$$

Substituting Eqs (C8)-(C9) into the small- λ expansion of Φ_0 used in the main text gives explicit solutions of $\Phi_0(x)$ to $\mathcal{O}(\lambda)$.

Quadrupole coefficients

We solve the inhomogeneous first-order linear system (3.64) with the coefficient matrix (3.65) and the coefficients (3.66) For the branch choice used in the numerics, we take

$$\Pi_2(x; \lambda) = -4 X_2(x) m_{2,0}(x; \lambda), \quad (\text{C10})$$

where $m_{2,0}$ is the vacuum function (C2) and $X_2(x)$ is the $\ell = 2$ $\mathcal{O}(\varepsilon_q^2)$ profile appearing in

$$X = X_\star + \varepsilon_q^2 \left[X_{2,0}(x) + X_2(x) P_2(\cos \theta) \right] + \mathcal{O}(\varepsilon_q^4).$$

In the implementation we use the explicit model profile

$$X_2(x) = \frac{\tilde{C}_X}{x^2 N(x)}, \quad (\text{C11})$$

and the source entering (3.64) is then

$$S_K(x; \lambda) = \frac{3x^2}{4(3 - \lambda x^3)} \Pi_2(x; \lambda), \quad (\text{C12})$$

which yields the closed form

$$S_K(x; \lambda) = -\frac{3\tilde{C}_X}{(3 - \lambda x^3) N(x)} \left(\frac{5-x}{x^4} + \frac{\lambda}{3x} \right). \quad (\text{C13})$$

Any overall coupling constants multiplying Π_2 can be absorbed into \tilde{C}_X for the purposes of numerics.

Numerical outline

We solve (3.64) on a static-patch interval $x \in [x_0, x_{\text{out}}]$. Let x_h be the outer black-hole horizon (a root of $N^2(x) = 0$ in the static region). To regulate the coordinate singularity at the horizon, we start at

$$x_0 = x_h + \varepsilon, \quad \varepsilon \ll 1.$$

For $\lambda \leq 0$ we take $x_{\text{out}} \gg 1$ as a large-radius proxy, and for $\lambda > 0$ (dS static patch) we take x_{out} just inside the

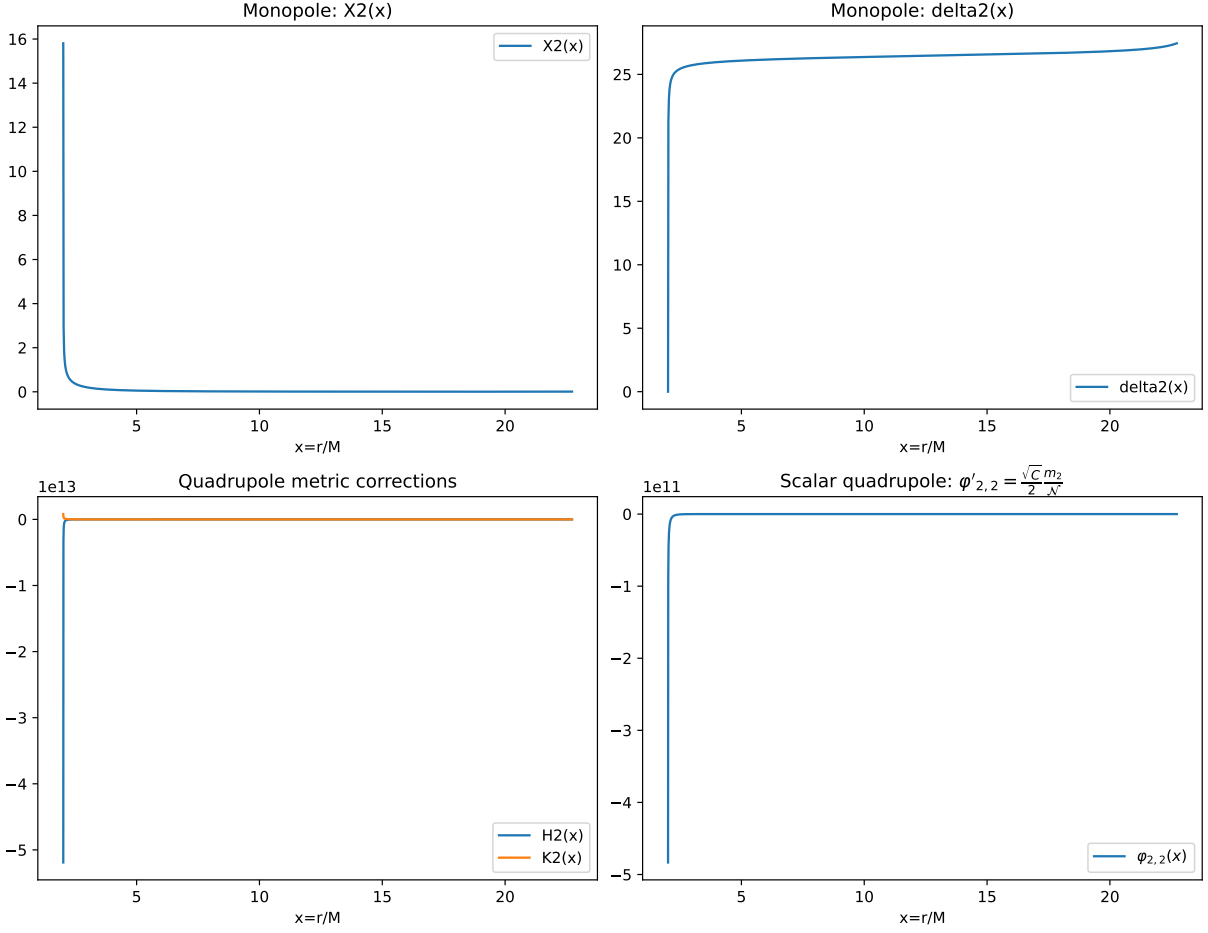


FIG. 10: Numerical solutions for the monopole and quadrupole metric corrections.

cosmological horizon, e.g. $x_{\text{out}} = 0.97 x_c$. We impose two Dirichlet conditions at $x = x_{\text{out}}$ as

$$H_2(x_{\text{out}}) = 0, \quad K_2(x_{\text{out}}) = 0. \quad (\text{C14})$$

Equivalently, we may implement the system as

$$K_2' = a_{KH}(x; \lambda) H_2 + a_{KK}(x; \lambda) K_2 + S_K(x; \lambda), \quad H_2' = c_{HH}(x; \lambda) H_2 - K_2', \quad (\text{C15})$$

with coefficients (3.66) and source as in Eq. (C13). We iterate over $(\lambda, \varepsilon_a, \varepsilon_q)$ and solve the system at each step using the following logic. We determine horizons x_h (and x_c for dS) from $N^2(x) = 0$, fix the branch profile $X_2(x)$ (e.g. (C11) with fixed \tilde{C}_X), solve the BVP (3.64) for (H_2, K_2) using horizon regularity and the outer conditions (C14). Then, we solve the $\ell = 2$ scalar ODE for Φ_2 using the obtained (H_2, K_2) . We construct the corrected metric and evaluate the CTC conditions ($g_{\phi\phi}$ and k_{min}^2) for (r, θ) outside the horizon, and finally, we extract $\lambda_{\text{crit}}(\varepsilon_a, \theta, \varepsilon_q)$, or equivalently, (α, β) .

Appendix D: Fully expanded polynomials for metric radial functions

Here, we list the polynomials referred to in the text. Each of the radial functions is of the form

$$X_i(r) = \varepsilon^2 \frac{1}{r^{n_i} f(r)^{p_i}} \left[P_{X_i}(r) + (r - 2GM) Q_{X_i}(r) \ln \left(1 - \frac{2GM}{r} \right) \right]. \quad (\text{D1})$$

Frame-drag polynomials $P_\Omega(r)$ and $Q_\Omega(r)$

Already given in the main text, we repeat them here for completeness:

$$\begin{aligned} P_\Omega(x) &= -8(40x^5 + 120x^4 + 180x^3 + 180x^2 + 90x + 20)(GM)^6, \\ Q_\Omega(x) &= (8x^5 + 20x^4 + 40x^3 + 60x^2 + 60x + 20)(GM)^6. \end{aligned} \quad (\text{D2})$$

Monopole polynomials $A_0(r)$, $B_0(r)$, $C_0(r)$

We choose normalisation such that

$$A_0(r) = \frac{\varepsilon^2}{r^6} \left[P_{A_0}(r) + (r - 2M) Q_{A_0}(r) \ln(1 - 2GM/r) \right], \quad (\text{D3})$$

where

$$P_{A_0}(r) = (GM)^6 \cdot p_{A_0}(x), \quad Q_{A_0}(r) = (GM)^6 \cdot q_{A_0}(x), \quad (\text{D4})$$

and

$$\begin{aligned} p_{A_0}(x) &= -\frac{1}{15} (720x^8 + 2880x^7 + 5760x^6 + 7200x^5 + 5400x^4 + 2160x^3 + 480x^2 + 60x + 10), \\ q_{A_0}(x) &= \frac{1}{30} (48x^6 + 120x^5 + 240x^4 + 360x^3 + 360x^2 + 150x + 30). \end{aligned} \quad (\text{D5})$$

Similarly, we have for $B_0(r)$

$$B_0(r) = \frac{\varepsilon^2}{r^6 f(r)^2} \left[P_{B_0}(r) + (r - 2GM) Q_{B_0}(r) \ln(1 - 2GM/r) \right], \quad (\text{D6})$$

where

$$P_{B_0}(r) = (GM)^6 \cdot p_{B_0}(x), \quad Q_{B_0}(r) = (GM)^6 \cdot q_{B_0}(x), \quad (\text{D7})$$

and

$$\begin{aligned} p_{B_0}(x) &= \frac{1}{15} (240x^8 + 960x^7 + 1920x^6 + 2400x^5 + 1800x^4 + 720x^3 + 160x^2 + 20x + 4), \\ q_{B_0}(x) &= -\frac{1}{30} (48x^6 + 120x^5 + 240x^4 + 360x^3 + 360x^2 + 150x + 30). \end{aligned} \quad (\text{D8})$$

For $C_0(r)$

$$C_0(r) = \frac{\varepsilon^2}{r^6} \left[P_{C_0}(r) + (r - 2GM) Q_{C_0}(r) \ln(1 - 2GM/r) \right], \quad (\text{D9})$$

with

$$P_{C_0}(r) = (GM)^6 \cdot p_{C_0}(x), \quad Q_{C_0}(r) = (GM)^6 \cdot q_{C_0}(x), \quad (D10)$$

and

$$\begin{aligned} p_{C_0}(x) &= \frac{1}{30} (120x^8 + 480x^7 + 960x^6 + 1200x^5 + 900x^4 + 360x^3 + 80x^2 + 10x + 2), \\ q_{C_0}(x) &= \frac{1}{60} (48x^6 + 120x^5 + 240x^4 + 360x^3 + 360x^2 + 150x + 30). \end{aligned} \quad (D11)$$

Quadrupole polynomials $A_2(r)$, $B_2(r)$, $C_2(r)$

For $A_2(r)$, we have

$$A_2(r) = \frac{\varepsilon^2}{r^8} \left[P_{A_2}(r) + (r - 2GM) Q_{A_2}(r) \ln(1 - 2GM/r) \right], \quad (D12)$$

with polynomials now scaled by M^8

$$P_{A_2}(r) = (GM)^8 p_{A_2}(x), \quad Q_{A_2}(r) = (GM)^8 q_{A_2}(x), \quad (D13)$$

where

$$\begin{aligned} p_{A_2}(x) &= -\frac{1}{420} (6720x^{10} + 33600x^9 + 100800x^8 + 201600x^7 + 302400x^6 \\ &\quad + 302400x^5 + 201600x^4 + 80640x^3 + 20160x^2 + 3360x + 280), \\ q_{A_2}(x) &= \frac{1}{840} (224x^8 + 560x^7 + 1120x^6 + 1680x^5 + 1680x^4 + 840x^3 + 280x^2 + 56x + 8). \end{aligned} \quad (D14)$$

For $B_2(r)$ we have

$$B_2(r) = \frac{\varepsilon^2}{r^8 f(r)^2} \left[P_{B_2}(r) + (r - 2GM) Q_{B_2}(r) \ln(1 - 2GM/r) \right], \quad (D15)$$

with

$$P_{B_2}(r) = (GM)^8 p_{B_2}(x), \quad Q_{B_2}(r) = (GM)^8 q_{B_2}(x), \quad (D16)$$

and the polynomials

$$\begin{aligned} p_{B_2}(x) &= \frac{1}{420} (2240x^{10} + 11200x^9 + 33600x^8 + 67200x^7 + 100800x^6 \\ &\quad + 100800x^5 + 67200x^4 + 26880x^3 + 6720x^2 + 1120x + 112), \\ q_{B_2}(x) &= -\frac{1}{840} (224x^8 + 560x^7 + 1120x^6 + 1680x^5 + 1680x^4 + 840x^3 + 280x^2 + 56x + 8). \end{aligned} \quad (D17)$$

Finally, we have $C_2(r)$ as

$$C_2(r) = \frac{\varepsilon^2}{r^8} \left[P_{C_2}(r) + (r - 2GM) Q_{C_2}(r) \ln(1 - 2GM/r) \right], \quad (D18)$$

with

$$P_{C_2}(r) = (GM)^8 p_{C_2}(x), \quad Q_{C_2}(r) = (GM)^8 q_{C_2}(x), \quad (D19)$$

and the polynomials

$$\begin{aligned} p_{C_2}(x) &= \frac{1}{840} (1120x^{10} + 5600x^9 + 16800x^8 + 33600x^7 + 50400x^6 \\ &\quad + 50400x^5 + 33600x^4 + 13440x^3 + 3360x^2 + 560x + 56), \\ q_{C_2}(x) &= \frac{1}{1680} (224x^8 + 560x^7 + 1120x^6 + 1680x^5 + 1680x^4 + 840x^3 + 280x^2 + 56x + 8). \end{aligned} \quad (D20)$$

Source terms

At $\mathcal{O}(\varepsilon^2 \varepsilon_a^2)$, the only non-vanishing source functions are: $A_{00}^{(0)}$, A_{00} , $G_{00}^{(s)}$ in the $\ell = 0$ sector, and $A_{20}^{(0)}$, A_{20} , B_{20} , $G_{20}^{(s)}$, F_{20} in the $\ell = 2$ sector. For $\ell = 0$ sources, we have

$$\begin{aligned} A_{00}^{(0)}(r) &= -24\sqrt{\pi} \varepsilon^2 \frac{(GM)^4 \varepsilon_a^2}{r^6 f(r)^2} \left[1 - \frac{101(GM)}{18r} + \frac{25(GM)^2}{r^2} - \frac{877(GM)^3}{18r^3} - \frac{1022(GM)^4}{15r^4} - \frac{2224(GM)^5}{9r^5} \right. \\ &\quad \left. + \frac{107786(GM)^6}{45r^6} - \frac{53452(GM)^7}{15r^7} - \frac{208(GM)^8}{45r^8} + \frac{5920(GM)^9}{3r^9} \right], \end{aligned} \quad (D21)$$

$$\begin{aligned} A_{00}(r) &= -2\sqrt{\pi} \varepsilon^2 \frac{(GM)^2 \varepsilon_a^2}{r^4 f(r)^4} \left[1 - \frac{4(GM)}{r} + \frac{16(GM)^2}{3r^2} + \frac{40(GM)^3}{3r^3} - \frac{236(GM)^4}{3r^4} + \frac{482(GM)^5}{3r^5} \right. \\ &\quad + \frac{13672(GM)^6}{15r^6} - \frac{6416(GM)^7}{3r^7} - \frac{15288(GM)^8}{5r^8} + \frac{13808(GM)^9}{5r^9} + \frac{84928(GM)^{10}}{5r^{10}} \\ &\quad \left. - \frac{18560(GM)^{11}}{r^{11}} \right], \end{aligned} \quad (D22)$$

$$\begin{aligned} G_{00}^{(s)}(r) &= \frac{56\sqrt{2\pi}}{3} \varepsilon^2 \frac{(GM)^4 \varepsilon_a^2}{r^6 f(r)} \left[1 - \frac{5(GM)}{4r} + \frac{333(GM)^2}{28r^2} + \frac{157(GM)^3}{14r^3} - \frac{969(GM)^4}{70r^4} - \frac{1807(GM)^5}{5r^5} \right. \\ &\quad \left. + \frac{2068(GM)^6}{5r^6} + \frac{1320(GM)^7}{7r^7} \right]. \end{aligned} \quad (D23)$$

Moreover $B_{00}(r) = 0$ and $F_{00}(r) = 0$.

For $\ell = 2$ sources, we have

$$\begin{aligned} A_{20}^{(0)}(r) &= -\frac{44\sqrt{5\pi}}{15} \varepsilon^2 \frac{(GM)^5 \varepsilon_a^2}{r^7} \left[1 + \frac{7737(GM)}{110r} - \frac{4201(GM)^2}{55r^2} + \frac{1047(GM)^3}{11r^3} - \frac{22086(GM)^4}{11r^4} \right. \\ &\quad \left. + \frac{194424(GM)^5}{55r^5} - \frac{8880(GM)^6}{11r^6} \right], \end{aligned} \quad (D24)$$

$$\begin{aligned} A_{20}(r) &= -\frac{236\sqrt{5\pi}}{75} \varepsilon^2 \frac{(GM)^4 \varepsilon_a^2}{r^6 f(r)^2} \left[1 + \frac{163(GM)}{59r} - \frac{2913(GM)^2}{118r^2} + \frac{3183(GM)^3}{59r^3} - \frac{4587(GM)^4}{59r^4} \right. \\ &\quad \left. + \frac{25798(GM)^5}{59r^5} - \frac{59448(GM)^6}{59r^6} + \frac{34800(GM)^7}{59r^7} \right], \end{aligned} \quad (D25)$$

$$B_{20}(r) = \frac{92\sqrt{15\pi}}{75} \varepsilon^2 \frac{(GM)^4 \varepsilon_a^2}{r^6 f(r)} \left[1 + \frac{153(GM)}{46r} - \frac{651(GM)^2}{23r^2} - \frac{513(GM)^3}{23r^3} - \frac{1682(GM)^4}{23r^4} + \frac{33704(GM)^5}{69r^5} - \frac{2000(GM)^6}{23r^6} \right], \quad (D26)$$

$$G_{20}^{(s)}(r) = \frac{2\sqrt{10\pi}}{15} \varepsilon^2 \frac{(GM)^4 \varepsilon_a^2}{r^6} \left[1 - \frac{15(GM)}{r} - \frac{4963(GM)^2}{5r^2} - \frac{1164(GM)^3}{r^3} - \frac{2910(GM)^4}{r^4} + \frac{96528(GM)^5}{5r^5} - \frac{2640(GM)^6}{r^6} \right], \quad (D27)$$

$$F_{20}(r) = -\frac{4\sqrt{15\pi}}{15} \varepsilon^2 \frac{(GM)^4 \varepsilon_a^2}{r^6} \left[1 + \frac{8(GM)}{r} + \frac{809(GM)^2}{5r^2} - \frac{358(GM)^3}{5r^3} + \frac{1386(GM)^4}{5r^4} - \frac{25888(GM)^5}{15r^5} + \frac{2160(GM)^6}{r^6} \right]. \quad (D28)$$

-
- [1] A. Bourgoïn, A. Hees, S. Bouquillon, C. Le Poncin-Lafitte, G. Francou, and M. C. Angonin, Testing Lorentz symmetry with Lunar Laser Ranging, *Phys. Rev. Lett.* **117**, 241301 (2016), [arXiv:1607.00294 \[gr-qc\]](#).
- [2] A. Bourgoïn, C. Le Poncin-Lafitte, A. Hees, S. Bouquillon, G. Francou, and M.-C. Angonin, Lorentz Symmetry Violations from Matter-Gravity Couplings with Lunar Laser Ranging, *Phys. Rev. Lett.* **119**, 201102 (2017), [arXiv:1706.06294 \[gr-qc\]](#).
- [3] A. Fienga and O. Minazzoli, Testing theories of gravity with planetary ephemerides, *Living Rev. Rel.* **27**, 1 (2024), [arXiv:2303.01821 \[gr-qc\]](#).
- [4] A. Hees, A. Bourgoïn, P. Delva, C. Le Poncin-Lafitte, and P. Wolf, Use of Geodesy and Geophysics Measurements to Probe the Gravitational Interaction, *Fundam. Theor. Phys.* **196**, 317 (2019).
- [5] J. Schwab, A. S. Bolton, and S. A. Rappaport, Galaxy-scale strong-lensing tests of gravity and geometric cosmology: Constraints and systematic limitations, *The Astrophysical Journal* **708**, 750–757 (2009).
- [6] B. P. Abbott *et al.* (LIGO Scientific, Virgo), Observation of Gravitational Waves from a Binary Black Hole Merger, *Phys. Rev. Lett.* **116**, 061102 (2016), [arXiv:1602.03837 \[gr-qc\]](#).
- [7] R. Abbott *et al.* (LIGO Scientific, Virgo), GWTC-2: Compact Binary Coalescences Observed by LIGO and Virgo During the First Half of the Third Observing Run, *Phys. Rev. X* **11**, 021053 (2021), [arXiv:2010.14527 \[gr-qc\]](#).
- [8] R. Abbott *et al.* (LIGO Scientific, VIRGO), GWTC-2.1: Deep extended catalog of compact binary coalescences observed by LIGO and Virgo during the first half of the third observing run, *Phys. Rev. D* **109**, 022001 (2024), [arXiv:2108.01045 \[gr-qc\]](#).
- [9] B. P. Abbott *et al.* (LIGO Scientific), Exploring the Sensitivity of Next Generation Gravitational Wave Detectors, *Class. Quant. Grav.* **34**, 044001 (2017), [arXiv:1607.08697 \[astro-ph.IM\]](#).
- [10] E. Belgacem *et al.* (LISA Cosmology Working Group), Testing modified gravity at cosmological distances with LISA standard sirens, *JCAP* **07**, 024, [arXiv:1906.01593 \[astro-ph.CO\]](#).
- [11] S. Perlmutter *et al.* (Supernova Cosmology Project), Measurements of Ω and Λ from 42 High Redshift Supernovae, *Astrophys. J.* **517**, 565 (1999), [arXiv:astro-ph/9812133](#).
- [12] A. G. Riess *et al.* (Supernova Search Team), Observational evidence from supernovae for an accelerating universe and a cosmological constant, *Astron. J.* **116**, 1009 (1998), [arXiv:astro-ph/9805201](#).
- [13] J. Martin, Everything You Always Wanted To Know About The Cosmological Constant Problem (But Were Afraid To Ask), *Comptes Rendus Physique* **13**, 566 (2012), [arXiv:1205.3365 \[astro-ph.CO\]](#).
- [14] E. Di Valentino *et al.* (CosmoVerse), The CosmoVerse White Paper: Addressing observational tensions in cosmology with systematics and fundamental physics, (2025), [arXiv:2504.01669 \[astro-ph.CO\]](#).
- [15] S. V. Krasnikov, Paradoxes of time travel, (1996), [arXiv:gr-qc/9603042](#).
- [16] M. Carrillo Gonzalez, C. de Rham, V. Pozsgay, and A. J. Tolley, Causal effective field theories, *Phys. Rev. D* **106**, 105018 (2022), [arXiv:2207.03491 \[hep-th\]](#).
- [17] C. de Rham, S. Melville, A. J. Tolley, and S.-Y. Zhou, Positivity bounds for scalar field theories, *Phys. Rev. D* **96**, 081702

- (2017), [arXiv:1702.06134 \[hep-th\]](#).
- [18] C. P. Burgess, Quantum gravity in everyday life: General relativity as an effective field theory, *Living Rev. Rel.* **7**, 5 (2004), [arXiv:gr-qc/0311082](#).
- [19] E. Palti, The Swampland: Introduction and Review, *Fortsch. Phys.* **67**, 1900037 (2019), [arXiv:1903.06239 \[hep-th\]](#).
- [20] C. Vafa, The String landscape and the swampland, (2005), [arXiv:hep-th/0509212](#).
- [21] S. Melville, Causality and quasi-normal modes in the GREFT, *Eur. Phys. J. Plus* **139**, 725 (2024), [arXiv:2401.05524 \[gr-qc\]](#).
- [22] C. de Rham and A. J. Tolley, Causality in curved spacetimes: The speed of light and gravity, *Phys. Rev. D* **102**, 084048 (2020), [arXiv:2007.01847 \[hep-th\]](#).
- [23] L. Alberte, C. de Rham, S. Jaitly, and A. J. Tolley, Positivity Bounds and the Massless Spin-2 Pole, *Phys. Rev. D* **102**, 125023 (2020), [arXiv:2007.12667 \[hep-th\]](#).
- [24] J. Tokuda, K. Aoki, and S. Hirano, Gravitational positivity bounds, *JHEP* **11**, 054, [arXiv:2007.15009 \[hep-th\]](#).
- [25] C. Y. R. Chen, C. de Rham, A. Margalit, and A. J. Tolley, A cautionary case of casual causality, *JHEP* **03**, 025, [arXiv:2112.05031 \[hep-th\]](#).
- [26] M. Carrillo González, C. de Rham, S. Jaitly, V. Pozsgay, and A. Tokareva, Positivity-causality competition: a road to ultimate EFT consistency constraints, *JHEP* **06**, 146, [arXiv:2307.04784 \[hep-th\]](#).
- [27] M. Carrillo González, Bounds on EFT's in an expanding universe, *Phys. Rev. D* **109**, 085008 (2024), [arXiv:2312.07651 \[hep-th\]](#).
- [28] D. Lovelock, The Einstein tensor and its generalizations, *J. Math. Phys.* **12**, 498 (1971).
- [29] D. Lovelock, The four-dimensionality of space and the einstein tensor, *J. Math. Phys.* **13**, 874 (1972).
- [30] A. Biswas, A. Kar, B.-H. Lee, H. Lee, W. Lee, S. Scopel, L. Velasco-Sevilla, and L. Yin, Gauss-Bonnet Cosmology: large-temperature behaviour and bounds from Gravitational Waves, *JCAP* **09**, 007, [arXiv:2405.15998 \[hep-ph\]](#).
- [31] A. Salvio, Quadratic Gravity, *Front. in Phys.* **6**, 77 (2018), [arXiv:1804.09944 \[hep-th\]](#).
- [32] C. de Rham, Massive Gravity, *Living Rev. Rel.* **17**, 7 (2014), [arXiv:1401.4173 \[hep-th\]](#).
- [33] P. Aschieri, M. Dimitrijevic, F. Meyer, and J. Wess, Noncommutative geometry and gravity, *Class. Quant. Grav.* **23**, 1883 (2006), [arXiv:hep-th/0510059](#).
- [34] M. Herrero-Valea, The status of Hořava gravity, *Eur. Phys. J. Plus* **138**, 968 (2023), [arXiv:2307.13039 \[gr-qc\]](#).
- [35] G. W. Horndeski, Second-order scalar-tensor field equations in a four-dimensional space, *Int. J. Theor. Phys.* **10**, 363 (1974).
- [36] B.-H. Lee, W. Lee, E. Ó. Colgáin, M. M. Sheikh-Jabbari, and S. Thakur, Is local H_0 at odds with dark energy EFT?, *JCAP* **04** (04), 004, [arXiv:2202.03906 \[astro-ph.CO\]](#).
- [37] S. Shankaranarayanan and J. P. Johnson, Modified theories of gravity: Why, how and what?, *Gen. Rel. Grav.* **54**, 44 (2022), [arXiv:2204.06533 \[gr-qc\]](#).
- [38] S. Nojiri, S. D. Odintsov, and V. K. Oikonomou, Modified Gravity Theories on a Nutshell: Inflation, Bounce and Late-time Evolution, *Phys. Rept.* **692**, 1 (2017), [arXiv:1705.11098 \[gr-qc\]](#).
- [39] W. J. van Stockum, The gravitational feild of a distribution of particles rotating about an axis of symmetry, *Proc. Roy. Soc. Edinburgh* **57**, 135 (1937).
- [40] K. Gödel, An example of a new type of cosmological solutions of einstein's field equations of gravitation, *Rev. Mod. Phys.* **21**, 447 (1949).
- [41] K. Lanczos, On a Stationary Cosmology in the Sense of Einstein's Theory of Gravitation, *General Relativity and Gravitation* **29**, 363 (1997).
- [42] F. J. Tipler, Rotating cylinders and the possibility of global causality violation, *Phys. Rev. D* **9**, 2203 (1974).
- [43] S. W. Hawking, Chronology protection conjecture, *Phys. Rev. D* **46**, 603 (1992).
- [44] E. Minguzzi, Lorentzian causality theory, *Living Rev. Rel.* **22**, 3 (2019).
- [45] R. Bousso, Z. Fisher, S. Leichenauer, and A. C. Wall, Quantum focusing conjecture, *Phys. Rev. D* **93**, 064044 (2016), [arXiv:1506.02669 \[hep-th\]](#).
- [46] M. Visser, The Quantum physics of chronology protection, in *Workshop on Conference on the Future of Theoretical Physics and Cosmology in Honor of Steven Hawking's 60th Birthday* (2002) pp. 161–176, [arXiv:gr-qc/0204022](#).
- [47] X. O. Camanho, J. D. Edelstein, J. Maldacena, and A. Zhiboedov, Causality Constraints on Corrections to the Graviton Three-Point Coupling, *JHEP* **02**, 020, [arXiv:1407.5597 \[hep-th\]](#).
- [48] G. D'Appollonio, P. Di Vecchia, R. Russo, and G. Veneziano, Regge behavior saves String Theory from causality violations, *JHEP* **05**, 144, [arXiv:1502.01254 \[hep-th\]](#).

- [49] F. S. N. Lobo, Closed timelike curves and causality violation, (2008), [arXiv:1008.1127 \[gr-qc\]](#).
- [50] J. B. Hartle and K. S. Thorne, Slowly Rotating Relativistic Stars. II. Models for Neutron Stars and Supermassive Stars, *Astrophys. J.* **153**, 807 (1968).
- [51] R. M. Wald, *General Relativity* (Chicago Univ. Pr., Chicago, USA, 1984).
- [52] N. D. Birrell and P. C. W. Davies, *Quantum Fields in Curved Space*, Cambridge Monographs on Mathematical Physics (Cambridge University Press, Cambridge, UK, 1982).
- [53] B. O’Neill, *Semi-Riemannian Geometry with Applications to Relativity*, Pure and Applied Mathematics, Vol. 103 (Academic Press, 1983).
- [54] F. Gray, J. Santiago, S. Schuster, and M. Visser, “Twisted” black holes are unphysical, *Mod. Phys. Lett. A* **32**, 1771001 (2017), [arXiv:1610.06135 \[gr-qc\]](#).
- [55] T. Kobayashi, Horndeski theory and beyond: a review, *Rept. Prog. Phys.* **82**, 086901 (2019), [arXiv:1901.07183 \[gr-qc\]](#).
- [56] P. Kanti, N. E. Mavromatos, J. Rizos, K. Tamvakis, and E. Winstanley, Dilatonic black holes in higher curvature string gravity, *Phys. Rev. D* **54**, 5049 (1996), [arXiv:hep-th/9511071](#).
- [57] C. Armendariz-Picon, V. F. Mukhanov, and P. J. Steinhardt, Essentials of k essence, *Phys. Rev. D* **63**, 103510 (2001), [arXiv:astro-ph/0006373](#).
- [58] T. Kobayashi, M. Yamaguchi, and J. Yokoyama, Generalized G-inflation: Inflation with the most general second-order field equations, *Prog. Theor. Phys.* **126**, 511 (2011), [arXiv:1105.5723 \[hep-th\]](#).
- [59] W. Israel, Event horizons in static vacuum space-times, *Phys. Rev.* **164**, 1776 (1967).
- [60] P. T. Chrusciel, J. Lopes Costa, and M. Heusler, Stationary Black Holes: Uniqueness and Beyond, *Living Rev. Rel.* **15**, 7 (2012), [arXiv:1205.6112 \[gr-qc\]](#).
- [61] C. Misner, K. Thorne, and J. Wheeler, *Gravitation*, Gravitation No. pt. 3 (W. H. Freeman, 1973).
- [62] D. Ayzenberg and N. Yunes, Slowly-Rotating Black Holes in Einstein-Dilaton-Gauss-Bonnet Gravity: Quadratic Order in Spin Solutions, *Phys. Rev. D* **90**, 044066 (2014), [Erratum: *Phys.Rev.D* 91, 069905 (2015)], [arXiv:1405.2133 \[gr-qc\]](#).
- [63] N. Yunes and L. C. Stein, Non-Spinning Black Holes in Alternative Theories of Gravity, *Phys. Rev. D* **83**, 104002 (2011), [arXiv:1101.2921 \[gr-qc\]](#).
- [64] V. Cardoso, S. Hopper, C. F. B. Macedo, C. Palenzuela, and P. Pani, Gravitational-wave signatures of exotic compact objects and of quantum corrections at the horizon scale, *Phys. Rev. D* **94**, 084031 (2016), [arXiv:1608.08637 \[gr-qc\]](#).
- [65] P. Heidmann, N. Speeney, E. Berti, and I. Bah, Cavity effect in the quasinormal mode spectrum of topological stars, *Phys. Rev. D* **108**, 024021 (2023), [arXiv:2305.14412 \[gr-qc\]](#).
- [66] L. Pierini and L. Gualtieri, Quasi-normal modes of rotating black holes in Einstein-dilaton Gauss-Bonnet gravity: the first order in rotation, *Phys. Rev. D* **103**, 124017 (2021), [arXiv:2103.09870 \[gr-qc\]](#).
- [67] R. S. Conklin, *Gravitational Wave Echoes: Theory and Application*, Ph.D. thesis, Toronto U., Toronto U. (2021).
- [68] R. S. Conklin, B. Holdom, and J. Ren, Gravitational wave echoes through new windows, *Phys. Rev. D* **98**, 044021 (2018), [arXiv:1712.06517 \[gr-qc\]](#).
- [69] V. Cardoso, E. Franzin, and P. Pani, Is the gravitational-wave ringdown a probe of the event horizon?, *Phys. Rev. Lett.* **116**, 171101 (2016), [arXiv:1602.07309 \[gr-qc\]](#).
- [70] J. Abedi, H. Dykaar, and N. Afshordi, Echoes from the abyss: Tentative evidence for planck-scale structure at black hole horizons, *Phys. Rev. D* **96**, 082004 (2017), [arXiv:1612.00266 \[gr-qc\]](#).
- [71] R. Dong and D. Stojkovic, Gravitational wave echoes from black holes in massive gravity, *Phys. Rev. D* **103**, 024058 (2021), [arXiv:2011.04032 \[gr-qc\]](#).
- [72] D. Wu, X.-L. Zhang, Q.-G. Huang, and J. Ren, Model-independent search of gravitational wave echoes in LVK data, (2025), [arXiv:2512.24730 \[gr-qc\]](#).
- [73] K. H. Tsang *et al.*, Search for rotating black hole horizonless echoes in the ligo-virgo-kagra o3 run, *Phys. Rev. D* **108**, 084041 (2023), [arXiv:2305.10430 \[gr-qc\]](#).
- [74] Z. Mark, A. Zimmerman, S. M. Du, and Y. Chen, A recipe for echoes from exotic compact objects, *Phys. Rev. D* **96**, 084002 (2017), [arXiv:1706.06155 \[gr-qc\]](#).
- [75] Q.-C. Wang, E. Berti, V. Cardoso, *et al.*, Mode mixing and superradiant amplification in gravitational-wave echoes, *Phys. Rev. D* **99**, 064016 (2019), [arXiv:1810.04667 \[gr-qc\]](#).
- [76] E. Maggio, N. Oshita, and P. Pani, Testing near-horizon quantum structures via gravitational-wave propagation, *Phys. Rev. D* **101**, 064030 (2020), [arXiv:2001.03620 \[gr-qc\]](#).
- [77] E. Barausse *et al.*, Prospects for Fundamental Physics with LISA, *Gen. Rel. Grav.* **52**, 81 (2020), [arXiv:2001.09793 \[gr-qc\]](#).

- [78] G. Papallo, On the hyperbolicity of the most general Horndeski theory, *Phys. Rev. D* **96**, 124036 (2017), [arXiv:1710.10155 \[gr-qc\]](#).
- [79] A. Adams, N. Arkani-Hamed, S. Dubovsky, A. Nicolis, and R. Rattazzi, Causality, analyticity and an IR obstruction to UV completion, *JHEP* **10**, 014, [arXiv:hep-th/0602178](#).
- [80] F. Echeverria, Gravitational Wave Measurements of the Mass and Angular Momentum of a Black Hole, *Phys. Rev. D* **40**, 3194 (1989).
- [81] E. Berti, V. Cardoso, and C. M. Will, On gravitational-wave spectroscopy of massive black holes with the space interferometer LISA, *Phys. Rev. D* **73**, 064030 (2006), [arXiv:gr-qc/0512160](#).
- [82] J. Maldacena, S. H. Shenker, and D. Stanford, A bound on chaos, *JHEP* **08**, 106, [arXiv:1503.01409 \[hep-th\]](#).
- [83] B.-H. Lee, N. A. Nilsson, and S. Thakur, (2026).